RSS BASED LOCALIZATION FOR PARTIAL DISCHARGE SOURCE USING RECEIVED SIGNAL STRENGTH ONLY.

By

UMAR F. KHAN

A thesis submitted to the University of Huddersfield in partial fulfilment of the requirements for the degree of Doctor of Philosophy

In the School of Computing and Engineering

Supervisor: Professor Pavlos I. Lazaridis

Co-Supervisor: Professor Ian A. Glover

December 2018

ABSTRACT

Partial discharge (PD) localization has been performed on a periodic or on a request basis to assess the health of high-voltage (HV) systems mainly due to lack of feasibility of techniques for continuous monitoring and localization. Advancements in the field of communication technology have made it possible to detect and locate PD activity in HV systems on a continuous basis. Existing PD localization techniques mainly include the time of arrival (TOA), time difference of arrival (TDOA) and angle of arrival (AOA) methods. These techniques require time-based synchronization of sensor nodes that are involved in the receiver system resulting in expensive and complex hardware and software solutions.

In this thesis, a received signal strength (RSS) based localization of PD is proposed. It is demonstrated that RSS based localization can be used under anonymous and harsh industrial environments for PD localization. RSS based localization does not require synchronization because unlike TOA, TDOA and AOA, it processes the amplitude of the received signal and not its phase.

A theoretical model of the algorithm has been developed based on the path loss model equation. Simulations have been performed to prove the principle in noiseless and noisy conditions before the experimental study was conducted. Artificial noise has been generated to test the performance of the algorithm in different noise conditions.

To explore the algorithm in real substation environments, an empirical study was performed in indoor and outdoor environments. Artificial PD signal is generated by using a high voltage partial discharge (HVPD) Pico Coulomb (pc) calibrator to perform the field trials at two different sites i.e., power network distribution centre (PNDC) at the University of Strathclyde and TATA Steel at Port Talbot, Wales. A specialised radiometer sensor is used to measure PD signals. Received signals from voltage levels are converted into power signals (dBm) as input to the location algorithm. Various sensors configurations in indoor and outdoor environments were used. The algorithm's performance was evaluated based on four parameters which include, the estimated location, localization error, the path loss exponent (PLE) optimisation and the scalability. Simulation and experimental studies show that there is sufficient agreement

and RSS based localization is a promising technique that can be used autonomously in future condition monitoring of HV systems on a continuous basis.

Acknowledgments

First and foremost, I would like to thank Almighty Allah for providing me the ability, courage, strength and opportunity to complete this work.

I want to express my sincere gratitude to my supervisors Dr. Pavlos Lazaridis and Prof. Ian Glover for their continuous support and guidance throughout this work. Without their support and guidance, it would have been a real challenge to complete this study.

Besides my supervisors, I would like to thank my colleagues who were working on the partial discharge project for their help and support towards experimental work and taking measurements.

I want to thank the University of Huddersfield for having me to complete this work.

Finally, I would like to thank all my family and friends for their support.

Author's statement of originality

I hereby certify that all the work presented in this thesis is the author's original work. Where ideas or techniques have been used from other's work, they are acknowledged fully by using the standard referencing system according to the University of Huddersfield's guidelines. Any publications that have arisen from this work are listed in chapter 1 section 1.7 as "major contributions". A copy of each of the published paper is submitted to the School's research office at time of thesis submission.

Umar F. Khan

1076750

01/12/2018

List of abbreviations

AE	…….	Acoustic emissions
AIS	…….	Air insulated sub-systems
AOA	…….	Angle of arrival
CRLB	…….	Cremer row lower bound
DOA	…….	Direction of arrival
DVB	…….	Digital video broadcasting
EM	…….	Electromagnetic
FM	…….	Frequency modulation
GHz	…….	Gigahertz
GIS	…….	Gas insulated sub-systems
HF	…….	High frequency
HVPD	…….	High voltage partial discharge
HV	…….	High-voltage
LIS	…….	Liquid insulated sub-system
LS	…….	Least squared
LNA	…….	Low noise amplifier
LOS	…….	line of sight
MHz	…….	Megahertz
ns	…….	Nanosecond
PD	…….	Partial Discharge
PDF	…….	Probability density function
pC	…….	Pico Coulomb
PLE	…….	Path loss exponent
PNDC	…….	Power network demonstration centre
RAM	…….	Random access memory
RF	…….	Radiofrequency
RMS	…….	Room mean squared
RSS	…….	Received signal strength
TDOA	…….	Time difference of arrival

TOA	…….	Time of arrival
UHF	…….	Ultra-high frequency
VHF	…….	Very high frequency
WSN	…….	Wireless sensor networks
RUL	…….	Remaining useful life

TABLE OF CONTENTS

List of figures

List of tables

Chapter 1: PARTIAL DISCHARGE LOCALIZATION: AN INTRODUCTION AND PROBLEM STATEMENT

1.1 Introduction to partial discharge

The demand for electricity has grown exponentially in recent times. It implies that non-stop provision is necessary to ensure the smooth running of services. Insulation materials used in power devices deteriorate with time and become the main cause of equipment outage or failure. Keeping in view such issues, it becomes necessary to monitor the health of high-voltage (HV) systems continuously to detect any issues and solve them before equipment failure to avoid cost and disruptions. Partial discharge (PD) detection is one of the key methods to evaluate the ageing of such HV systems. The term partial discharge (PD) refers to the release of energy that occurs due to cracks in insulations that partially bridge two conductors [1, 2]. PD is an ionization process that changes the physical and chemical structure of the dielectric materials and finally weakens them if left unresolved. The occurrence of PD in HV systems is a complex phenomenon [1, 3, 4]. IEC 60270 defines partial discharge as a localized electrical discharge that only partially bridges the insulation between two conductors and which may or may not occur adjacent to a conductor [4].

1.2 An overview of PD activity and localization

Changes in PD characteristics often precede catastrophic failures. The existence of PD in the insulation structure is termed as one of the major causes of failure in high-voltage systems [5-7]. If PD events occur in the long term, they can result in failure of high-voltage systems. [8, 9]. Usually, PD activity takes place mainly in power transmission lines, power transformers, generators and power cables. PD generally arises at sites such as voids, joints, cavities and delamination zones in high-voltage components insulation systems [8, 10]. The repetitive occurrence of PD activity can lead to system degradation and can affect the performance of the system and consequently may lead to the breakdown of the whole insulation system [8, 11]. Different PD types such as corona and surface discharges are observed from electrode edges, point edges or cylindrical wires in case of gases[12, 13]. Usually, the surface PD is observed

at the insulation boundaries [14]. A common perception regarding PD activity is that it appears typically in cavities or air inclusions [14, 15]. The higher the number of cavities, the higher will be the number of PD pulses that will arise per unit time. If a breakdown occurs due to PD, it will be preceded by consecutive PD pulses [16]. A variety of PD types is determined based on electromagnetic (EM) radiation [17]. EM radiation of internal discharge is different from the surface or cavity discharge. PD pulses have a frequency spectrum in the Megahertz (MHz) and the Gigahertz (GHz) range, a large amount of which is radiated from conductors that are in the close vicinity of the PD source [18-20].

Continuous monitoring of PD activity can have a significant impact on mitigating catastrophic failures. Continuous monitoring of PD activity can, therefore, help in several ways including:

- Delaying the replacement of an ageing power plant and sustaining service life until it becomes necessary to replace it to save the cost
- Risk-based maintenance can overtake the routine maintenance if there is unusual activity, i.e. PD.
- A plant can be de-rated, and the energy flow can be re-routed [21]

It is pivotal to realise that the ultimate consequence of PD is a catastrophic failure. Early diagnosis of PD can save energy and costs. When energy companies are fined, they face fines of millions of pounds [8, 15, 21]. Hence if one failure can be avoided, this can result in millions of pounds of savings and simultaneously avoiding disruptions to customers by either curing the problem or by re-routing the energy.

Partial discharge detection is not new. It can be achieved using various technologies. In relation to the detection mechanism, PD detection may broadly be categorised into three main generations as summarised in Figure 1.3 below:

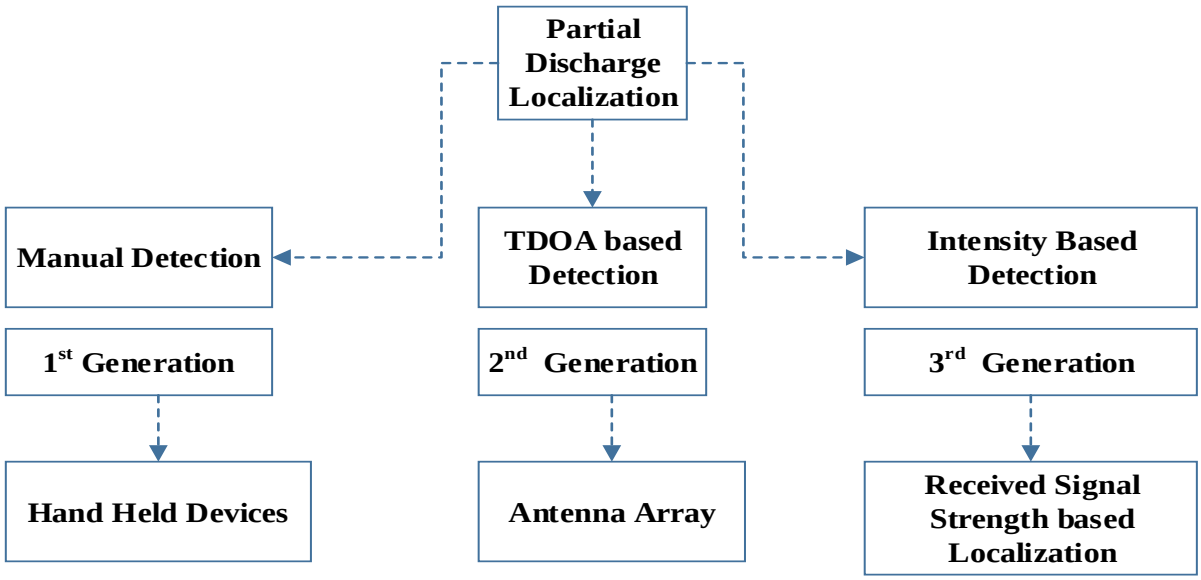

Figure 1.1. PD localization: three generations [22, 23].

The figure 1.3 above illustrates PD detection as a generation based approach. The manual detection is the first generation and a most commonly used approach. A technician with a handheld device mainly called PDS 100 surveys the high voltage system to monitor the state of the HV system. The frequency of the survey is normally twice or no more than three times a year.

The second generation is based on the time difference of arrival (TDOA). In TDOA based approach, mainly power companies request the survey of the high voltage system. It is available on request to power companies. The technique works on the entire pulse of the PD signal and hence demands expensive signal processing and synchronisation.

To overcome the limitations of the above two techniques, received signal strength (RSS) based techniques is proposed in the third generation of localization. The technique works on the total energy received rather than entire pulse of the PD signal. Due to the technique only working on the received signal, the signal processing requirements can be reduced significantly as well as the synchronisation between the receiving nodes is not required.

1.3 An overview of localization of an object on a plane

Before going into the details of a PD source localization, it is essential to understand the localization of an object on a plane. Object localization can be performed relative to a known position within a certain coordinate system. A localization system can be a self-localization system or a remote localization system. In a self-localization system, an object localizes itself with respect to a static point. In a remote localization system, receiving nodes are used to locate

an object or source within a boundary or a coverage area. Due to advancements in wireless communication technology, the remote localization has gained significant importance in recent times. Figure 1.4 below summarises the overall localization of an object within a certain coverage area.

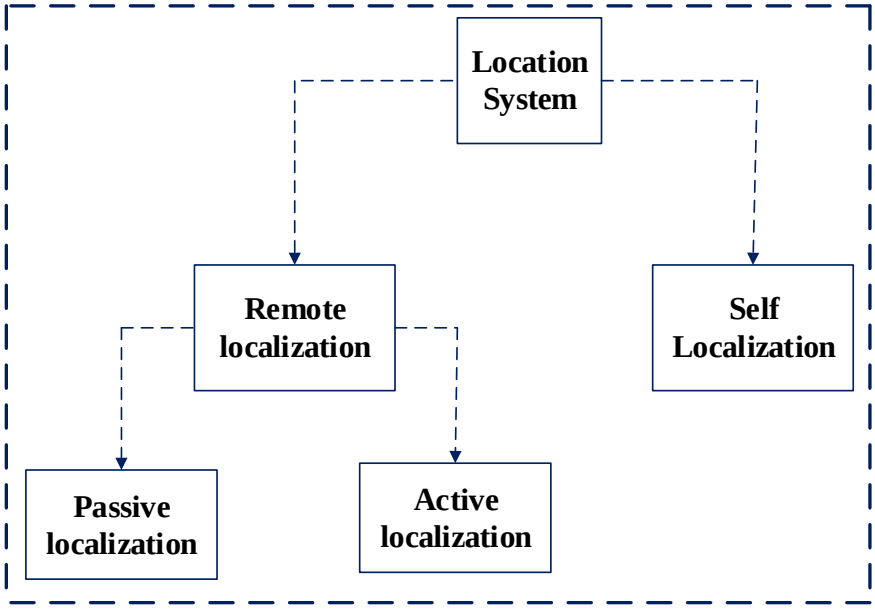

Figure 1.2. Localization of an object: a hierarchal approach.

The remote localization can be active or passive. In the active localization process, the source becomes the part of the localization process, whereas, in passive localization, the source does not involve in the localization process.

1.4 Prediction of the future state of insulations

Prediction of the future state of insulation materials is important in assessing the overall condition of the HV equipment. [24] Have performed a prognostic study. The goal of the study is to predict the failure in terms of remaining useful life (RUL). The main reason for the catastrophic failures is the establishment of a treeing mechanism that develops in HV systems. Due to the treeing, electric field in a local area will become highly concentrated. PD monitoring can detect the electrical treeing by continuously monitoring the insulation state. The work proposed in [25] explores the scope by using various materials. This study aims to detect the PD and locate the source of the discharge.

1.5 Problem statement

To deploy wireless sensor networks (WSNs) for a wide variety of applications, accuracy and cost are the key requirements [26]. In recent times, it has become possible to detect and locate a PD activity on an automated basis by using the techniques such as the time of arrival (TOA) and the time difference of arrival (TDOA). Real-time monitoring of PD activity can help to recognize the PD pattern and feature extraction [22, 27]. TDOA is currently used successfully by companies such as Elimpus, which provide PD services principally to the National Grid. Although TDOA based PD monitoring is effective and accurate at the commercial level, however, it cannot be deployed for continuous PD monitoring due to its complexity and cost.

Nevertheless, the approach proposed in this thesis, i.e. PD location estimation based on received signal strength, has several advantages over all other PD detection and location mechanisms. The main advantages of the proposed mechanism include:

- The intensity-based approach is simpler and hence economical. There are no expensive clock requirements for synchronization of nodes. In TOA synchronization between the source and the receiving nodes is necessary. In TDOA synchronization between the receiving nodes only is necessary. RSS based localization does not require both, hence becomes simple and cost-effective.
- The approach is scalable. If any modifications are required, they can be performed easily without any alterations in the whole system. For example, if additional receiving nodes are required to cover more area and, to increase coverage, nodes can be added without any challenges.
- There is no requirement of line of sight (LOS) when PD localization is based on RSS. In other techniques such as TDOA, TOA and DOA/AOA etc. there is a need for LOS for accurate localization of the PD source.
- The major advantage that the proposed technique offers over existing ones is that existing techniques offer on-demand PD detection at a particular time when scheduled or requested. With the proposed technique based on monitoring of PD using received signal strength (RSS), PD activity is monitored every e.g. hour and updated regularly to be used to monitor the health of the high-voltage systems. Existing techniques either require manual detection (manual handheld devices) or they are available commercially at the request of the power companies (TDOA).

A comparison between the techniques in terms of various parameters is outlined in Table 1.1 below:

Table 1.1. Comparison between techniques.

Parameter	TOA	TDOA	RSS
Complexity	Very high due to synchronisation at the source and the receiving ends. Need expensive clock [28, 29].	High, there is no synchronisation requirement at the source, however, between the node pairs is mandatory. Again there is need for expensive clock [28, 29].	No synchronisation required, no expensive clock required [28].
Signal processing	Expensive due to high requirements because the scheme works on the entire pulse and it leads to expensive solutions in terms of use of smart antennae array [30].	Again works on the entire PD pulse, hence there is expensive signal processing and requirement of smart antenna [31].	No requirements of smart antennae array. A simple dipole antenna can perform the job well.
Cost	Very high	High	Low
Accuracy	Very high but on the condition that LOS and synchronisation requirements are met fully. A small synchronisation error can lead to big localization error [32].	High, but again on the condition that requirements in terms of LOS and synchronisation at the receiving end at met fully [32].	Moderate, works on the received signal which is exposed to many interferences and noise signals. Its accuracy is mainly dependent on propagation environment [32, 33].

Keeping in view these factors, the RSS based measurement of PD seems an integral part of future smart grids.

1.6 Aims and objectives of the study

The key aim of this research is to design and implement a location algorithm based on intensity, i.e. the strength of the received signal. Main objectives include the following:

1. To review the wireless-based detection and localization techniques used for PD monitoring.
2. To identify the scope of intensity-based PD measurement and its applications in future smart grids.
3. To identify a plausible way of implementing intensity-based PD localization in an anonymous environment.
4. To model and evaluate an intensity-based location algorithm for continuous PD monitoring.
5. To optimise the emerging parameters of the PD localization algorithm by using mathematical and statistical modeling tools.
6. To deploy a proof-of-principle system with one or more location algorithms, as part of "whole system integration" in a wireless sensor system.

1.7 Major contributions

In this thesis, received signal strength (RSS) is utilised to locate a partial discharge source. To locate the PD source, the path loss model is used. The major challenge that exists is that, both, the source transmitted power and the path loss power are unknown. A novel algorithm for localization of PD source has been developed by using received signal strength (RSS) in an environment where no prior information is available about the propagation environment. The proposed algorithm attempts to localize PD source by using the amplitude of the PD pulse rather than the phase. The algorithm's testing was performed by using simulations and field trials. An empirical study was conducted in at least three different substation environments based on indoor and outdoor localizations. The results obtained show that the proposed algorithm offers a simple RSS based localization solving issues of complexity and cost associated with other existing approaches. Results obtained from different field trials have been presented.

Although there are over twenty publications where the author has contributed to the PD project, however, the main contributions to the field are listed in the papers below:

I. Khan, U.F., et al., *An Efficient Algorithm for Partial Discharge Localization in High-Voltage Systems Using Received Signal Strength.* 2018. 18(11): p. 4000.

II. Khan, U., et al. *Localization of Partial Discharge by Using Received Signal Strength*. in *2018 2nd URSI Atlantic Radio Science Meeting (AT-RASC)*. 2018. IEEE.

III. Khan, U., et al. *Received Signal Strength Intensity based localization of partial discharge in high-voltage systems.* ICAC-Newcastle 09/2018. IEEE

IV. Saeed, B., et al. *A supervisory system for partial discharge monitoring*. in *2018 2nd URSI Atlantic Radio Science Meeting (AT-RASC).* 2018. IEEE.

V. D W Upton., et al. *Wireless Sensor Network for Radiometric Detection and Assessment of Partial Discharge in HV Equipment.* URSI GASS 2017, Montreal, Canada; 08/2017, DOI:10.23919/URSIGASS.2017.8104973.

VI. Jaber, A., et al. *Diagnostic potential of free-space radiometric partial discharge measurements*. in *General Assembly and Scientific Symposium of the International Union of Radio Science (URSI GASS), 2017 XXXIInd*. 2017. IEEE.

VII. Jaber, A., et al. *Validation of partial discharge emulator simulations using free-space radiometric measurements*. in *Students on Applied Engineering (ICSAE), International Conference for*. 2016. IEEE.

VIII. Mohamed, H., et al. *Partial discharge detection using software defined radio*. in *Students on Applied Engineering (ICSAE), International Conference for*. 2016. IEEE.

1.8 Research methodology

The methodology is mainly based on three main parts, which include the following:

- Theoretical modeling of the algorithm.
- Validation and verification of using a simulation of the algorithms in MATLAB.
- Proof of concept through empirical study.
- The final part of the methodology is based on the performance evaluation of the proposed algorithm, and hence the comparison of the proposed algorithm is made with other algorithms that work on received signal strength.

The first stage of the methodology was based on the development of the mathematical model based on the literature review. To develop the mathematical model, earlier work conducted was used to elaborate the need and scope of the algorithm based on RSS. By using a statistical approach, a mathematical model was developed by the end of year 1 to establish the key principles of source localization using received signal strength (RSS).

The second stage was based on the simulation model. There were various tools available and were under consideration to develop the simulation model of the location algorithm. The main options under consideration include NS2, Prowler, C/C++ and MATLAB. The author's preference was to use MATLAB software due to familiarity. Also, for the majority of the localization algorithms that required programming and testing the proof of principle, MATLAB was the best option.

The third stage of the methodology entailed the physical implementation of the location algorithm based on RSS. The whole system is an integration of various components including analogue and digital electronic parts, front-end and communication system. The physical implementation was performed in a real-life scenario where localization of the source was a part of a whole wireless sensor network system. RSS based localization was successfully achieved with errors that were acceptable based on expected input coming from the analogue circuitry.

1.9 Structure of the thesis

The structure of the remaining thesis is organised as follows. Chapter 2 mainly focuses on the survey of existing technologies regarding localizations. In chapter 2, various localization techniques are discussed including TOA, TDOA, AOA and RSS. Chapter 3 is mainly based on various RSS based localization techniques that all work in an anonymous environment by using the path loss model equation. The performance of such techniques in harsh industrial environments such as PD detection and localization is explored in this chapter. Chapter 4 focuses on the theoretical modeling of the location algorithm based on RSS. Chapter 5 focuses on the use of a radiometer sensor and its explanation for detecting the PD signal and the use of that signal to determine the input to the location algorithm. Mainly the focus is on solving the mathematical challenges to implement the algorithm by using the path loss model equation. Chapter 6 discusses the results obtained from field trials scenarios to perform the empirical study. The results obtained are based on indoor and outdoor measurements with a range of sensors configurations. In chapter 7, the performance evaluation of the proposed algorithm is

performed by comparing it with the other RSS based algorithms where path loss parameters are unknown, and results are evaluated by using the comparison. Chapter 8 is about the conclusion and future work.

1.10 Overall work summarised

An overall overview of the work conducted is summarised in Figure 1.5 below:

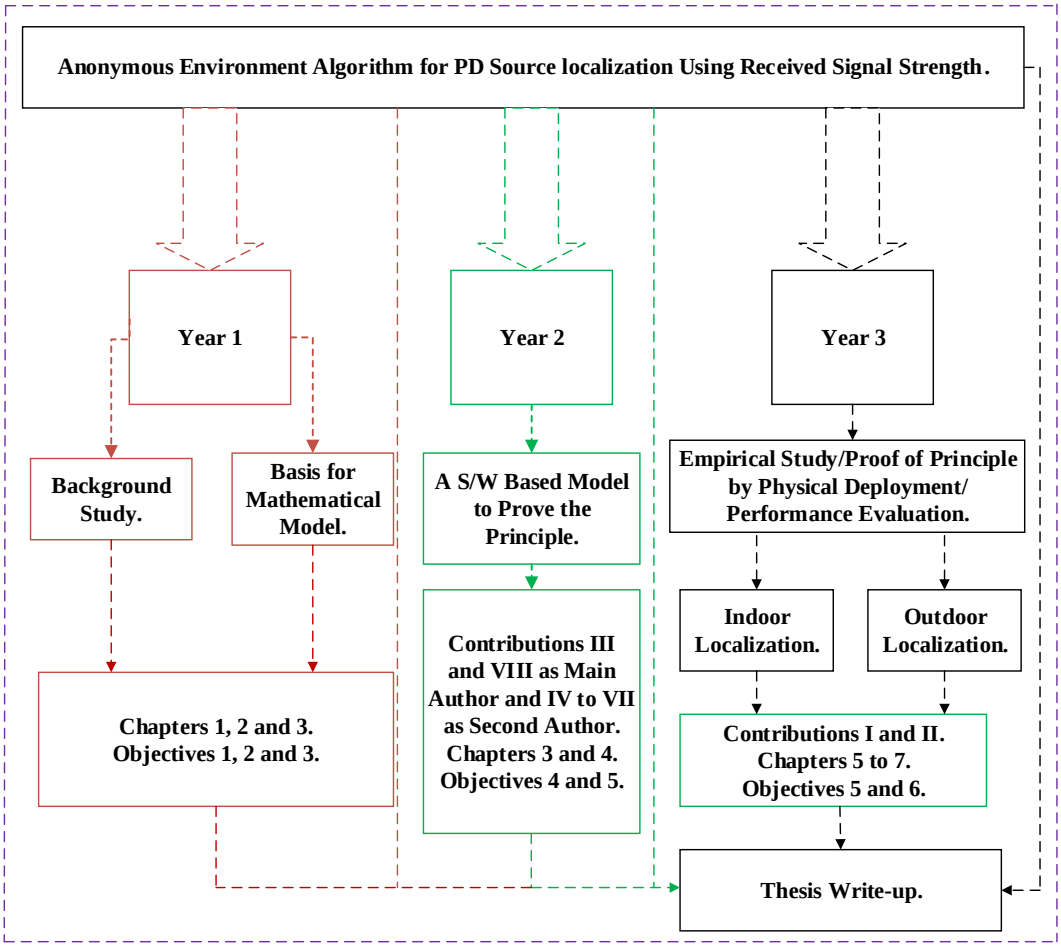

Figure 1.3. A summary of the work conducted contributions.

1.11 Chapter 1 summary

Chapter 1 presented a brief overview of the partial discharge activity and PD pulse properties. The chapter also presented the key objectives of the research and the expected outcome of the research. The problem statement is identified as well as the methodology of the research. This leads to chapter 2, where existing localization techniques and their scope will be discussed for continuously detecting and locating a PD source.

Chapter 2: A REVIEW OF EXISTING LOCALIZATION TECHNIQUES AND THEIR APPLICATION TO CONTINUOUS PD MONITORING

2.1 Overview of the PD activity

In high-voltage (HV) systems, the existence of partial discharge is a physical phenomenon that can be lethal and costly [34, 35]. Within electrical systems, the PD occurrences have been

appreciated from the beginning of the 20th century. PD occurs due to various reasons, e.g. cracks inside the insulation, impurities, voids and ageing of the equipment etc. Within insulation systems, PD is a physical activity that can be low, medium or high-intensity. A PD activity is highly confined electrical discharge within an insulating material bridging two conductors [36-39]. There can be various reasons for a PD activity within high-voltage (HV) power systems. It could occur because of the insulation breakdown or floating components due to aging, or it could happen due to significant cracks in the insulation system that bridges the electrodes [39-41]. A PD can also occur due to the breakdown between a floating electrodes, the breakdown of gas in a cavity and breakdown between floating and an energized electrode [4, 42]. Under varying acoustic emissions (AE) measurement conditions, PD can be classified into four main types, which include the PD from a sharp point to the ground plane, PD arising from insulation voids, surface discharge (corona) and PD arising from semi-parallel planes [43, 44].

Low-intensity PD activity results due to the emission of charge carriers from surfaces of the insulators, glow and sub-critical avalanche charge carriers [45]. Medium intensity PD activity results due to electrical treeing that is established between insulators and conductors, however, it can get severe with time. Highly intense PD activity occurs due to partial arcs and electric sparks [46, 47]. The majority of such activities cause degradation of electrical equipment and often lead to electrical breakdowns or catastrophic failures if unresolved for a long time. Some of the key equipment that experience PD include switchgear, power cables, stator windings and power transformers. For PD to occur, the supply voltage that conductors experience should be high. The high-voltage between the conductors will create electrical stress. For example, for most of the dry gases, at a pressure value of 100KPa, if the electrical stress exceeds 3000V/mm, electrons from the gas atom will be stripped off. These stripped electrons will run through the air and will strike the liquids or solids and hence will cause ageing of the insulation materials used. The movement of electrons through space will result in the creation of electric current. This current will be equal to the rate of change of charge q, as shown in the equation below:

$$I = \frac{dq}{dt} \qquad \text{Equation 2.1}$$

Figure 2.1 below illustrates the electrical representation of the partial discharge activity in a stator of a motor.

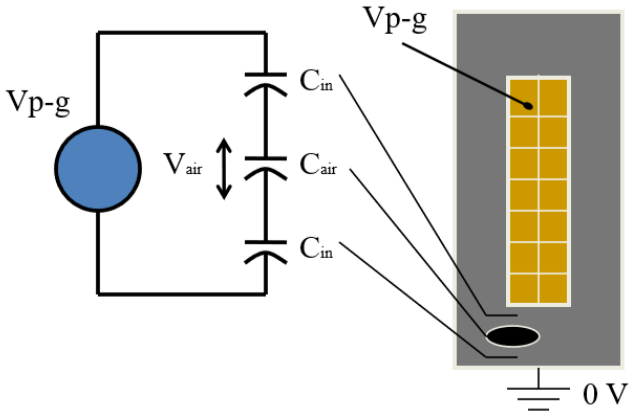

Figure 2.1. An example of PD in a stator of a motor [48].

In Figure 2.1 above, V_{p-g} act as the supply voltage to the capacitive voltage divider circuit that consists of C_{in} and two C_{air} capacitors. Due to the capacitive divider circuit, the voltage will develop across the void that is air filled. PD will occur if the strength of the electric field is high enough. The electrical field strength can be determined by using equation 2.2 below:

$$E = \frac{V}{d} \qquad \text{Equation 2.2}$$

The electrical stress will occur if:

$$E = \frac{V}{d} > 3000V/mm \qquad \text{Equation 2.3}$$

The strength of the discharge depends upon the size of the void. The overall PD is highly dependent upon the voltage that is applied.

PD can be of different types including external or surface discharge, corona and internal discharge etc. Due to PD, the insulation in HV systems can deteriorate, and this can result in the breakdown of the electrical system [21, 49]. As an example, Figure 2.2 below shows the internal discharge occurring in a failed transformer.

Figure 2.2. Power transformer failure (http://electrical-engineering-portal.com).

PD can occur in a cavity within a dielectric material, or it can originate at an electrode itself. Typical partial discharges include:

Corona discharge: It occurs in air insulated system (AIS), gas insulated systems (GIS) or liquid insulated systems (LIS). Corona discharge usually occurs to the non-uniform electric field at sharp edges etc. Figure 2.3 (i) below shows a typical corona discharge in HV systems. Relatively, corona discharge is a low power discharge that can exist in the form of a spark, glow or a steamer. The discharge will increase with an increase in the voltage due to the strength of the electric field. Corona discharge can be positive or negative.

Surface discharge: it occurs due to the relative permittivity of the dielectric materials increase due to stresses. Figures 2.3 (ii) and (iii) illustrate the surface discharges

Cavity discharge: Cavity discharge occurs due to the formation of cavities in solid and liquid dielectric materials. When such cavities are established in the insulating materials, the gas inside the materials becomes overstressed, and as a result, the discharge occurs. Figure 2.3 (iv) illustrates the cavity discharge.

Treeing: in such cases, the insulating materials deteriorate due to the formation of strong electric fields at the sharp edges which result in treeing. Figure 2.3 (v) illustrates the treeing process.

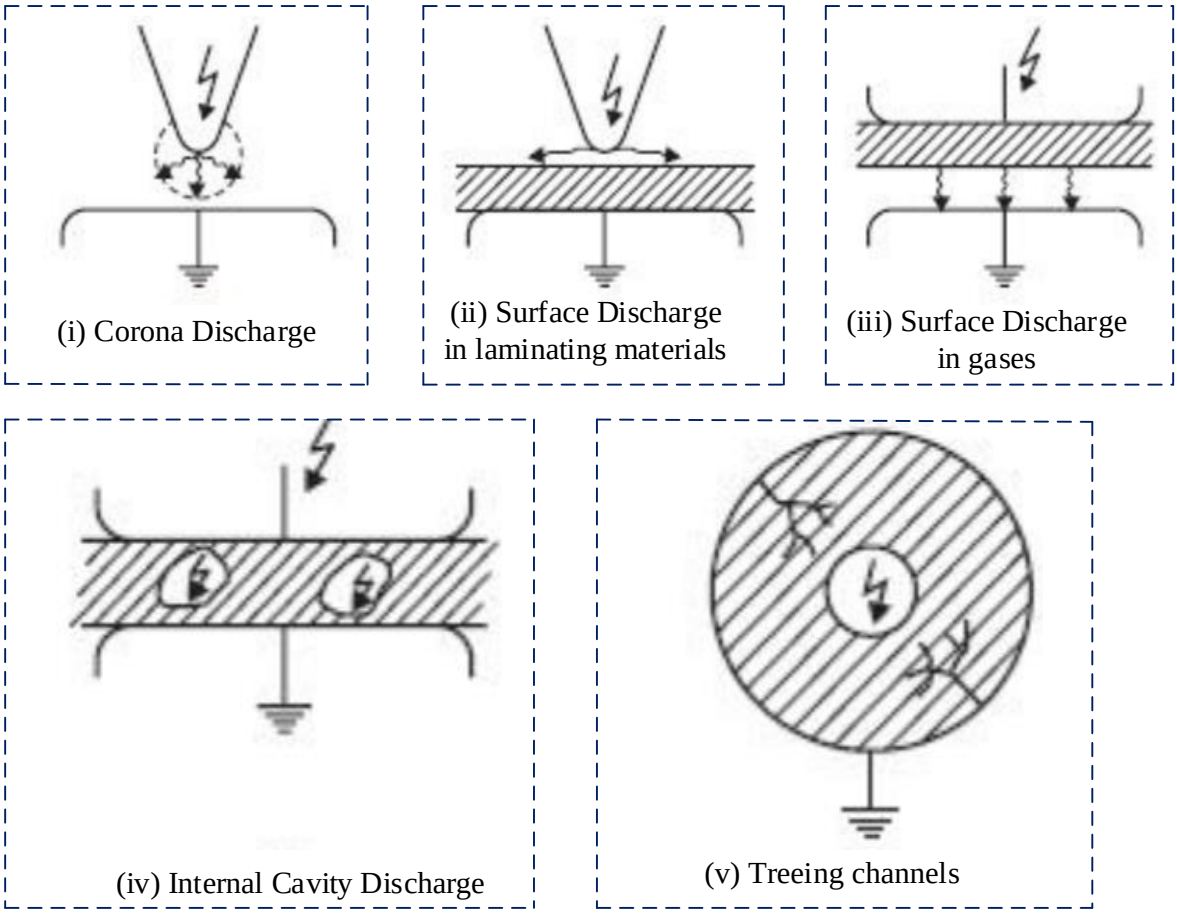

Figure 2.3. Typical PDs in HV systems [50].

As mentioned above, PD may not cause instant failure of high-voltage systems. However, PD becomes damaging when electrical treeing is established between the dielectric material and the conductor. Electrical treeing in electrical equipment takes place due to two main reasons which include chemical degradation and physical degradation due to nitrogen ions bombardments. The whole process is termed electrochemical treeing [51]. The process of electrochemical treeing is quite familiar in the field of power electronics and has been most recently replaced by the term “water treeing”. The stress increases initiate the process in high-voltage systems at the operating voltages. If the process of electrical treeing is continuous at operating voltages, it will accelerate the erosion and PD activity will be initiated continuously and hence will result in the break of insulation sooner than later [50, 52, 53]. Various PD occurrences and their causes are summarised in Table 2.1 below:

Table 2.1. A summary of PD types and reasons in HV systems.

Discharge type	Reason
Void discharge	Poor impregnation of coil.
Delamination zones discharge	Coils overheating
Slot discharge	Within slots windings looseness
End winding discharge	The looseness of end windings
Voids created next to copper	Thermal cycling
Electrical tracking discharge	Due to contaminations in windings

Table 2.1 above shows some but not all of the PD reasons and their existence that are commonly found in HV systems and become the main source of equipment degradation.

Considering the nature of PD activity and its effects economically and in terms of energy losses, brings the need to continuously monitor the PD rather than periodically. To robustly assess the quality of high-voltage systems, PD location and diagnosis is considered as one of the most useful methods to assess the condition of HV systems.

2.2 Origin of partial discharge: An overview

The presence of PD in HV systems does not lead to instant failures. When PD occurs in an HV system, it causes a gradual degradation. PD becomes more damaging when it occurs in microscopic insulation voids. This happens due to a microscopic void having a lower permittivity than its surrounding insulation, which results in an electric field in the void that is higher than the electric field in its surrounding material, which results in a discharge occurring inside the void. Figure 2.4 represents the equivalent circuit for PD.

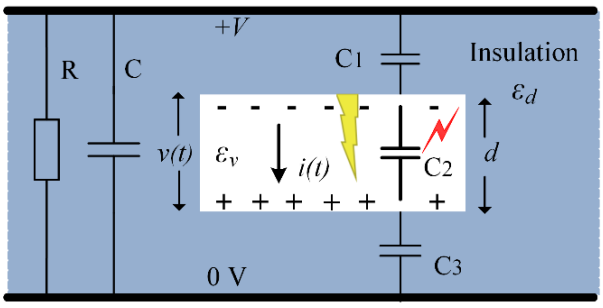

Figure 2.4. PD equivalent circuit [54].

Figure 2.4 above is an illustration of PD due to the presence of a cavity within an insulation material. Capacitors C_1, C_2 and C_3 form a voltage divider circuit. When a spark is created with in the gap in the void, a small current flows through the conductor. Overall capacitance of the three capacitors forming a voltage divider depends upon the dielectric permittivity of the material.

PD pulses have a frequency spectrum in the very-high frequency (VHF) and the ultra-high frequency (UHF) range, a large amount of which is radiated from conductors that are in the close vicinity of the PD source.

2.2.1 PD signal generation

In the majority of cases, PD occurs due to rapid changes in the electric field configuration as a result of an electrical activity, which results in the flow of current through a conductor connected to the external world [55]. For example, a PD signal is usually a PD pulse in solid or fluid dielectrics which is the result of voids or bubbles that are mainly created within or at the surface of the dielectric materials [56, 57]. The duration of a PD pulse may vary, and it is in the range of 1ns [4, 58]. A typical PD pulse is shown in Figure 2.5 below:

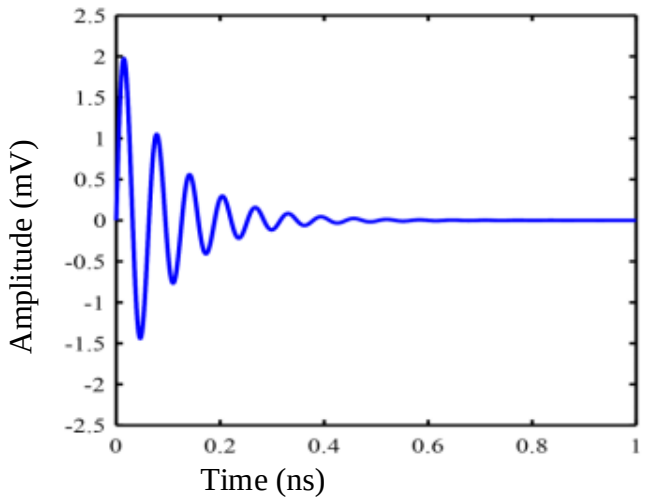

Figure 2.5. A typical PD pulse.

To monitor the high-voltage system's state, normally PD detection is performed on a periodic basis. Power companies usually measure PD activity every few months. The frequency of measurements is typically twice a year or not more than once every quarter. The main reason to detect and measure PD is to identify a problem if it exists, and also to repair it as soon as possible. This will ensure the early diagnosis and treatment of PD. If PD remains unidentified

or undetected, it may lead to catastrophic failures in high-voltage power systems. The consequences of such catastrophic failures can result in fires, explosions, loss of power and ultimately loss of revenue regarding energy and legislative costs. Figure 2.6 is an example of PD within the insulation system.

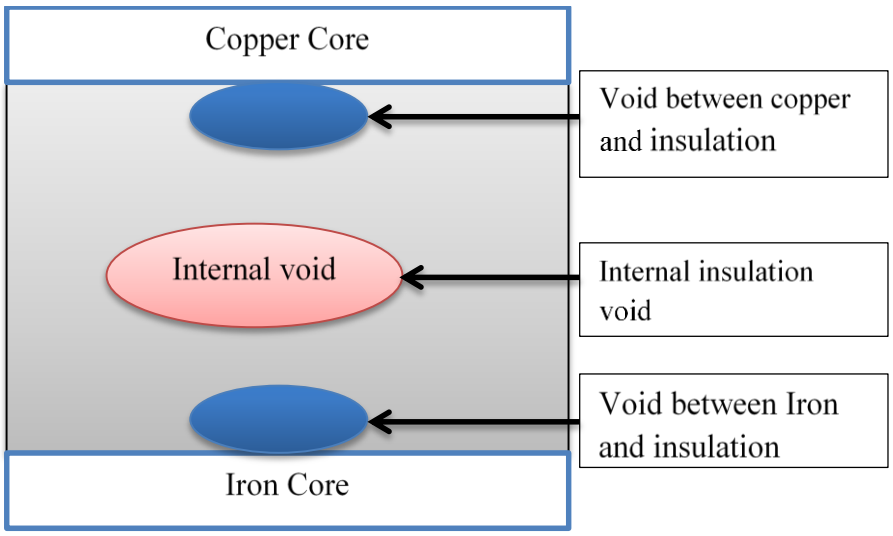

Figure 2.6. A depiction of PD activity [52].

2.2.2 Failures associated with PD

PD activity initiates slowly, and immediate failure may not happen [4]. In some cases, A PD activity will last for years before a failure takes place. For example, a discharge occurring between the insulating shield of a cable and the neutral wire does not cause an immediate failure [59]. Failure because of PD will take place if an electrical tree is grown between the insulation material and the conductor. Some of the major causes of electrical treeing include:

- A PD activity occurring within a cavity erodes gradually and creates a hole in the surface. Some PD can increase the conductivity of the cavity wall, and a short circuit may be created which may result in PD extinction [4, 60, 61].
- Switching impulse or lightening can result in the conversion of a water tree [62].
- High AC voltage can result in the conversion of a large water tree [62].
- The presence of metallic contaminants in the insulating materials can cause stress in the HV system that results in charge injection.

2.3 Classification of PD mechanisms

PD can be classified into three broad categories as summarised in Figure 2.7 below:

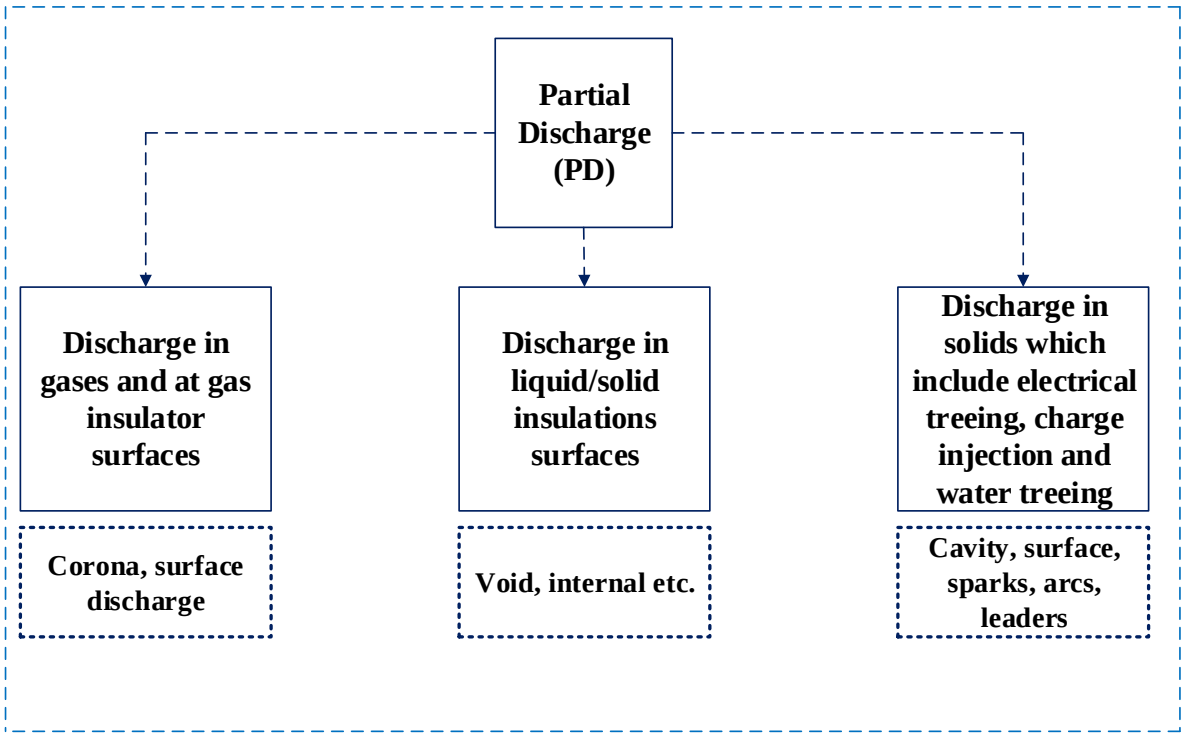

Figure 2.7. Classification of PD mechanisms.

Some of the weakest discharges include the charge carries emissions as a result of a leakage current that is caused by weakly conducting insulation surfaces. Such discharges include the flow of current along the insulation surfaces, glow discharges and cathode conductors because of electric field development. Various PD types with their duration and the magnitude of charges are summarised in Table 2.2 below:

Table 2.2. Some of the key PD types and their characteristics [2, 55].

Type of PD	Duration of the pulse	The magnitude of the charge or current
Partial arcs	100ms to 1s	10A
Electric sparks	100μs to 1ms	1 to 10A
Leader	1000μs to 1ms	1 to 10A
Surface emissions	10ns	100μC
Glow	100ns	10nC

2.4 PD pulse localization: An overview of the approaches being used

In high-voltage systems such as transformers, the capital costs are extremely high. Economic penalties due to transformer failures and as a result, the outage costs are significant [63]. If PD is the source of insulation deterioration in such systems, which it commonly is, early detection on a periodic basis of incipient insulation faults may assist in avoiding failures, and preventive maintenance measures can be taken [64]. A difficulty with the PD pulse is that it attenuates and distorts quite quickly as it travels from the source to the measuring system. However, even distorted or attenuated PD pulses still contain significant information about the nature and the location of the discharge [65]. When PD occurs, the energy present has different forms including mechanical, electrical and thermal etc. The detection of PD means identification of one or more of these forms of energy [66].

The PD pulse phenomenon is random. The quality of HV systems and cables can be assessed by measurement and diagnosis of the PD [67]. Various methods have been deployed in the past for localization of different PD types [31]. Continuous monitoring of the PD band-limited signal phenomenon requires real-time location system. Real-time location system implemented in the past for mobile devices positioning can be classified into lateration, angulation and pattern recognition [68].

Lateration techniques used for PD localization are based on distance. PD source location based on spatially-separated sensors has been explored in the past by using various techniques including radiofrequency (RF) antenna array, time of arrival (TOA), time difference of arrival (TDOA), direction of arrival (DOA), use of SDR USRP N200 and RTL-SDR etc. [16, 17, 19, 66, 69, 70]. The cost of hardware at HF, VHF and UHF operating bands has reduced significantly in recent times, which makes it affordable to detect PD in these frequency bands [71-74], [70, 75].

PD localization's accuracy is limited by the fact that PD pulse is time-limited i.e. it has a certain rise time. The typical rise time of a PD pulse is about 0.3 to 0.8 ns and the pulse duration is around 1.5 ns [76]. Owing to measurement system limitations and propagation effects, the received RF signal will be a band-limited signal. This brings uncertainty in the time-of-flight of the PD pulse and hence will cause inaccuracy in location measurement [77].

The electrical method is a key technique employed historically to estimate the PD location [25]. Electrical methods for PD location require system parameters to determine the PD location [78]. With new systems, detailed specifications may be available. Conversely with old systems

- due to their reaching the so-called “outage limit”- there may not be sufficient details, or it may not be very easy to access their interior. Hence this sort of measurement approach can be useful for such systems irrespective of whether they are old or new. For example, in power transformers, to determine the PD location, transformer parameters such as inductance and capacitance can be used. Various object localization techniques that can be used for PD localization are addressed one by one next.

2.4.1 TOA localization technique

Time of arrival (TOA) enables localization of an object by measuring the distance. TOA technique is based on the unidirectional propagation time of the travelling signals between the sender and the receiver. With one directional propagation, it becomes necessary that source, and the receivers are synchronized precisely. TOA technique uses multiple receiving nodes to locate the position of a source. To get the precise location of the source, at least three receiving nodes are required. In TOA based localization, the accuracy is high, however, on the condition that both the source and receivers are properly synchronized. If there is a small timing error, it may lead to a high localization error of the target source.

When TOA based localization is performed, in addition to nodes synchronization, it is the requirement that source transmitted signal is time stamped. This is to enable the nodes to see the time the source signal was initiated or transmitted. This is the additional requirement that increases the complexity of the scheme. In harsh industrial conditions such as localization of PD, it becomes challenging to cope with such requirements.

2.4.2 TDOA localization technique

The time difference of arrival (TDOA) works on the time difference of the arrived signal at two receiving nodes. The main advantages that TDOA offers over TOA are that there is no requirement for synchronization between the source and the receiving nodes. However, synchronization between the receiving nodes is necessary for the technique to estimate the location with enough accuracy [22]. This removes complexity to a great extent as the source synchronization is a quite complex procedure. TDOA also does not require a time stamp of the originated signal because the measurement itself is the difference of the time at the two receivers which eliminates the requirements of the time stamp. In this way, TDOA offers a better opportunity to be used for localization than TOA [33, 79].

2.4.3 DOA localization technique

Direction of arrival (DOA) also sometimes called an angle of arrival (AOA). In DOA, the receiving nodes determine the angle of the arriving signal by using an antenna array [80]. A key requirement for DOA technique is that for each antenna of the antenna array, there is a need for an RF front-end component. With these requirements, three main drawbacks include the high cost, higher power consumption and complexity of the overall detection system. For a harsh industrial environment, such requirements can prove to be challenging as a system to be deployed should be cost-effective and running continuously [81].

2.4.4 RSS localization technique

Received signal strength (RSS) based localization works on the multiple nodes receiving the energy and conversion of that energy into the distance to estimate the source locations. This technique works similarly to TOA and TODA regarding the receiving nodes used. The major difference between RSS and other techniques is that it does not require any synchronization which is a big advantage regarding the overall simplicity and cost of the receiving system. The reason being no synchronisation is required because RSS based localization works on the signal strength rather than the entire PD pulse. Converting the received signal strength into distance determines the physical location of the source [82, 83]. Another big advantage that RSS offers over other techniques is that there is no requirement of line of sight (LOS) which is the requirement in case of TOA, TDOA and DOA [31]. All these advantages may cost in accuracy as the received signal may contain noise or unwanted signals that may come from the propagation environment. This can be resolved by adding more receiving nodes in the receiving system.

2.5 Lateration techniques for PD localization

Lateration techniques used for PD localization are based on the distance. PD source location based on spatially-separated sensors has been explored in the past by using various techniques including RF antenna array, time of arrival (TOA), time difference of arrival (TDOA) and direction of arrival (DOA) etc. [80, 84, 85]. In recent years, the radiometric RF detection of partial discharge has gained significant popularity due to advancements in the field of communication engineering. The cost of hardware at VHF and UHF operating bands has reduced significantly in recent times which make it affordable to detect PD in these frequency bands [23]. All these methods are classified as range-based methods, i.e. they form matrices

bearing location information, and furthermore, they estimate the position of the source based on the information held in location matrices.

2.5.1 Radiometric PD localization based on time synchronization and distance

The radiometric PD localization is based on the use of RF antenna array. Wideband RF interference is generated by the partial discharge (PD) which can be intercepted by using the radio receiver [86]. The work of [79] has used a 4-antenna array for the three-dimensional location of PD sources. The antenna array with direct sampling can measure the time of arrival of the wave to the nanosecond accuracy [79]. Figure 2.8 below shows the configuration of the 4-antenna array.

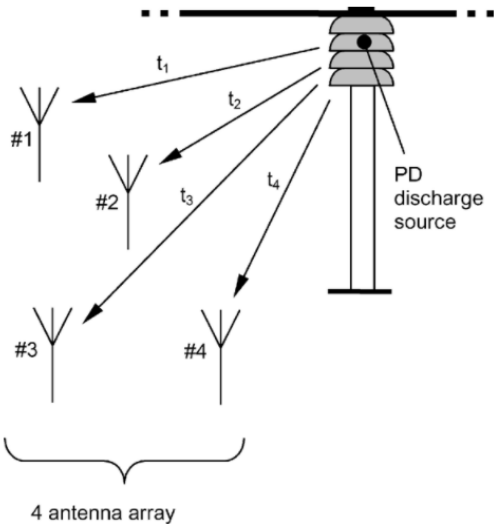

Figure 2.8. An antenna array for PD localization [79].

In the above antenna array, the arrival time difference is calculated by using two main steps. Firstly, from the digital record of each antenna signal, the time of arrival of direct wave is obtained by applying the threshold technique. Secondly, by using a cross co-relation technique, the difference of arrival of the wave is calculated in comparison with the direct wave. Similarly, the work carried out in [33] is based on a similar approach where four discone antennas are used with a frequency response from 10MHz to 1GHz which is the range of PD signal. Figure 2.9 below shows the overall system overview of the whole monitoring system.

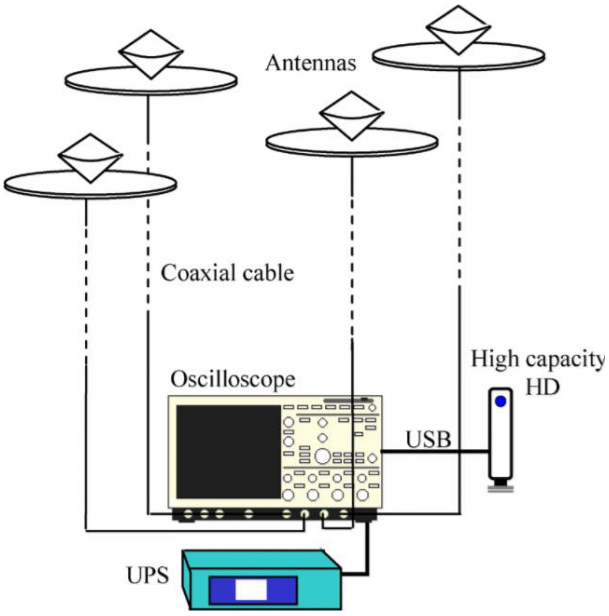

Figure 2.9. System overview of RF monitoring system for PD activity [33].

In both of the above radiometric systems, it can be understood that time synchronization is the key. Without time synchronization it will be impossible to estimate the true location of the source.

The work carried out in [87] is based on TOA calculation initially and then uses TOA to calculate the time difference of arrival (TDOA) between different signals received by different sensors. TOA in this approach is based on the time required by the signal to reach the maximum or the peak value. Figure 2.10 shows the approach used for the location of PD using UHF detection method [87].

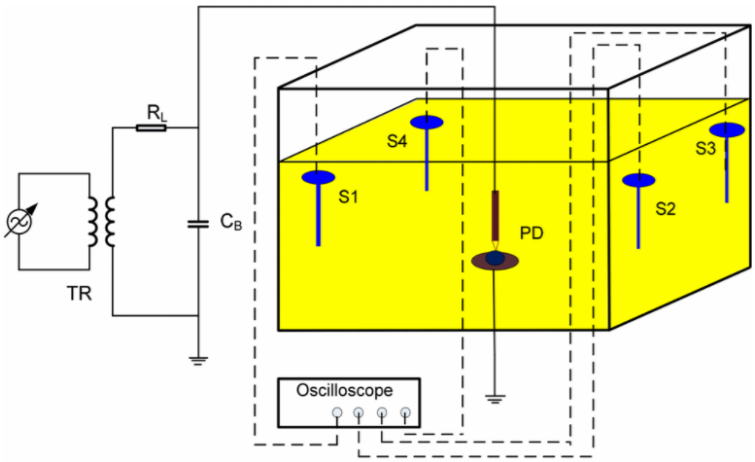

Figure 2.10. TDOA based source localization [87].

The approach is based on three-dimensional coordinate systems for source localization. The coordinate system for the above setup is depicted in Figure 2.11 below:

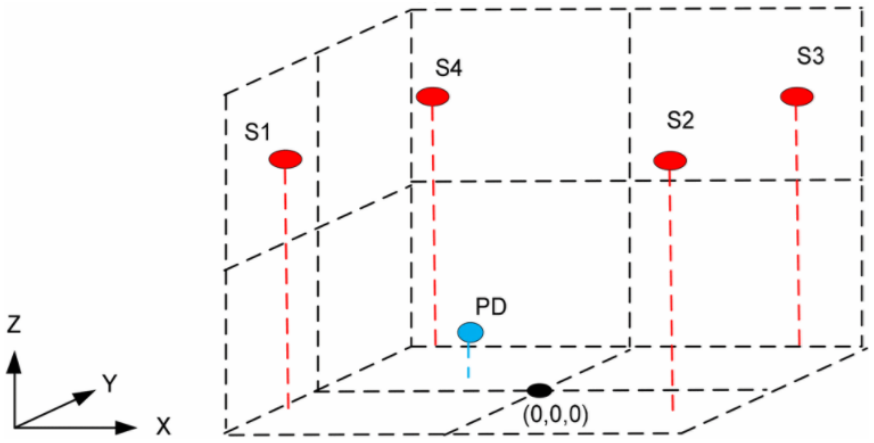

Figure 2.11. The coordinate system for source location [87].

All the above techniques are termed as lateration or distance based techniques. The next part is to discuss the angle based techniques that are again based on time synchronization.

2.5.2 Angulation technique

The angulation technique is mainly based on the angle of arrival of the wave. AOA location of the source is based on angulation rather than lateration and is also referred to as the angle of arrival of the signal emitted by the source at the receiving node [88]. The source location can be estimated by drawing the line of bearing from source to receiver, and at least two lines of bearing must intersect [31, 89]. Figure 2.12 next shows how the schemes work on a two-dimensional plane.

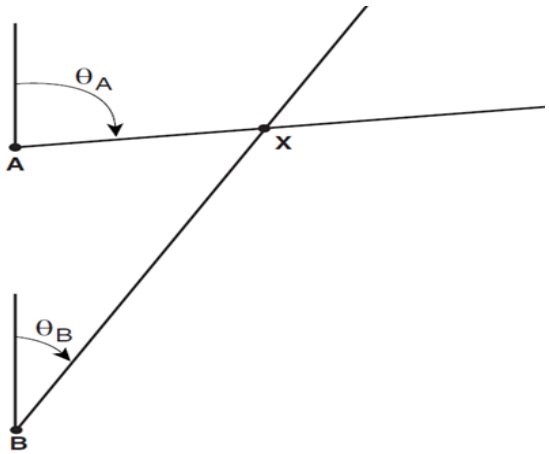

Figure 2.12. AOA scheme for localization [90].

The problem with this technique is that it works well only for situations where there is a direct line of sight. It is a technique susceptible to multipath interference. In the case of PD detection where the PD pulse phenomenon is random in nature, the DOA scheme may become barely usable in some cases.

2.6 The issues of time synchronisation based lateration and angulation techniques

Whether it is lateration or angulation technique, the key issue associated with them is that of time synchronizations. The receiver nodes must be time synchronized. This makes the system complex and brings complications when there is a need to perform modifications in the system in terms of software and hardware. For autonomous PD localization, the system should be cost-effective that can be deployed for continuous monitoring of PD signal. Both TOA and TDOA methods implemented for PD location are based on time-based measurements. In such algorithms, clock synchronization is essential for a location to be accurate [91, 92]. In TOA both transmission and receiver synchronizations are necessary. In TDOA only receiver synchronization is necessary. In both these schemes, a small inaccuracy can lead to bigger location errors. In AOA again the location accuracy is mainly dependent on the line of sight. Multipath interference may lead to inaccuracy and hence may sometimes hardly be applicable in practical applications. An overall summary of the potential techniques is summarised in Table 2.3 below:

Table 2.3 Comparison of PD detection techniques [33, 79, 86].

Technique used	Advantages	Disadvantages
TOA	• High accuracy • Performs well when accurately synchronisation is done between node pairs and the source.	• Time-based synchronization is required for all nodes and receivers. • The line of sight (LOS) is assumed in TOA based localization • Scalability is a challenge
TDOA	• Accuracy is high • Synchronization at the source is not required that makes it simpler than TOA	• The line of sight (LOS) is assumed in TOA based localization • Scalability can be a challenge as still receiving nodes synchronization is required.

DOA/AOA	• No synchronization required • Two receivers can perform the localization	• The line of sight (LOS) is assumed • Requirements of smart antenna can make is expensive. For example in such localization, antennae with smart signal processing are required, which do not provide a cost effective solution.
RSS	• Simple and cost-effective • No synchronization required • No challenges of synchronization	• Accuracy can be low due to the propagation environment and losses as this technique works on the received energy. The spatial distance between the receiving nodes is based on inverse square law. The distance can be reduced by placing more receiving nodes. The cost for each receiving node does not exceed $150. Addition of a single node can enhance the localization accuracy significantly.

To overcome the above issues, the author has elected to utilize the PD locations method based on received signal strength (RSS) only which is explained in the next chapter.

2.7 Chapter 2 summary

Chapter 2 focused on existing techniques that can be utilized when the location of an unknown source requires estimating. Key techniques that have been discussed in this chapter include TOA, TDOA, AOA and RSS. In harsh industrial environments such as localization of PD, the advantage of each technique and its limitations are summarised in table 2.3. It is concluded that that RSS based localization is worth investigating due to limitations the other techniques are

suffering from. This leads to an investigation of RSS based localization and a range of algorithms are discussed in chapter 3 next.

Chapter 3: RECEIVED SIGNAL STRENGTH (RSS) INTENSITY BASED LOCALIZATION AND ITS APPLICATION IN PD LOCALIZATION.

3.1 An overview of RSS based localization techniques

Like TOA and TDOA, the RSS technique is based on lateration or distance. Source localization based on RSS can be divided into two main categories. These include:

i. Physical localization of the source
ii. Symbolic localization of the source

In physical localization of the source, the coordinates of the source are obtained by using the measured signal from the measurement receivers [93]. In symbolic localization, the received signals are used to get to the vicinity of the source [94, 95]. In a physical localization, the physical location of the source is determined. The ideal result will be to determine the exact location of the source, however, in a real environment under harsh industrial conditions, a localization error of below 2 meters will be considered as plausible. For symbolic localization, the location of the source is considered to within a certain range [96, 97].

In the RSS based methods, however, there is no major synchronization between nodes required, and this, therefore, enhances the scalability. In all non-RSS schemes mentioned above, scalability remains the biggest constraint due to the synchronization requirement. However, on the other hand, scalability also improves accuracy. This means that although RSS eliminates the issues associated with its counterparts, it remains to be shown that it can serve as an alternative than TOA, TDOA and AOA.

In recent times, RSS based localization has attracted strong attention. The work of [82] is based on WiFi access point localization by using received signal strength (RSS). The approach employs a multi-lateration technique to locate a WiFi access point in an anonymous environment. Similarly, source localization, when path loss model parameters are unknown, has been applied by [96].

Some of the key algorithms that use RSS in the localization of a source are discussed next

3.1.1 Centroid algorithm

The centroid algorithm is one of the simplest algorithms that can be used for estimation of a source transmitting an electromagnetic signal. The centroid algorithm works similar to triangulation in the way that, the exact position is determined. The centroid is the estimated version of the triangulation because here the position is estimated rather than ideally located. The way the algorithm works is such that, sensors are placed over an entire grid. The received signal is converted into distance between the target source and the receivers. The distance between each sensor and the target will make a matrix of x and y coordinates [91]. The main emphasis of the centroid algorithm is based on calculating the area and finding x and y positions where the maximum area is concentrated. For the location of a source by using received signal strength (RSS), the target source location can be calculated by taking the mean of all x and all y values between the individual sensors to the source [98, 99].

The traditional centroid algorithm is based on triangulation measurements.

- In the triangulation approach, there are three receiving nodes used.
- For each receiver, there is a locus, and hence for three receivers, there will be three different loci.
- The point where three loci intersect is the location of the targeted source.

The triangulation approach can be understood by considering Figure 3.1 below:

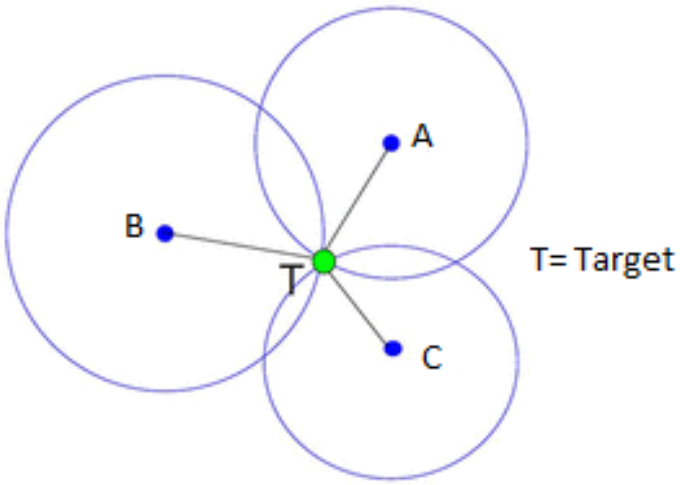

Figure 3.1. Triangulation mechanism.

In Figure 3.1 above, A, B and C are the three sensors nodes, and T is the unknown location of the source. The coordinates of the receivers are named as (x_A, y_A), (x_B, y_B), (x_C, y_C) respectively and the coordinates of the source are assigned as (x, y).

The distance of the individual receiving node from the unknown source is calculated as given in the equations below:

$$d_A = \sqrt{(x - x_A)^2 + (y - y_A)^2} \qquad \text{Equation 3.1}$$

$$d_B = \sqrt{(x - x_B)^2 + (y - y_B)^2} \qquad \text{Equation 3.2}$$

$$d_C = \sqrt{(x - x_C)^2 + (y - y_C)^2} \qquad \text{Equation 3.3}$$

When considering the practical propagation environment, the factors such as reflections, refractions and interferences will bring errors to the signals measurements and hence the above three circles will not intersect as shown in Figure 3.1.

To account for this effect, the equations for lines are determined by squaring the above three equations and then subtracting them respectively. The equations for three line are determined as below [100]:

$$d_A^2 = x^2 + x_A^2 - 2xx_A + y^2 + y_A^2 - 2yy_A \qquad \text{Equation 3.4}$$

$$d_B^2 = x^2 + x_B^2 - 2xx_B + y^2 + y_B^2 - 2yy_B \quad \text{Equation 3.5}$$

$$d_C^2 = x^2 + x_C^2 - 2xx_C + y^2 + y_C^2 - 2yy_C \quad \text{Equation 3.6}$$

To obtain the equation for the line, the equations are subtracted respectively as shown in the equations below. For line 1, the equation is below:

$$d_A^2 - d_B^2 = (x^2 + x_A^2 - 2xx_A + y^2 + y_A^2 - 2yy_A) - (x^2 + x_B^2 - 2xx_B + y^2 + y_B^2 - 2yy_B) \quad \text{Equation 3.7}$$

$$d_A^2 - d_B^2 - x_A^2 - y_A^2 + x_B^2 + y_B^2 = 2(x_B - x_A)x + 2(y_B - y_A)y \quad \text{Equation 3.8}$$

Similarly, the questions for line 2 and line 3 are obtained as well and the point where the three lines meet each other is the location of the source as shown in Figure 3.2 below.

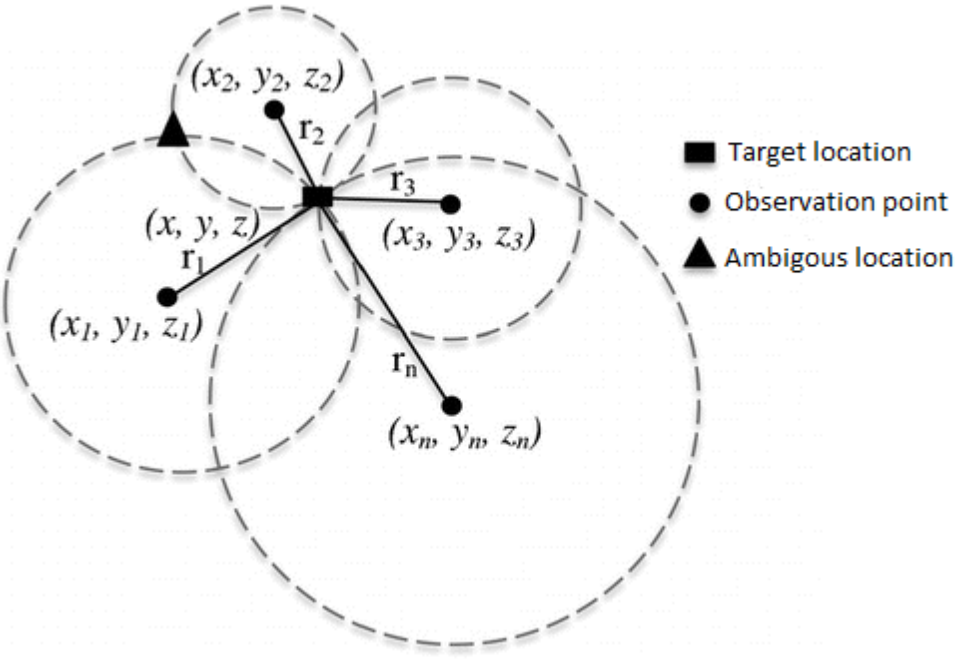

Figure 3.2. Consideration of practical situation for trilateration method.

In the figure 3.2 above, when all circle intersect at a single point, the target location is expressed as a rectangle. However, if multiple circles intersect each other at multiple positions, then

rectangle represents the ambiguous location because there are multiple locations that can be considered as the target location and it will be a challenge to decide the true location.

In the trilateration algorithm, if the lines above do not intersect each other, there will be no solution. For RSS based localization, the localization accuracy will increase with a decrease in distance measurement.

- In the centroid algorithm, the distance between the unknown nodes to the receiving nodes is ranked in ascending order.
- Four nodes with the minimum distance are selected and are termed as anchor nodes
- Each of the anchor nodes will use three nodes to estimate the location of the source.
- Other three anchors will repeat the same, and hence there will be four estimated locations by the four anchor nodes.
- The centroid point is the mean of the location coordinates as shown in the equation below:

$$x = \frac{(x_1 + x_2 + x_3 + x_4)}{4} \qquad \text{Equation 3.9}$$

$$y = \frac{(y_1 + y_2 + y_3 + y_4)}{4} \qquad \text{Equation 3.10}$$

Where x and y is the mean x and y coordinates obtained from four anchor nodes with minimum distance from the unknown source. The flowchart for the algorithm is given in Figure 3.3 below:

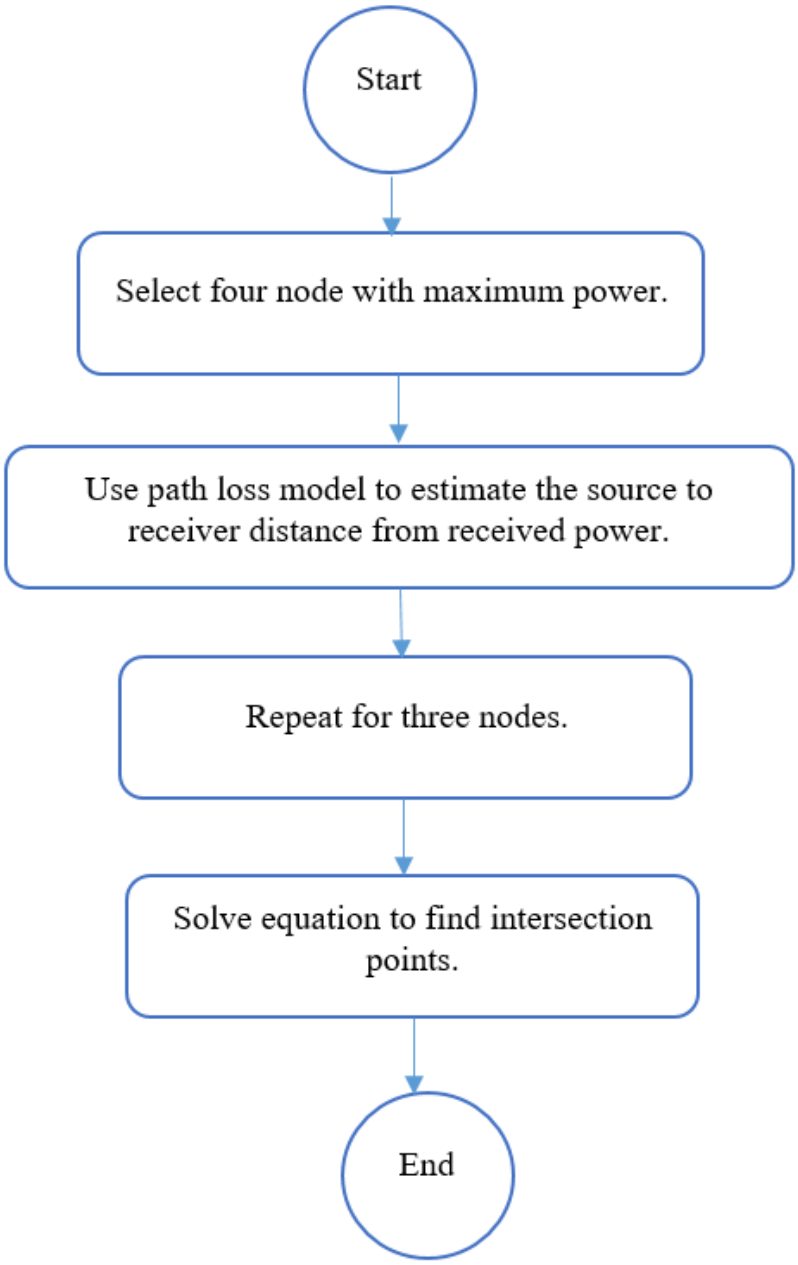

Figure 3.3. Flowchart for the centroid algorithm.

An overall summary of the centroid algorithm is described next.

3.1.1.1 Centroid algorithm summary

i. First, find the distance of the receiver from the unknown source by using the path loss model equation.
ii. Rank the distances in ascending order.
iii. Take the four receiving nodes that have the least distance.
iv. Estimate the coordinates by using trilateration.

v. There are four estimated coordinates of the unknown source because of four combinations.
vi. Find the mean x and mean y locations by using the four combinations.
vii. This will be the estimated location of the source by using the centroid algorithm as shown in equations 3.9 and 3.10.

The centroid algorithm as mentioned above is the simplest version and can be used in an improved form which is termed as weighted centroid form. The weighted centroid form of the centroid algorithm is explained next.

3.1.2 Weighted centroid algorithm

The weighted centroid algorithm is an improved version of the centroid algorithm. With the traditional centroid algorithm, the location accuracy is not very high. When estimating RSS based locations, the selection of the correct model is important [100, 101]. The weighted centroid algorithm improves the accuracy of the centroid algorithm by path loss smoothing or position estimation. The traditional centroid algorithm does not optimise the path loss exponent that is the environment dependent and can vary between pairs of nodes. This would mean that using the traditional centroid algorithm for a fixed value of path loss exponent may be useful, but the real environment is quite complex and of varying nature [99-101].

Equations 3.9 and 3.10 determine the source locations based on the centroid algorithm. The location accuracy is enhanced by improving the above (x, y) coordinates by using the weighted factor. To determine the weighting factor, the approach used by [100] is based on the reciprocal of the sum of the distances from the unknown source to the receiving nodes.

Assuming that there are four nodes involved in localization having coordinates (x_1, y_1), (x_2, y_2), (x_3, y_3) and (x_4, y_4) respectively. The distance of each node from the unknown source is termed as d_1, d_2, d_3 and d_4 respectively. At a single instant three of the four nodes are involved in the localization. By calling the coordinates of the unknown source as (x_s, y_s), the coordinates (x_s, y_s) can be estimated as below.

There will be four different locations estimated including location 1 based on nodes (1, 2, 3). The location 2 will be based on nodes (1, 2, and 4), location 3 will be based on nodes (1, 3, and 4) and location 4 will be based on nodes (2, 3, and 4). Finally, the coordinates (x_s, y_s) by using the weighted centroid algorithm can be calculated as shown in the equations below:

$$x_s = \frac{\left(\frac{x_1}{d_1 + d_2 + d_3} + \frac{x_2}{d_1 + d_3 + d_4} + \frac{x_3}{d_1 + d_2 + d_4} + \frac{x_4}{d_2 + d_3 + d_4}\right)}{\left(\frac{1}{d_1 + d_2 + d_3} + \frac{1}{d_1 + d_3 + d_4} + \frac{1}{d_1 + d_2 + d_4} + \frac{1}{d_2 + d_3 + d_4}\right)} \quad \text{Equation 3.11}$$

Similarly, the value of x_s will be calculated as given below:

$$y_s = \frac{\left(\frac{y_1}{d_1 + d_2 + d_3} + \frac{y_2}{d_1 + d_3 + d_4} + \frac{y_3}{d_1 + d_2 + d_4} + \frac{y_4}{d_2 + d_3 + d_4}\right)}{\left(\frac{1}{d_1 + d_2 + d_3} + \frac{1}{d_1 + d_3 + d_4} + \frac{1}{d_1 + d_2 + d_4} + \frac{1}{d_2 + d_3 + d_4}\right)} \quad \text{Equation 3.12}$$

Equations 3.11 and 3.12 represent the coordinates of the unknown source by using the weighted centroid algorithm [100]. For the weighted centroid algorithm, the flowchart is shown in Figure 3.4 next:

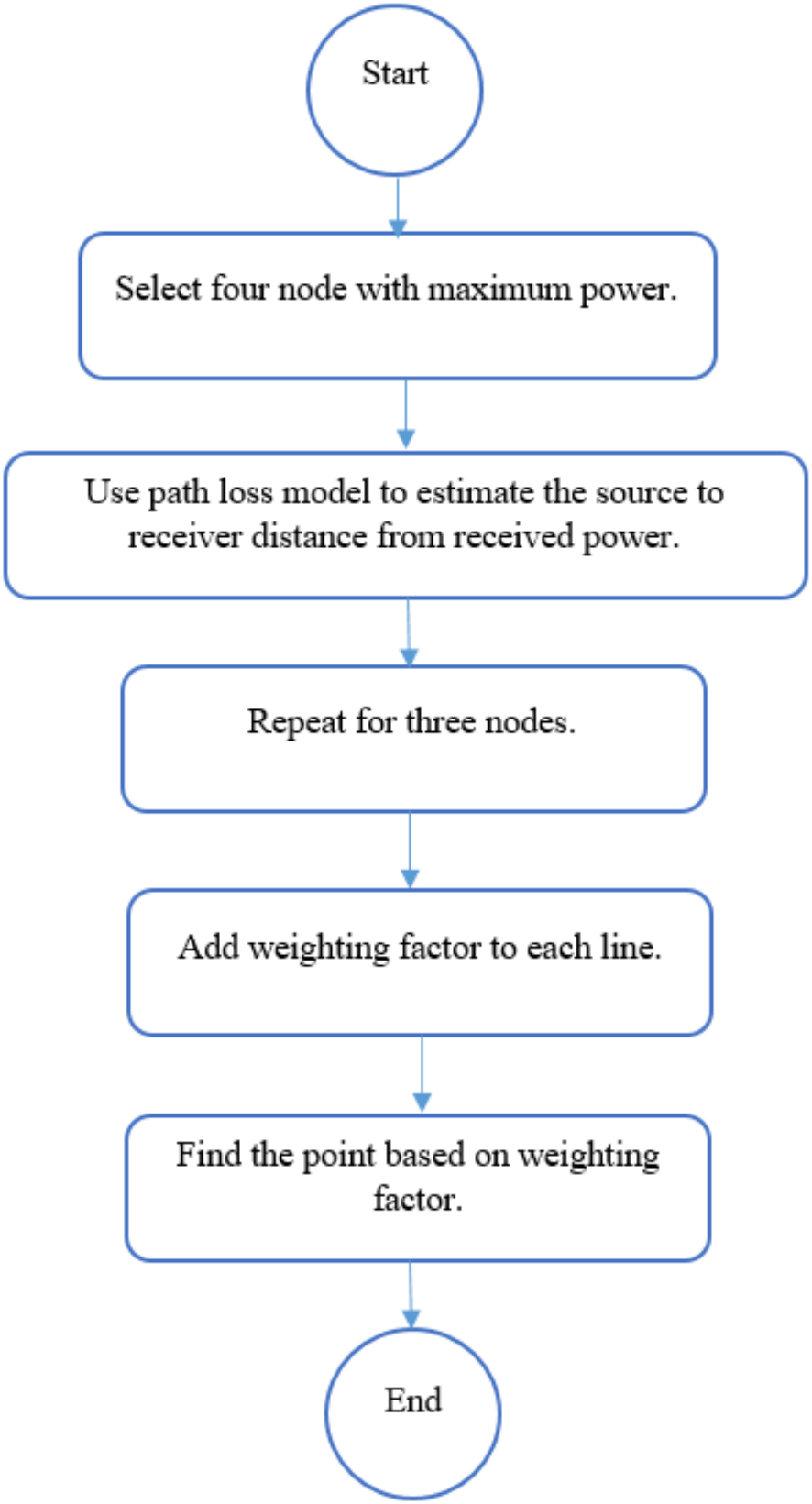

Figure 3.4. Weighted centroid algorithm flowchart.

Weighted centroid algorithm can be summarised in main steps below.

3.1.2.1 Summary of weighted centroid algorithm

i. This is an extension of the centroid algorithm. The algorithm improves the centroid algorithm by using the weighting factor.

ii. Calculate the weighting factor by dividing individual estimated locations $(x_1 - x_4)$, by the distances of the receiving nodes involved as shown below for x location of the unknown source as numerator part of equation 3.11:

$$\frac{x_1}{d_1 + d_2 + d_3} + \frac{x_2}{d_1 + d_3 + d_4} + \frac{x_3}{d_1 + d_2 + d_4} + \frac{x_4}{d_2 + d_3 + d_4}$$

iii. Estimate the source location by dividing (ii) by the sum of reciprocal of distances of each node involved in each estimated location from $(x_1 - x_4)$ as shown in equation 3.11.

The next part describes the least squares algorithm.

3.1.3 Least square algorithm

The least square algorithm is another algorithm that can be used to estimate the location of the transmitting source. When performing RSS based localization, the least square algorithm will best approximate the sum of squared differences between the sensors and the source.

Let the unknown coordinates of the source are denoted as (x, y) and the known coordinates of the receiving notes are denoted as (x_i, y_i) where $i = 1,2,3, \dots n$. The distance between the source and the ith receiving nodes can be expressed as d_i, which is given below:

$$d_i = \sqrt{(x_i - x)^2 + (y_i - y)^2} \qquad \text{Equation 3.13}$$

Where d_i is the distance of the ith receiver from the source, (x_i, y_i) are the coordinates of the ith receiver and (x, y) are the coordinates of the source. Linear least square is utilized in the majority of the approaches in addition to many other techniques especially when using the received signal strength based localization [89].

The least square algorithm utilizes the received signal strength (RSS) by converting the received signal into a distance by using the path loss model equation. If the source power transmitted is expressed as P_t and received power by an ith receiver is expressed as P_r, the average that is received by an individual receiver is expressed as:

$$P_{r,i} = \frac{K_i P_t}{d_i^{\alpha}}$$ Equation 3.14

In the above equation, K_i is the factor that accounts all the factors that affect the received power and α is the path loss exponent. The value of path loss exponent is constrained by the minimum and maximum limits and a typical value is 2 in a free space wireless environment. The disturbance to the RSS is log-normal distributed and the above equation can be converted into logarithmic form as below:

$$10\ log\left(P_{r,i}\right) = 10\ log(K_i) + 10\ log(P_t) - 10\alpha\ log(d_i) + \omega_i$$ Equation 3.15

ω_i is the normally distributed error signal in the received signal $10\ log\left(P_{r,i}\right)$ with zero mean and a known value of standard deviation.

The RSS can be converted into a linear model by first introducing the range variable as:

$$R = x^2 + y^2$$ Equation 3.16

By squaring equation (3.13), we get:

$$d_i^2 = (x_i - x)^2 + (y_i - y)^2$$ Equation 3.17

The equation then can be re-written as:

$$d_i^2 - (x_i)^2 - (y_i)^2 = -2x_i x - 2y_i y + R$$ Equation 3.18

Based on the number of receivers, the equations can be written in the matrix form as:

$$A\theta = b$$ Equation 3.19

Where each of the matrices is:

$$A = \begin{bmatrix} -2x_1 & -2y_1 & 1 \\ -2x_2 & -2y_2 & 1 \\ -2x_3 & -2y_3 & 1 \\ & . & \\ & . & \\ -2x_n & -2y_n & 1 \end{bmatrix}$$ Equation 3.20

$$\theta = \begin{bmatrix} x \\ y \\ R \end{bmatrix}$$ Equation 3.21

$$b = \begin{bmatrix} d_1^2 - x_1^2 - y_1^2 \\ d_2^2 - x_2^2 - y_2^2 \\ d_3^2 - x_3^2 - y_3^2 \\ \vdots \\ \vdots \\ d_n^2 - x_n^2 - y_n^2 \end{bmatrix}$$ Equation 3.22

The matrix A is known, θ is the unknown and b is the observation matrix. The least square estimator can be obtained as:

$$\theta = A^{-1}b$$ Equation 3.23

The least square algorithm requires that source transmitted power P_t is a known parameter. However, in real environment, it is an unknown parameter. In the localization of PD source, the source transmitted power is definitely unknown. An overall summary of least squares algorithm is described next.

3.1.3.1 Summary of least squares algorithm

i. The least squares algorithm is based on a multilateration technique.
ii. For each receiving node involved in the system a distance equation is obtained.
iii. A matrix is established in the form of:

$$A\theta = b$$

iv. The least squares approach is used to solve for unknowns by using a fixed value of PLE.
v. Chosen PLE has to be closer to the average value of the propagation environment to minimise the localization error.

Next part describes CRLB algorithm.

3.1.4 Cramer Rao lower bound (CRLB) algorithm

For an estimation problem, the variance of the best estimator is given by the Cramer Rao Lower Bound (CRLB). It is a method that provides the estimator that fits the best.

For the problems based on RSS, the received power contains the error that has zero mean and a known value of variance. The CRLB determines the minimum variance to bring sharpness to the probability density function (PDF) to maximize the location accuracy.

By using equation 3.24 below:

$$10\ log\left(P_{r,i}\right) = 10\ log(K_i) + 10\ log(P_t) - 10\alpha\ log(d_i) + \omega_i \quad \text{Equation 3.24}$$

Where ω_i is the error or noise signal with zero mean and standard deviation σ. For simplicity let's call:

$$10\ log\left(P_{r,i}\right) = x[n] \quad \text{Equation 3.25}$$

and

$$10\ log(K_i) + 10\ log(P_t) - 10\alpha\ log(d_i) = A \quad \text{Equation 3.26}$$

The above equation 3.24 can be rewritten as shown in equation 3.27:

$$x[n] = A + \omega_i \quad \text{Equation 3.27}$$

To simplify the problem further, the above equation (3.27) can be restricted to just a one receiving node and can be re-written as below:

$$x[1] = A + \omega_1 \quad \text{Equation 3.28}$$

The probability density function of the equation be expressed as:

$$p(x[1]; A) = \frac{1}{\sqrt{2\pi\sigma^2}} e^{\frac{1}{2\sigma^2}(x[1]-A)^2} \quad \text{Equation 3.29}$$

Once $x[1]$ is observed, some values of A are more likely than the others. This would mean the PDF of A and PDF of $x[0]$ will have the same form. For example if $x[1] = 2$, the PDF of A can be written as:

$$PDF\ of\ A = \frac{1}{\sqrt{2\pi\sigma^2}} e^{\frac{1}{2\sigma^2}(2-A)^2} \qquad \text{Equation 3.30}$$

This will mean that a sharp function, i.e., PDF with lower variance will provide more accurate results for estimation. CRLB in addition to least square estimation can provide more accurate results. However, it is difficult to implement in the anonymous environment [81].

3.1.4.1 Summary of CRLB algorithm

i. CRLB algorithm is again based on the path loss model equation.
ii. The algorithm uses probability density function (PDF) to maximize the location accuracy by determining the minimum variance of PDF.
iii. To estimate the source location, the algorithm utilises the least squares estimation.
iv. The algorithm is unfeasible for anonymous environments because there is a requirement to have prior information about the source power.

The next section describes the ratio and search algorithm.

3.1.5 Ratio and search algorithm

In its essence, ratio and search is one algorithm that is truly applicable for the anonymous environment, i.e., when both the source power transmitted and path loss exponent is unknown.

The ratio and search algorithm is based on a path loss model derived from the Friis equation. The algorithm uses the ratio approach to eliminate the source transmitted power unknown. To overcome the issue with the path loss exponent, the algorithm uses the constraint value initially and later optimises the path loss exponent.

The algorithm works in such a way that unknown coordinates of the source that are defined as (x, y). The coordinates of the receiving nodes are defined as (x_i, y_i). The minimum numbers of receiver nodes required for the algorithm to work are three. In the first step, the algorithm converts the power received by the ith node is converted into distance. If the received power by the ith node is R_i, the corresponding converted distance is defined as d_i. The equation modelling the received signal strength is given below as:

$$R_i = R_0 - 10\alpha log_{10}\left(\frac{d_i}{d_0}\right) + \mu \quad \text{Equation 3.31}$$

Where, R_i is the received signal by the ith receiver. R_0 is the source transmitted power constant. μ is the path loss exponent (PLE), $d_i$is the distance of the ith receiver, $d_0$is the distance of the reference receiver and σ is the shadowing loss.

In equation 2.31 above, the source transmitted power and path loss exponent are both unknown. To overcome the issue of source transmitted power, a reference power at a reference distance is used, and hence by taking one of the nodes as the reference node, the ratio approach has been used to eliminate the power [96, 102]. The algorithm uses the least square algorithm initially to calculate the distance between the source and the ith receiver as given in equation 3.32. The ratio approach to eliminate the source transmitted power is given in the equation below:

$$di = d_0\left(\text{antilog}\frac{R_0 - R_i}{10\alpha}\right) \quad \text{Equation 3.32}$$

The algorithm uses the linear least square matrix as given in equations 3.20 to 3.23.

The main challenge is the optimisation of the path loss exponent. To optimise the path loss exponent, the algorithm considers the matching of distance ratios as below:

$$\frac{d_i}{d_1} = \quad \left(\frac{p_i}{p_1}\right)^{\frac{1}{\alpha}} \quad \text{Equation 3.33}$$

When the above distance ratios match with the distance ratio obtained in equation 3.33, the value of the path loss exponent will be the optimum value and the location will be the optimum location. The good thing about the path loss exponent is that it remains within a minimum to maximum limit with the optimum value in an ideal environment being 2. If the path loss exponent is constrained between 1 and 6, the optimum value of path loss exponent will remain between 1 and six as shown below:

$$\alpha_{MIN} \leq \alpha_{OPT} \leq \alpha_{MAX} \quad \text{Equation 3.34}$$

The ratio and search algorithm is useful and is very close to the requirements considering that its implementation is based on an anonymous environment. The main issue that is associated with the ratio and search algorithm is that it results in higher localization errors. The other sort of limitation of the algorithm is that it does not account for variations in the path loss exponent for individual paths between sources to sensors. In a real environment, the source to the receiving node will have variations in the path loss exponent.

The flowchart for the ratio and search algorithm is given in figure 3.5 below:

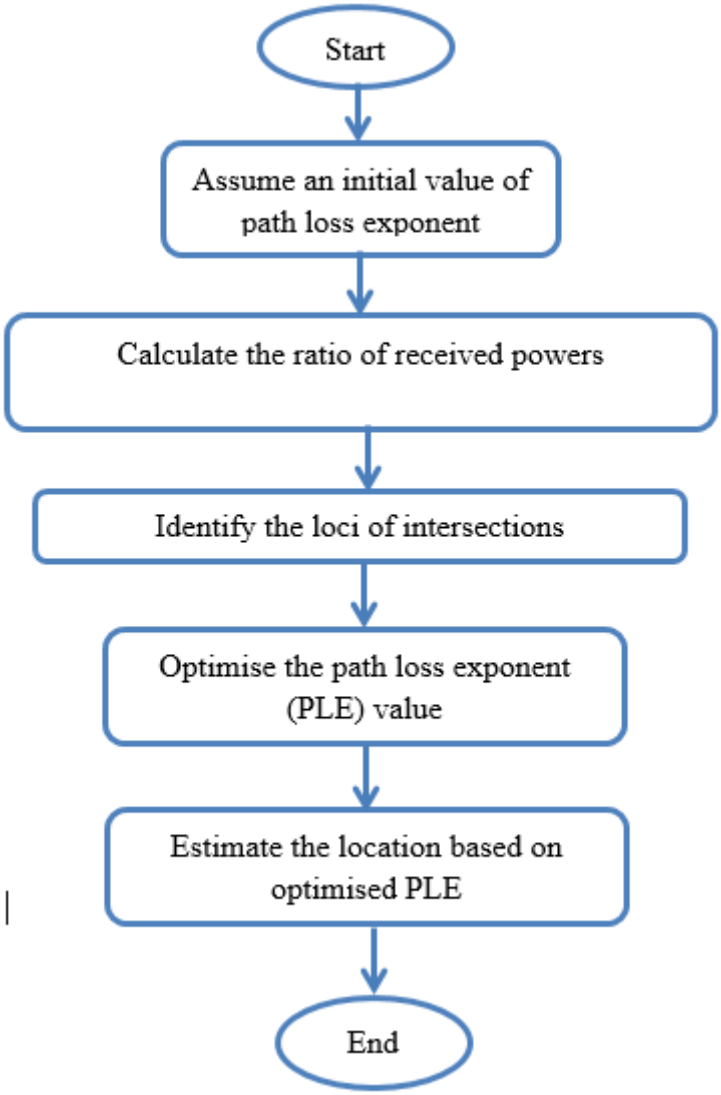

Figure 3.5. Ratio and search flowchart.

The algorithm will be used in the performance evaluation of a new proposed algorithm as this algorithm is a very good example of RSS based localization when path loss model parameters are unknown. A summary of the ration and search algorithm is described below.

3.1.5.1 Ratio and search algorithm summary

i. Ratio and search algorithm uses the path loss model equation.
ii. Path loss model equation is converted into the distance that determines the distance between the receiving node and the unknown source.
iii. The algorithm works in such a way that unknown source power is eliminated by using the ratio approach by choosing one of the receiving nodes as the reference node.
iv. There are as many equations as the number of receiving nodes.
v. Multilateration technique is used to estimate the location of the source.
vi. PLE is optimized by using the search approach within a given range as below:

$$1 \leq \alpha \leq 6$$

vii. Algorithm's accuracy is dependent on the number of receiving nodes used.

The next section describes the cognitive algorithm based on RSS.

3.1.6 A cognitive algorithm based on the received signal strength

The cognitive algorithm is another algorithm that uses the received signal strength for localization of a source that transmits an electromagnetic signal. The algorithm again is based on the statistical model and sees the propagation environment in two ways, i.e., homogeneous or non-homogeneous. For homogeneous environment, the algorithm sees all links share the same attenuation factor. For the non-homogeneous environment, every link has a different attenuation factor. The cognitive algorithm adopted by [103] consists of two main stages. At first, a hypothesis test is performed, which is based on the receiving nodes measurements that are arranged in a circular trajectory and measurements are taken in a clockwise direction. This will determine whether the propagation environment is homogeneous or non-homogeneous.

The second stage is based on the output of the first stage where, based on the received signals from various sensors, the maximum likelihood estimator algorithm is adopted. In conclusion, the cognitive algorithm proposed by [103] first identifies the nature of the propagation environment, i.e., homogeneous or non-homogeneous and then applies a maximum likelihood estimator algorithm.

3.2 A summary of the algorithms reviews

An overall summary of the algorithms reviewed so far is given in Table 3.1 below:

Table 3.1. A summary of algorithms reviewed based on RSS.

Algorithm	Advantages	Disadvantages

Centroid [81, 83, 96, 99, 103]	It is easy and simple to implement; an algorithm that can be used for detection of the PD source without much complexity	The simplicity of the algorithm costs localization accuracy. The algorithm is too simple and localization error is high.
Weighted centroid algorithm [81, 98, 100]	It is an extension of the centroid algorithm. It enhances the localization accuracy to an extent when compared with the centroid algorithm by assigning weighted factors based on distances	It needs more sensors nodes to enhance accuracy. Few sensors nodes will not contribute to significant localization accuracy. Hence it can become expensive regarding hardware deployment
Least square algorithm [89, 102]	It is the fundamental approach that is used when localizing the source using RSS. This approach is common and uses a least squares estimator	The algorithm does not optimise the PLE and only works on the given PLE value.
Cramer Rao Lower Bound algorithm (CRLB) [81, 96, 103]	It is more useful when an error in the received power is to be accounted for. The algorithm provides a sophisticated way to work with location estimation when using RSS to select the variance that will provide a more accurate location when there is noise in the received power	The algorithm is quite complex and is hard to implement in real situations.
Ratio and search algorithm [96, 102]	It is one of the sophisticated algorithms that is based on an anonymous environment,	The algorithm has a limitation in terms of localization accuracy. Also,

	i.e., prior knowledge of source transmitted power and path loss exponent is not required.	it requires a significant number of receiving nodes.

3.3 Chapter 3 summary

In chapter, a range of RSS based algorithms has been discussed. All algorithms do not require prior information about the path loss model. Centroid-based algorithms are too simple to be used for localization of PD source due to localization error being large. Least squares algorithms estimate the source at a given path loss exponent. However, they do not optimise the PLE. CRB may work better if source transmitted power is known, but that is not the case regarding PD localization. Ratio and search algorithm estimates the source as well as optimise the PLE. However, localization errors in real substation environment may end up being too large.

This leads to the development of a new algorithm to estimate the location of a PD source where the source transmitted power, and the PLE are unknown. Chapter 4 explains the algorithm and proof of principle by performing simulations in a noisy and noiseless environment.

Chapter 4: PARTIAL DISCHARGE LOCALIZATION ALGORITHM: THEORETICAL MODELING AND SIMULATIONS

This research aims to locate the partial discharge (PD) source by using received signal strength. The project methodology is a three-stage process. The overall project has split into three main phases which are:

a. Theoretical phase
b. Computational phase
c. Experimental phase

4.1 The theoretical modeling of the proposed algorithm

The algorithm is based on the path loss model equation 4.1. Assume that the source is located at the position (x, y) on a two-dimensional plane h;owever, the position (x, y) is unknown. The coordinates of the receiver that detect the signal emitted by the source are known because all receivers are placed at known locations around a substation and are named as (x_i, y_i). The proposed algorithm is based on the path loss model equation (4.1) below:

$$P_R = P_t - 10\alpha log\left(\frac{r_i}{r_1}\right) \qquad \text{Equation 4.1}$$

P_R is the measured signal strength by the receiving node in dBm, at a location (x_i, y_i). P_t is the transmitted power of the source at a reference distance and measured in dBm, α is the path loss exponent which again is unknown, however, it can be constrained. r_i and r_1 are the ith and the first node distances from the PD source in meters. The equation 4.1 can be derived as below:

The equation 4.1 is derived from the inverse square law as the received power at a distance d can be expressed as:

$$P_R = \frac{P_t G_t G_r \lambda^2}{4\pi^2 r^2} \qquad \text{Equation 4.1.1}$$

Where P_R is the received power at a distance r. P_t is the transmitted power, $G_t G_r$ are the gain of transmitter and receiver antennae, λ is the wavelength. The path loss is the ratio of transmitted to the received power and can be expressed as:

$$\frac{P_t}{P_R} = \frac{4\pi^2 r^2}{\lambda^2} \qquad \text{Equation 4.1.2}$$

The equation 4.1.2 assumes that both transmitter and receiver antennae gain are equation and unity i.e. omnidirectional. The equation can be converted into dB as below:

$$P_R = 10log(P_t) - 10\alpha log\left(\frac{r_i}{r_1}\right) \qquad \text{Equation 4.1.3}$$

Equation 4.1 describes the most commonly used propagation model based on the use of received signal strength (RSS). A major issue associated with a given environment is that path loss index (α) and source power are unknown and different for each source–sensor path in a substation environment. This makes it impossible to solve the equations since there are two unknowns and one equation. It is obvious that the source transmitted power $P_t$is unknown, but also the path loss exponent (PLE) is environment dependent and is different for each source–sensor path in a substation environment. The good thing about PLE is that it is constrained i.e., $1 \leq \alpha \leq 6$. The constrained nature of PLE makes it possible to solve the system of equations and estimate the location of the source.

Firstly, to overcome the source transmitted power issue, the source transmitted power is eliminated by using a ratio of distance approach. In the ratio of distance approach, one of the nodes in the receiving system is chosen as a reference node. The distance of all other receivers in the receiving systems is divided by the distance from the reference node. In this way, the uncertainty of the source transmitted power is eliminated. Each node in the receiving system is used as the reference node in turn, and a mean estimated location is estimated from all estimated locations for an initially chosen value of path loss exponent.

4.1.1 Key points of the algorithm

For known path-loss index (α), the ratio of received power at two nodes yields the ratio of the distance from these nodes and thus a locus on which the PD source must lie. Multiple node pairs yield the intersecting loci and thus the PD source location. The whole algorithm is summarised in the following steps:

- Assume a universal value of path loss exponent (α) from the given range $1 \leq \alpha \leq 6$.
- Select a reference node and use ratios of powers received by a pair of sensors to calculate an estimated PD location.
- Repeat for all other nodes set as reference nodes one by one.
- Calculate the mean spatial location from all the above-estimated locations.
- Calculate the RMS error of the spatial location distance from the mean location.
- Repeat for multiple values of α and select the final estimated location that has a minimum RMS error

A complete flowchart for the proposed algorithm is shown in Figure 4.1 next:

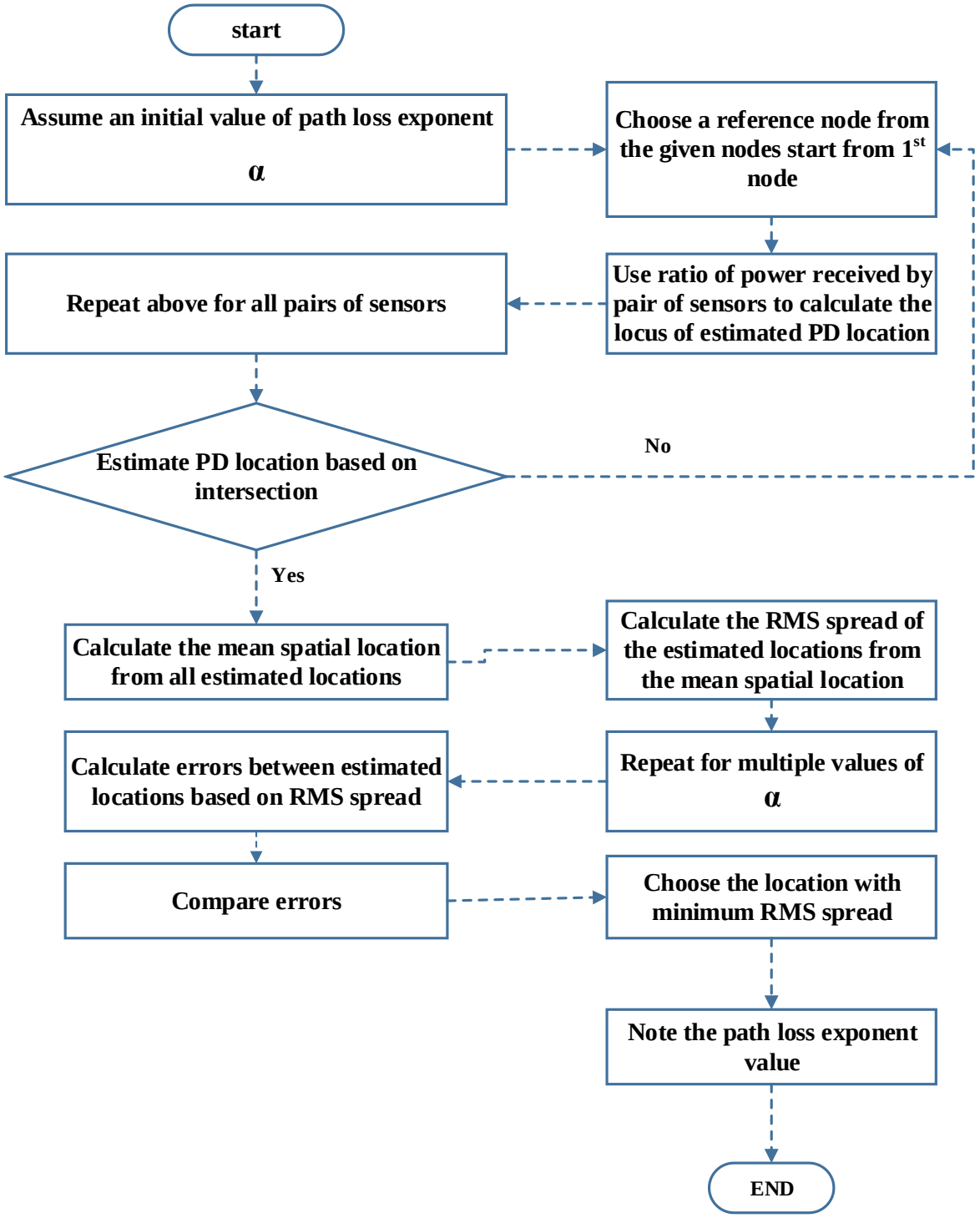

Figure 4.1 Algorithm flow chart.

To implement the above steps in the algorithm, the solution steps are described next.

4.2 The theoretical model of the algorithm.

The path loss model equation shown as 4.1 has been solved to develop the model. One of the nodes in the receiving system has been used as a reference and hence, starting from the first node as the reference node. This implies that r_1 represents the reference node distance from the

PD source. The distance between two sensors is estimated from measured values of the received signal. This implies that there will be as many distance values as the number of receiving sensors used in the receiving system. The source localization is performed by using the multilateration technique.

The RMS distance between the source and an ith receiver can be modelled by using the equation below:

$$d_i^2 = (x_i - x)^2 + (y_i - y)^2 \qquad \text{Equation 4.2}$$

When expanded, the equation (4.2) can be re-written as:

$$d_i^2 = x_i^2 + x^2 - 2x_i\ x + y_i^2 + y^2 - 2y_i\ y \qquad \text{Equation 4.3}$$

Equation (4.1) is converted into distance by re-arranging it in the form of distance as given in equation (4.4).

$$r_i = r_1\left(10^{\frac{P_t - P_R}{10\alpha}}\right) \qquad \text{Equation 4.4}$$

Then, equation (4.4) can be simplified by using equations (4.5) and (4.6) below:

$$p_i = 10^{\frac{P_R}{10}} \qquad \text{Equation 4.5}$$

$$p_1 = 10^{\frac{P_t}{10}} \qquad \text{Equation 4.6}$$

Equation (4.4) using equations (4.5) and (4.6) is compared with equation (4.2) as shown in equation (4.7) below:

$$(x_i - x)^2 + (y_i - y)^2 = \left(r_1 \left(\frac{p_i}{p_1} \right)^{\frac{1}{\alpha}} \right)^2 \quad \text{Equation 4.7}$$

The distance ratio of the reference node to the ith node is given in equation (4.8) below:

$$\frac{r_1^2}{(x_i - x)^2 + (y_i - y)^2} = \left(\frac{p_i}{p_1} \right)^{\frac{2}{\alpha}} \quad \text{Equation 4.8}$$

The reference node chosen initially is node 1. The distance r_1 of the reference node from the PD source is given in equation (4.9) below:

$$r_1 = \sqrt{(x_1 - x)^2 + (y_1 - y)^2} \quad \text{Equation 4.9}$$

Equation (4.8) in the ratio form is given in equation (4.10):

$$\frac{(x_1 - x)^2 + (y_1 - y)^2}{(x_i - x)^2 + (y_i - y)^2} = \left(\frac{p_i}{p_1} \right)^{\frac{2}{\alpha}} \quad \text{Equation 4.10}$$

By cross multiplying equation (4.10), expanding the square and by rearranging all terms in the form of x, y and z, where $z = x^2 + y^2$ is an extra variable, a system of matrices in the form of $AX = b$ is obtained with the co-efficients given in equation (4.11) below:

$$\left(p_1^{\frac{2}{n}} - p_i^{\frac{2}{n}} \right) z + 2 \left(p_i^{\frac{2}{n}} x_i - p_1^{\frac{2}{n}} x_1 \right) x + 2 \left(p_i^{\frac{2}{n}} y_i - p_1^{\frac{2}{n}} y_1 \right) y = p_i^{\frac{2}{n}} z_i - p_1^{\frac{2}{n}} z_1 \quad \text{Equation 4.11}$$

The coefficients of x, y and z for $i = 2$ are given from equations 4.12 to 4.14 respectively.

$$x = 2p_2^{\frac{2}{\alpha}}x_2 - 2p_1^{\frac{2}{\alpha}}x_1$$ Equation 4.12

$$y = 2p_2^{\frac{2}{\alpha}}y_2 - 2p_1^{\frac{2}{\alpha}}y_1$$ Equation 4.13

$$z = p_1^{\frac{2}{\alpha}} - p_2^{\frac{2}{\alpha}}$$ Equation 4.14

Similarly, the coefficients of x, y and z for $i = 3$ are given from equations 4.15 to 4.17 respectively.

$$x = 2p_3^{\frac{2}{\alpha}}x_2 - 2p_1^{\frac{2}{\alpha}}x_1$$ Equation 4.15

$$y = 2p_3^{\frac{2}{\alpha}}y_2 - 2p_1^{\frac{2}{\alpha}}y_1$$ Equation 4.16

$$z = p_1^{\frac{2}{\alpha}} - p_3^{\frac{2}{\alpha}}$$ Equation 4.17

Considering that the receiving system may be comprised of m number of receivers, where $m \geq 3$. The coefficients of x, y and z for $i = m$ are given from equations 4.18 to 4.20 respectively.

$$x = 2p_m^{\frac{2}{\alpha}}x_2 - 2p_1^{\frac{2}{\alpha}}x_1$$ Equation 4.18

$$y = 2p_m^{\frac{2}{\alpha}}y_2 - 2p_1^{\frac{2}{\alpha}}y_1$$ Equation 4.19

$$z = p_1^{\frac{2}{\alpha}} - p_m^{\frac{2}{\alpha}}$$ Equation 4.20

As mentioned above, if there are m receivers used to receive the signal, the matrix representation of the whole system is shown respectively, in equations (4.21), (4.22) and (4.23).

$$A = \begin{bmatrix} 2p_2^{\frac{2}{\alpha}}x_2 - 2p_1^{\frac{2}{\alpha}}x_1 & 2p_2^{\frac{2}{\alpha}}y_2 - 2p_1^{\frac{2}{\alpha}}y_1 & p_1^{\frac{2}{\alpha}} - p_2^{\frac{2}{\alpha}} \\ 2p_3^{\frac{2}{\alpha}}x_3 - 2p_1^{\frac{2}{\alpha}}x_1 & 2p_3^{\frac{2}{\alpha}}y_3 - 2p_1^{\frac{2}{\alpha}}y_1 & p_1^{\frac{2}{\alpha}} - p_3^{\frac{2}{\alpha}} \\ \vdots & \vdots & \vdots \\ 2p_m^{\frac{2}{\alpha}}x_m - 2p_1^{\frac{2}{\alpha}}x_1 & 2p_m^{\frac{2}{\alpha}}y_m - 2p_1^{\frac{2}{\alpha}}y_1 & p_1^{\frac{2}{\alpha}} - p_m^{\frac{2}{\alpha}} \end{bmatrix}$$ Equation 4.21

$$X = \begin{bmatrix} x \\ y \\ z \end{bmatrix}$$ Equation 4.22

$$b = \begin{bmatrix} p_2^{\frac{2}{\alpha}} - p_1^{\frac{2}{\alpha}} \\ p_3^{\frac{2}{\alpha}} - p_1^{\frac{2}{\alpha}} \\ \vdots \\ p_m^{\frac{2}{\alpha}} - p_1^{\frac{2}{\alpha}} \end{bmatrix}$$ Equation 4.23

The algorithm requires at least four nodes and one of the nodes will be used as the reference node. To enhance accuracy, the number of receiving nodes can increase to as many as fulfill the accuracy requirements. Increasing the number of nodes is better for two main reasons i.e. the source localization estimation will improve and the path loss exponent will be optimised better and will get closer to the average value of the propagation environment.

The above system of equations represented in matrix form is $AX = b$.

The system of equations shown in the above matrix form is overdetermined i.e. the number of unknowns is smaller than the number of equations. To solve the above system, the linear least squares approach has been used, based on equation (4.24), [89].

$$X = (A^T A)^{-1} A^T b$$ Equation 4.24

The above expression cannot be solved yet. Although the source transmitted power is eliminated by taking the ratio of distances, however, the path loss exponent (α) is still unknown. A positive aspect about the path loss exponent is that it is constrained i.e., it has a practical minimum and maximum. Theoretically and experimentally, it has been proven that for an ideal free space propagation, α is approximately 2. However, considering the factors such as multipath propagation and shadowing, it ranges from $1 \leq \alpha \leq 6$ [104, 105]. For this

reason, the initially chosen value of PLE is 2 because the measurements are performed in an approximately free space environment. The process is then repeated for multiple values of PLE by taking a reasonable step size, e.g., 0.01 keeping in view the runtime. A measure of the spread between the mean spatial location and the estimated location is calculated by using equation (4.25) below:

$$d_{RMS} = \sqrt{\frac{1}{N}\sum_{n=1}^{N} d_n^2} \qquad \text{Equation 4.25}$$

Where, d_n is the spatial location distance from the mean estimated location in meters, and d_{RMS} is the RMS spread of the spatial location distance in meters. The location that will have the minimum value of RMS spread will be the estimated location of the source, and the value of the path loss exponent will be an optimised value closest to an average PLE of the environment. Figure 4.2 below summarised the process.

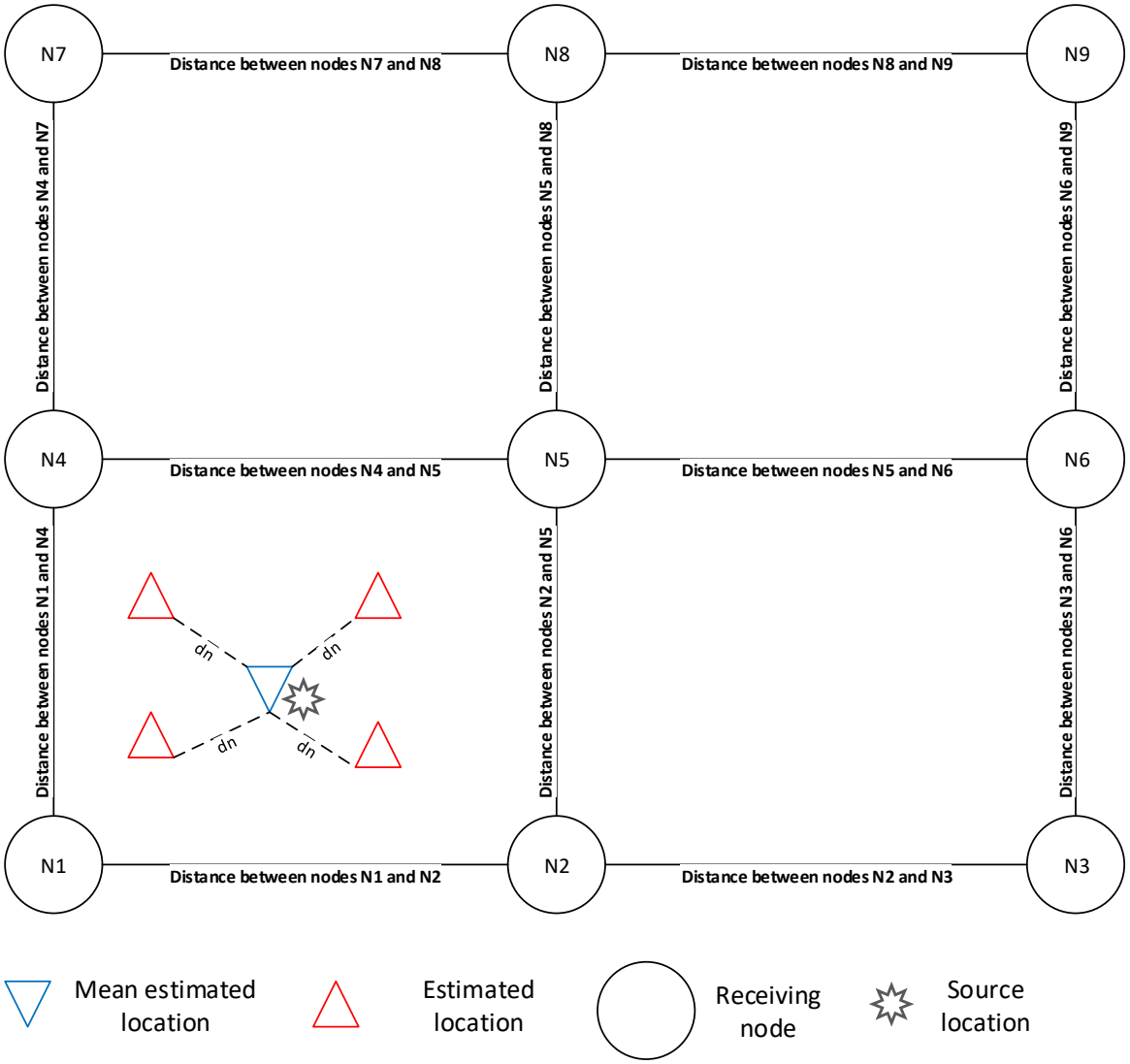

Figure 4.2. Loci intersection

Figure 4.2 above shows the multiple estimated locations in the form of a red triangle. From these multiple locations, the mean estimated location is calculated. The distance between each estimated location and mean estimated location is termed as d_n. d_{RMS} is calculated by using the equation 4.25 above once d_n is calculated.

To prove the principle, the simulations were performed. The algorithm simulations are explained next.

4.3 Simulation results

Simulations were performed in a noiseless and noisy environment. For a noiseless environment, the reason to perform the simulations were to check if the algorithm works correctly. This will be proved by the fact that without noise, there should not be any localization error.

4.3.1 Noiseless simulations

The location estimation was performed via simulations in MATLAB. The algorithm requires a minimum of four sensor nodes in order to converge. Simulations were performed including noise in a $20m \times 20m$ grid. The noise modelling was performed by using specified values of the noise figure and RF reception bandwidth. Simulations were performed for a source power of -30dBm and noise figure values of 2dB and 3dB and bandwidths of 10MHz and 100MHz, respectively. The chosen values of noise figure are based on the realistic requirements of the system considering the sensitivity of the receiver.

This was tested and is shown in Figure 4.2 below.

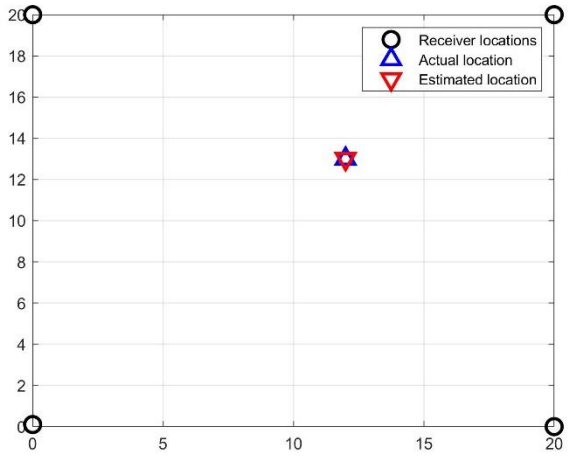

Figure 4.3. Simulation without noise.

The actual location of the source is (12,13), whereas, the estimated location is the same as the actual location. This proves that the algorithm works correctly as expected under ideal conditions. The algorithm was tested over the entire range with the source position to be placed at every 1m distance with the number of receiving sensors remaining the same.

The Figure below shows there is no error over the entire grid. The receivers were also placed irregularly to ensure that geometry of the receivers will not have any impact on the location accuracy. This was tested as shown in Figure 4.3 below:

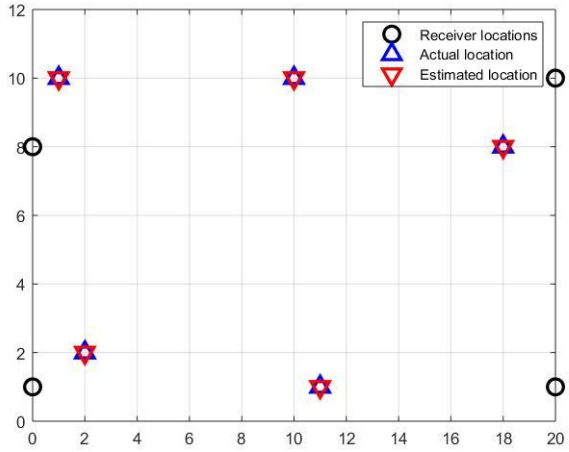

Figure 4.4. Simulation without noise at various locations.

4.3.2 Simulations by addition of noise in received power

The noisy signals were created by adding to the received signal random values generated by a Gaussian distribution with zero mean and the variance calculated as shown in the equation (4.26) below:

$$N = KT_{EQ}B = \sigma^2 \qquad \text{Equation 4.26}$$

Where T_{EQ} the equivalent temperature in K, and B is the bandwidth of the system in Hz. The numbers of sensors used are initially four. A simulation with an RF bandwidth of 10 MHz with

a noise figure of 2dB was carried out, and the results are shown in Figure 4.4. This Figure shows that there is an estimation error of around 1.19 meters.

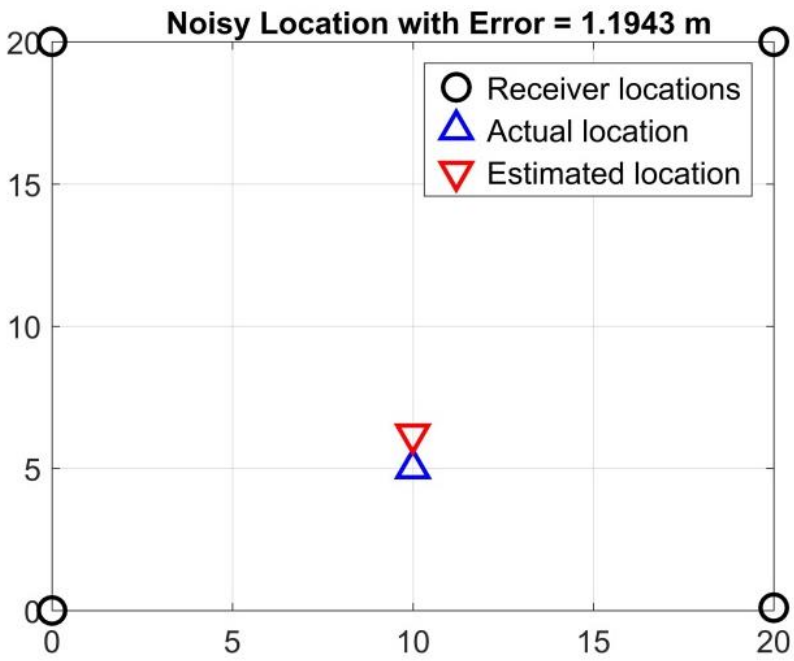

Figure 4.5. Simulation with Noise Figure =2dB and RF bandwidth of 10 MHz.

Figure 4.5 shows the results with a noise figure of 3dB and an RF bandwidth of 100 MHz This Figure shows that there is a much larger estimation error of around 2.25 meters, as expected. These results demonstrate the required specifications for the RF front-end of the system.

Regarding noise calculations, random noise signals with zero mean and a fixed value of standard deviation were generated. Dealing with random numbers was considered by running the program 100 times and taking the mean of the 100 estimated values. This means that there were 100 independent runs of the program and the final location was the mean 100 independent locations.

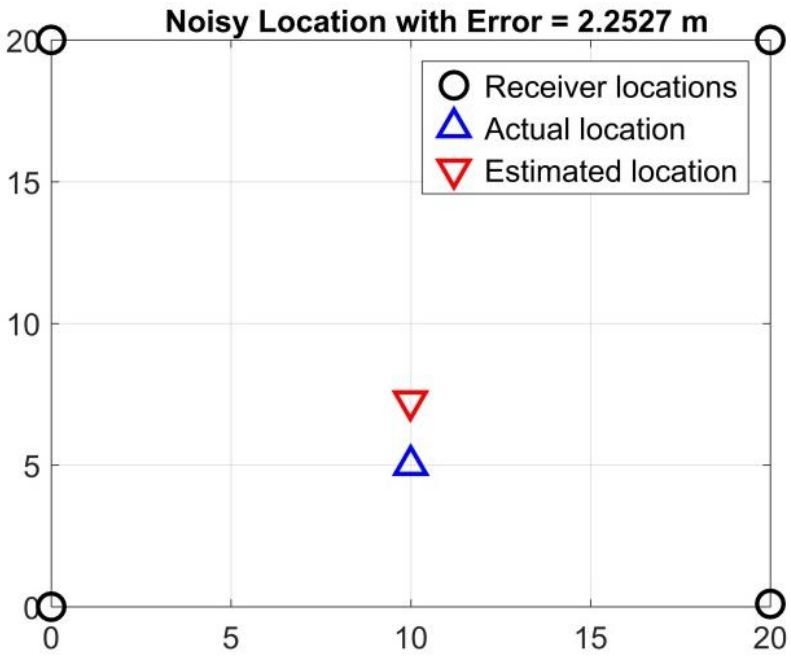

Figure 4.6. Simulation with Noise Figure = 3dB and RF bandwidth of 100MHz.

It can be summarised that RF bandwidth of 10 MHz and 100 MHz with noise figure of 2dB and 3dB respectively has produced licalization error of 1.19 meters and 2.25 meters respectively.

Simulations were also performed for ratio and search algorithm for exactly the same conditions in terms of bandwith and noise figure. The results are shown in Figures 4.7 and 4.8 respectively.

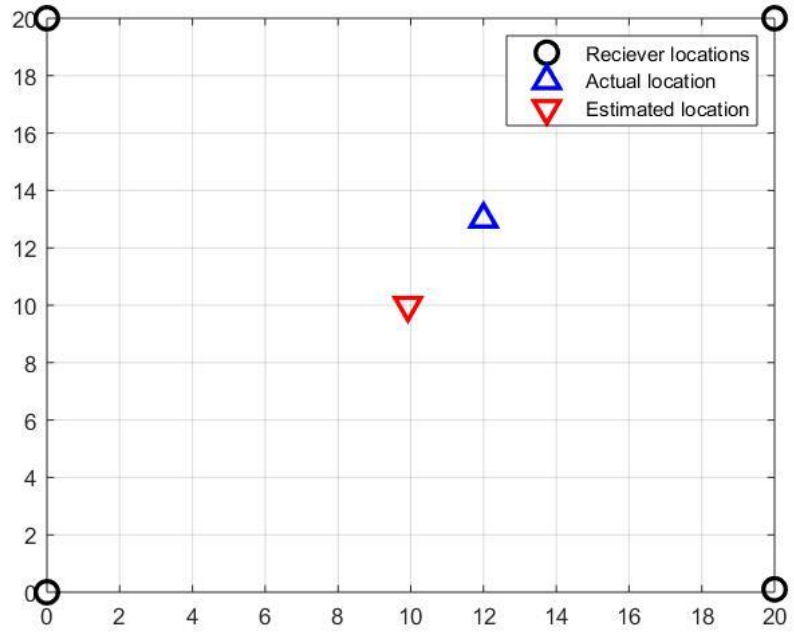

Figure 4.7. Ratio and search simulations for noisy conditions.

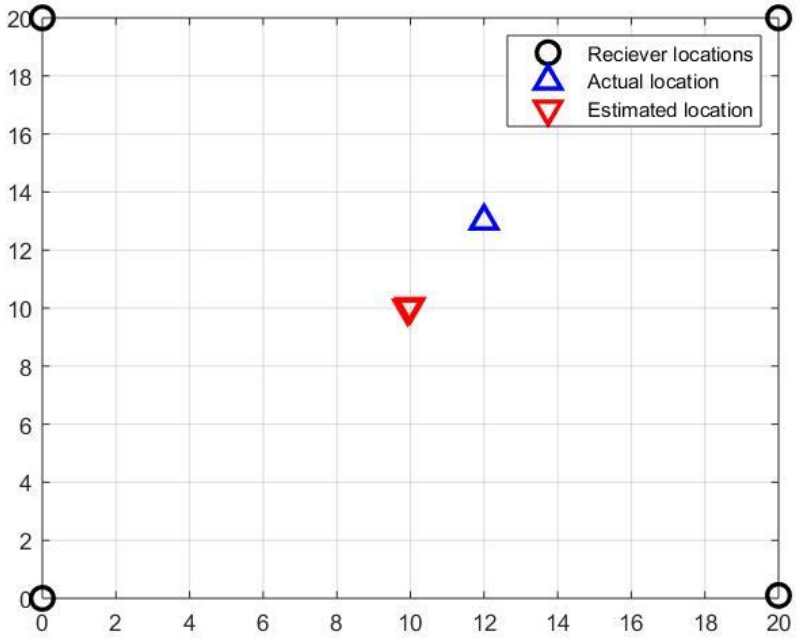

Figure 4.8. ratio and search simulations for lower noise figure.

4.4 Chapter 4 summary

The above results obtained from the noiseless and noisy conditions demonstrate that the localization algorithm works properly and the principle is proved as expected. Under an anonymous environment, the algorithm shows satisfactory results based on simulations. The

performance of the algorithm was tested with typical values of system noise figure and RF bandwidth.

To assess the performance of the algorithm, real measurements were required. An empirical study was performed by using field trials that were performed based on indoor and outdoor measurements that were obtained by using a radiometric wireless sensor system. The description of the radiometric wireless sensors system is provided in Chapter 5.

Chapter 5: DESCRIPTION OF THE RADIOMETER SENSOR AND SUPERVISORY SYSTEM

For the measurement of PD signal, an RF sensor was designed and implemented by [106] in the electronics lab. To locate a PD source, there was the requirement of a comprehensive supervisory system that could detect the signal which could be used for localization purposes. The supervisory system used is based on broadband PD radiometer sensors described in [107].

5.1 System overview

The complete system is based on three major components, which include:

i. A PD radiometer sensor
ii. A wirelessHART unit for communication
iii. A PD supervisory application

To detect a PD activity, there was an array of radiometric sensors deployed in an HV compound. Continuous collection of data and recording was made possible by using wirelessHART transceivers. The data from the supervisory application was utilized by the location algorithm to locate the PD source.

5.1.1 An overview of the PD radiometric sensor

Figures 5.1 and 5.2 show the RF measurement sensor and supervisory part, respectively.

Figure 5.1 is the radiometer sensor, and Figure 5.2 is the supervisory system. Sensor nodes used for measurement consisted of four major sub-systems, including the RF front end, signal conditioning, microcontroller unit, and the wirelessHART unit. Each unit consists of further sub-units. Such sensors are simple and cost-effective and can be deployed for continuous monitoring of PD.

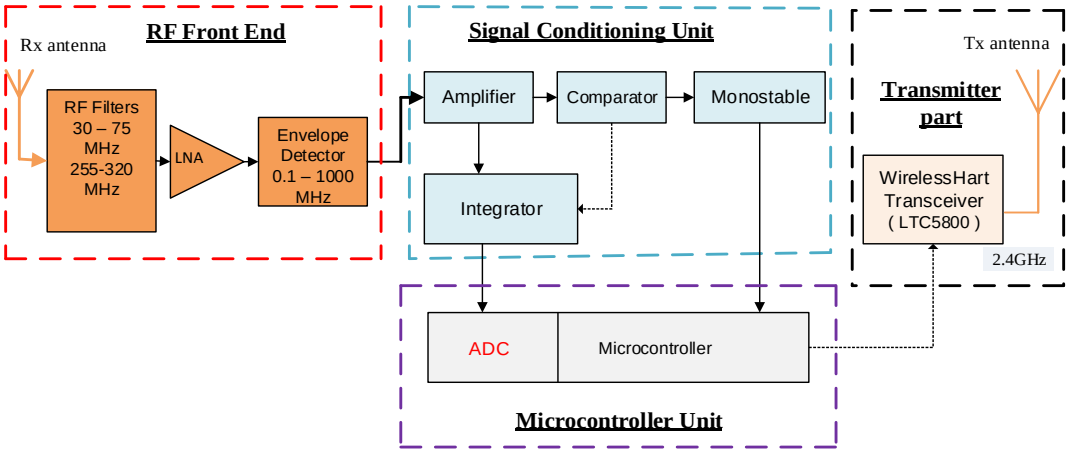

Figure 5.1. Block diagram of a PD signal measurement radiometer sensor system [107, 108].

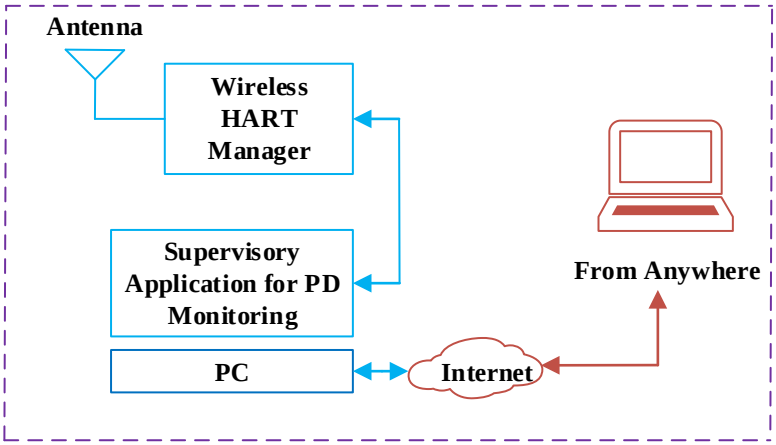

Figure 5.2. Overview of the supervisory system.

The explanation about each part of the sensor system is given next.

5.1.1.1 RF front end

The RF front end consists of four components which include:

- Receiving dipole antenna
- RF filters
- Low noise amplifier (LNA)
- RF peak envelope detector

A dipole receiving antenna is used to receive the PD signal that is emitted from the dielectric material under stress. The dipole antenna has a vertical polarization with a frequency range from 20MHz to 1GHz and an omnidirectional response. For the required passbands, the

performance of the dipole antenna used was compared with bi-conical antenna and results obtained were strong enough to conclude that bi-conical antenna was useful cost effective method to receive the PD signal for the given frequency range. Once received by the antenna, the signal is then passed to the RF filters. The experimental study suggests that PD signal bandwidth remains between 50-800 MHz, the used passbands have a frequency range from 30 to 75 MHz and 255 to 320 MHz [109-111]. To remove unwanted signals that could be present in the monitored signal from various sources such as TV, FM, digital radio and private radio, RF filters have been used at these two bands as shown in the RF front end part of Figure 5.1.

The function of the LNA is to increase the sensitivity of the sensor by providing a fixed gain value of 16.5 dB. The use of RF filters and LNA enables the RF front end part of the system to generate a passband frequency response in the range of 30 to 75 MHz and 255 to 320 MHz with the noise figure value from 5-7dB and passband gain value of 12-14 dB. By doing this, a 20-meter detection range is obtained from the PD source which is far above the minimum set requirement of 10 meters. The reason to set the minimum 10-meter range is to make the system cost effective and practically usable for continuous PD monitoring and localization. The function of the envelope detector is to reduce the signal bandwidth by removing the RF component and leaving the envelope only.

5.1.1.2 Signal conditioning unit

The output from the envelope detector is fed to the signal-conditioning unit where further amplification is performed via an amplifier, in addition to counting the PD events received. Within the signal-conditioning unit, the envelope-detected signal is integrated as well. The output from the signal conditioning unit is a collected PD activity in the form of a metric. The threshold value is set to 3V. When the output of the integrator reaches the threshold value, the integrator is set to zero [112]. The function of the comparator is to activate the integrator, provided that the PD signal is of the sufficient amplitude. This is vital to ensure that integrator's output voltage is not a result of envelope detected noise signals. Another function of the comparator is to count the number of PD events received. The integrator will stop integrating once the signal strength drops below the threshold. At this point, the output of the integrator is kept at a constant level. The signal then is passed to the microcontroller unit.

5.1.1.3 Microcontroller unit

From the signal conditioning unit, two parameters are received by the microcontroller unit which includes:

- The step size of the integrator
- Received PD pulses count

The function of the microcontroller within this entire system is to provide the interface between the sensor and the wirelessHART unit. The microcontroller used is PIC24EP512GP810 from Microchip. The microcontroller has a random access memory (RAM) of 52KB, program memory of 512 KB and speed of 70 million instructions per second (MIPS). The microcontroller unit offers analogue to digital conversion (ADC) that is configurable as 10 bits with 1.1 mega samples per second (MSa/s). There are four simultaneous channels provided that ensure that sampling of the PD pulses is performed adequately.

The second important function of the microcontroller unit is to establish and maintain the wireless connection via the wirelessHART unit. The microcontroller is brought to the sleep mode if there is no data collection to save energy. When the signal is received via a supervisory application, the microcontroller unit wakes up from the sleep mode. The data is collected and it is transferred to the system. PD occurrences are monitored by the microcontroller for one second i.e. 50 cycles of the power supply. During this one second, three main tasks are performed which include, the counting of PD pulses, sampling of integrator step size and recording of the relative time stamp of PD pulses. The data is then transferred to the supervisory application via the wirelessHART unit after calculating the average step size. The whole process is repeated on an hourly basis.

5.1.1.4 WirelessHART unit

To continuously monitor PD, it is pivotal to have robust interfacing of PD sensors to the wireless network. For this reason, WirelessHART IEC 62591 has been used as wireless communication technology. WirelessHART provides a continuous PD monitoring with the option of scalability if the scope of the system deployment gets bigger. It is a low power, low cost and easy to install a communication system that is based on IEEE 802.15.4. It is a self-forming multi-hop mesh technology. The technology is specifically designed for harsh industrial environments.

5.1.1.5 Supervisory application for PD

Supervisory application for PD monitoring has three main parts, which include:

- A data collection module
- A monitoring module
- A location algorithm

The data collection module collects data by interacting with a wirelessHART unit and stores it into a database. The monitoring module is a database system that is based on Indusoft web studio. The full details are described in [107]. The location algorithm uses the received signal and estimates the location of the PD source. A photo of the radiometer sensor used is shown in Figure 5.3 below:

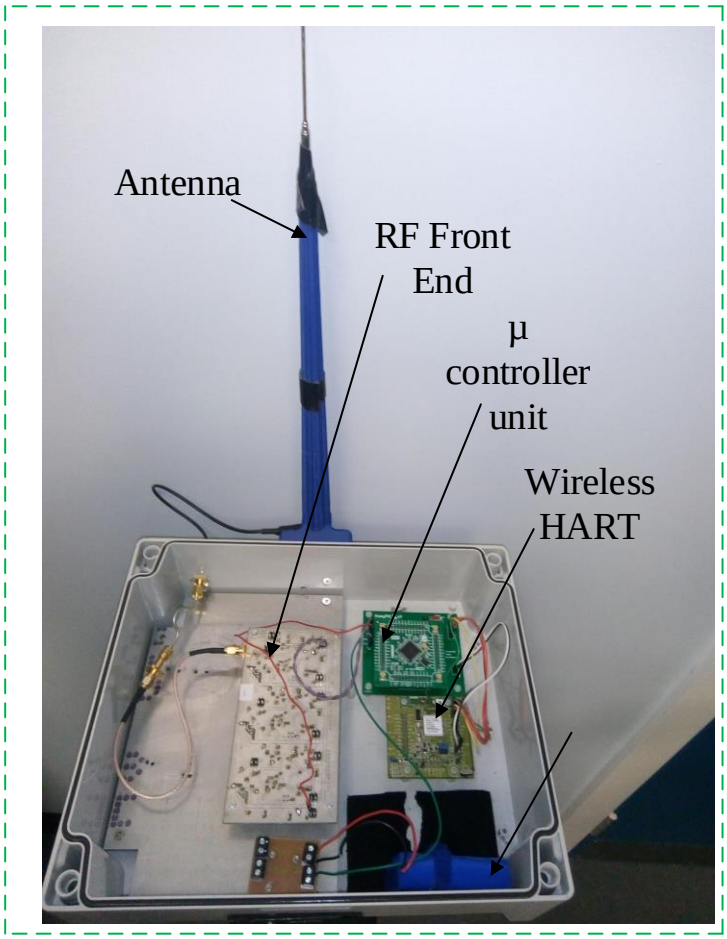

Figure 5.3. Radiometric sensor for PD monitoring and detection.

The above sensor is used for the detection and collection of data. The collected data is in the form of voltage levels that are converted into dBm power levels as an input to the location algorithm.

Performance evaluation of the algorithm in the real environment required the generation of a PD signal. To perform this task, a high-voltage PD (HVPD) calibrator was used. The calibrator was connected to a bi-conical Aaronia 2100E antenna, and a charge was emulated at a certain repetition frequency. The antenna connected with the PD calibrator together with the RF sensor is shown in Figure 5.4 below:

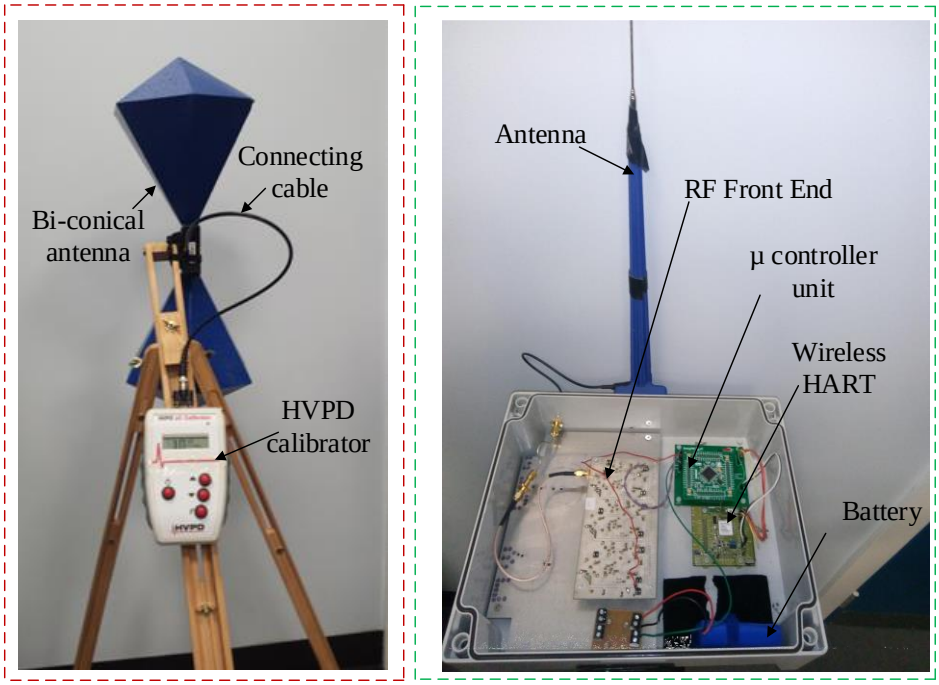

Figure 5.4. Antenna connected with the calibrator and the sensor.

The bi-conical antenna used for the experiment has the dimensions of $0.54\,m \times 0.225\,m \times 0.225\,m$, the frequency range from 20 MHz to 1GHz and the nominal input impedance is 50 Ω. The frequency range easily covers the required band of 50-850 MHz.

PD signal measurements were performed in some indoor and outdoor environments. There were a range of sensors configurations used, and signals were measured by using a range of sensors from 5 to 8. Source localization was performed by using the location algorithm based on the received signals under various configurations. Indoor and outdoor results obtained for various configurations are explained in the next chapter.

5.2 Chapter 5 summary

The radiometric sensors described in this chapter was used for the measurements to performed field trials in both indoor and outdoor environments. The sensors have a front end part where RF filters are used to suppress noise sources outside the desired frequency bands. For a location to be accurate, it is imperative to have the measurement sensor that measures the PD signal and not the noise. For this reason, when indoor measurements were performed, as explained in the next chapter, the spectral analysis of the algorithm was performed, and interference coming from the background was resolved.

Chapter 6: RESULTS OF LOCALIZATION OF PD SOURCE BASED ON INDOOR AND OUTDOOR MEASUREMENTS USING VARIOUS SENSORS CONFIGURATIONS

6.1 Practical results

To evaluate the performance of the algorithm and to ensure that the algorithm will work in a real environment, the algorithm testing was performed by generating artificial PD signals. Indoor and outdoor signal measurements were performed by using the radiometric sensors and the biconical antenna. A hypothetical view of the whole system as part of the detection and localization of PD can be illustrated in Figure 6.1 below:

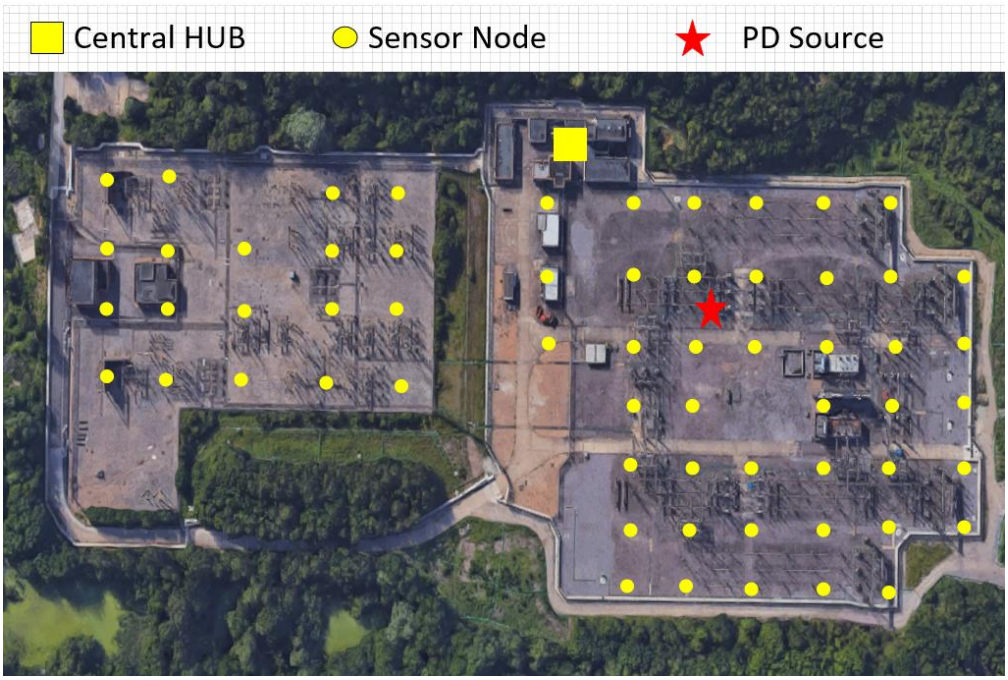

Figure 6.1. Hypothetical view of the whole PD detection and localization system.

Figure 6.1 above illustrates the entire system in terms of the sensors, the supervisory system and the localization of the source. Receiving nodes are deployed around a substation covering a particular area. The received signals are logged and stored in the central hub. The data then is used by the supervisory system, where within the supervisory system, received signals are used by the location algorithm to estimate the location of the source. Specialised PD emulators used in [35] and [113] were tested and produced similar results to the calibrator when proper averaging was used for the received signal

6.1.1 Indoor localization

For indoor localization, a sports hall was chosen as the measurement place. The reason to choose a sports hall was that it was big in the area and also would provide the propagation environment that was much closer to the free space environment. The environment was a homogeneous as this was quite useful to prove the principle to test the plausibility of the algorithm before it could be tested in a more realistic outdoor environment. There were nine different measurements taken within the sports hall. The artificial PD signals were generated by using an HVPD pC calibrator. The HVPD calibrator generated a $10\,nC$ charge as an emulated PD source with a repetition rate of 100 Hz. Measurements were performed in the unshielded sports hall environment. A range of services operate at the desired frequency band such as FM broadcast and digital video broadcasting (DVB-T) etc. Signals for such services could easily superimpose on the desired PD signal and could become a source of noise to the

desired signal. To evaluate such background interferences, a spectral analysis was performed inside the sports hall before measurements were conducted by using a high specification spectrum analyser as shown in Figure 6.2 below:

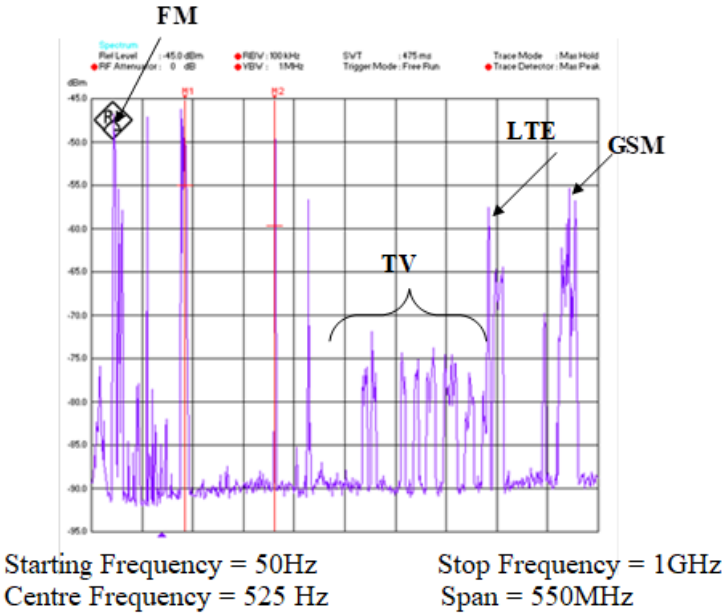

Figure 6.2 Spectral analysis inside the sports hall.

As illustrated in Figure 6.2, the frequency span was chosen from 50 MHz to 1GHz covering the whole desired band. As it is evident from Figure 6.2, interference from FM radio, TV, LTE-4G, GSM, and other communication signals were observed. To overcome such effects, bandpass RF filters have been used in the front-end part of the measurement sensor receiver as in Figure 5.1.

To measure the PD signal, eight receiving nodes were used. There were nine different measurements taken in this indoor environment. Measurements were performed in the sports hall by placing the receiving nodes at different locations and changing the position of the source. Source position was chosen at nine different locations. Source positions were chosen randomly considering the geometry of the grid. The idea was to prove the principle by placing the source at various geometries and obtaining the information about the decay of the signal. It was assumed that nodes near to the source would have higher signal strength to the ones far away from the source. This was confirmed from the received signals.

Receiving sensors were placed in known locations that remained unchanged. The location of the PD source was changed to nine different positions. This implies that the PD signal was

generated by using the HVPD pC calibrator at nine different positions by keeping the receiving nodes at the same position. The receiving nodes arrangements are shown in Figure 6.3 below over an 18 by 18-meters grid.

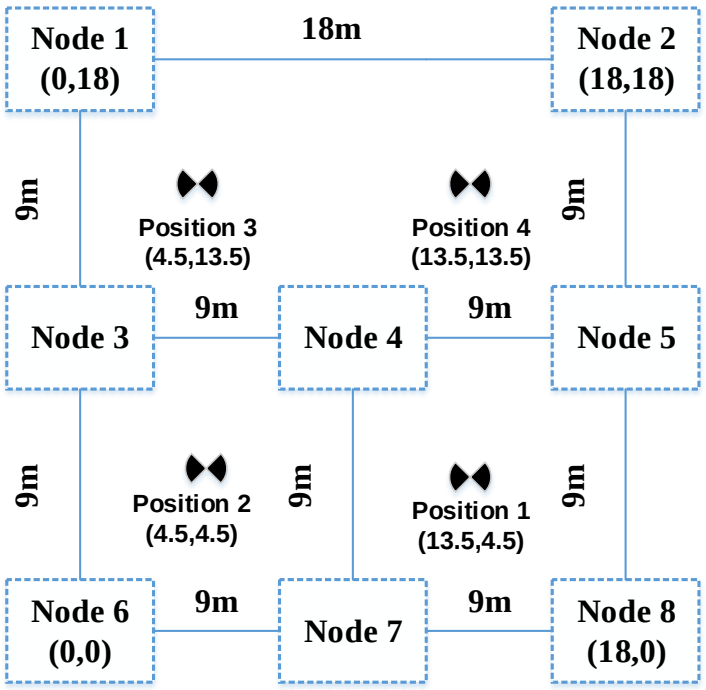

Figure 6.3 Arrangements of receiving nodes over an entire grid of 18 x 18 m.

Figure 6.3 above shows that position (0,18) corresponds to node 1 and position (18,0) correspond to node 8. Actual deployment of sensors nodes inside the sports hall is shown in Figure 6.4 below:

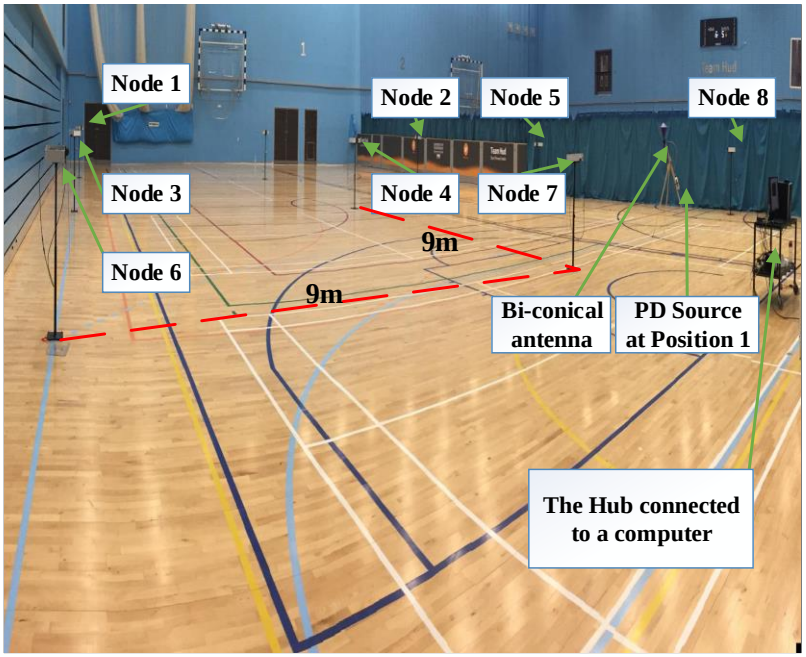

Figure 6.4 Sensor nodes deployments inside the sports hall.

Figure 6.4 above shows how the sensors were placed in the sports hall and the other parts of the receiving system including the central hub. The maximum number of receiving nodes that could be used was eight due to limited availability of sensors. Each receiving node in the system receives the signals and to ensure the validity of the received signals; the measurements were repeated at least five times. In addition to this, the trends were also showing that received signals were according to the expectations as the closer nodes had higher signal strength than the nodes that were far from the PD source. Repeated measurements, as well as changing positions, ensured that received signals were according to the expectations.

The received signals for each position were voltage levels and converted into power levels in dBm as input the location algorithm. The average-step voltage signal (U) was converted into dBm as an input to the location algorithm. The signal was converted as below:

$$dBm = 20log_{10}(U^2) + 30 \qquad \text{Equation (6.1)}$$

Where U is the average-step voltage signal. dBm conversion of the signal is shown in Table 6.1 for each node and all positions.

Table 6.1. Received signal power in dBm.

Source Position	Node 1	Node 2	Node 3	Node 4	Node 5	Node 6	Node 7	Node 8
Position 1	-12.49	-12.69	-12.32	-4.35	-4.56	-8.98	-3.58	-6.27
Position 2	-13.10	-14.38	-5.72	-4.05	-10.36	-6.87	-4.88	-14.33
Position 3	-1.91	-12.19	-4.43	-7.10	-11.99	-13.42	-12.44	-17.48
Position 4	-9.23	-2.56	-11.70	-5.16	-5.29	-13.33	-14.11	-18.50
Position 5	-11.91	-11.17	-10.47	2.30	-3.49	-9.69	-8.92	-10.50
Position 6	-9.41	-13.18	-3.07	1.28	-9.82	-9.75	-9.01	-14.69
Position 7	-6.10	-8.90	-8.53	-0.40	-7.76	-12.70	-12.78	-17.73
Position 8	-11.19	-6.56	-12.18	1.29	0.68	-12.13	-10.01	-13.58
Position 9	-18.49	-19.26	-14.94	-13.44	-15.21	-2.62	-4.96	-12.84

Table 6.1 shows the values in dBm for each position of the source for each node. For each position, several measurements were performed, and Table 6.1 shows the average of all measurements performed. From the measurements, it is clear that receiving nodes closer to the source have higher signal strength than the ones that are far from the source. For example, position 1(13.5,4.5) has the closest nodes 4, 5, 7 and 8. All four nodes have the strongest received signal than other nodes in the receiving system. Nodes 1 and 2 that are farthest have the least strength of the received signal. PD source localization was performed by using six, seven and eight receiving nodes. The performance parameters were estimated location and path loss exponent after optimisation.

6.1.1.1 PD localization using six receiving nodes in an indoor environment.

Firstly, the source localization was performed by using six receiving nodes for nine positions. The localization parameters included the estimated location of the source, the localization error and the optimised value of the path loss exponent. For each of the nine positions localized, the results of the estimated versus true locations, calculated error and optimised path loss exponent for each position are summarized in Table 6.2 below:

Table 6.2 True vs. estimated location when six receiving nodes used for indoor localization.

	True location		Estimated Location			
PD source location	$X\ (m)$	$Y\ (m)$	$X\ (m)$	$Y\ (m)$	Error (m)	Optimum PLE α
Position 1	13.50	4.50	10.30	7.62	4.47	2.70
Position 2	4.50	4.50	7.04	6.56	3.26	3.10
Position 3	4.50	13.50	5.90	13.08	1.47	4.50
Position 4	13.50	13.50	8.68	11.95	5.06	5.00
Position 5	10.00	6.00	8.75	8.66	2.94	5.00
Position 6	6.00	8.00	6.29	9.17	1.21	5.00
Position 7	8.00	12.00	7.38	11.57	0.76	4.70
Position 8	12.00	10.00	8.91	9.84	3.09	5.00
Position 9	4.5.0	-4.50	7.64	-3.23	3.39	4.65

From the results shown in Table 6.2 above, it appears that localization error is around 5 meters for position 4, for positions 3, 6 and 7, localization errors are reasonably low meeting the expectations. For position 1, the localization error is nearly 4.5 meters whereas, for positions 2, 8 and 9 the error is not very low but acceptable considering the number of receiving nodes used for the localization. Figure 6.5 shows the location results for position 1

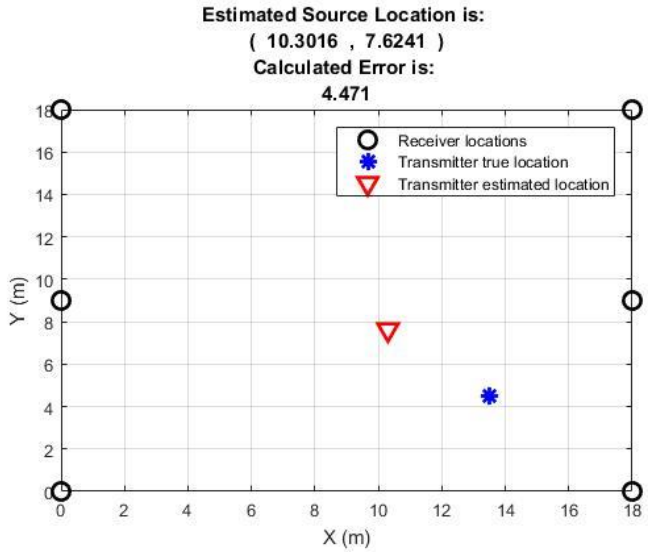

Figure 6.5. A position with six receiving nodes used.

Figure 6.5 above shows the estimated location and the localization error when six measurement sensors were used. Path loss exponent values seem a bit high as the optimised values for the majority of positions are in the range of 4 and 5 except for positions 1 and 2. Estimated locations for positions 2 and 3 are shown in Figures 6.6 and 6.7 next:

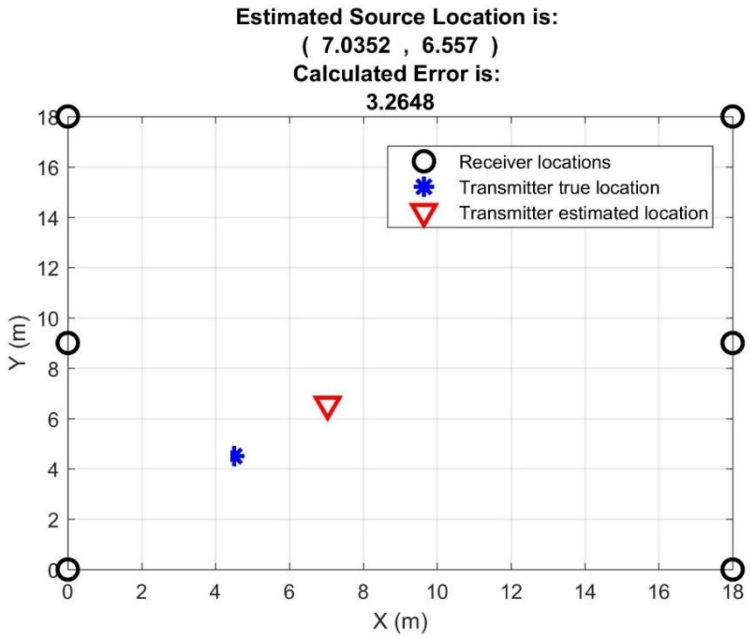

Figure 6.6. Position 2 with six receiving nodes used.

Position 2 results again show that localization error is not as low as desired; however, considering that only six measurement sensors were used, it can be considered as acceptable.

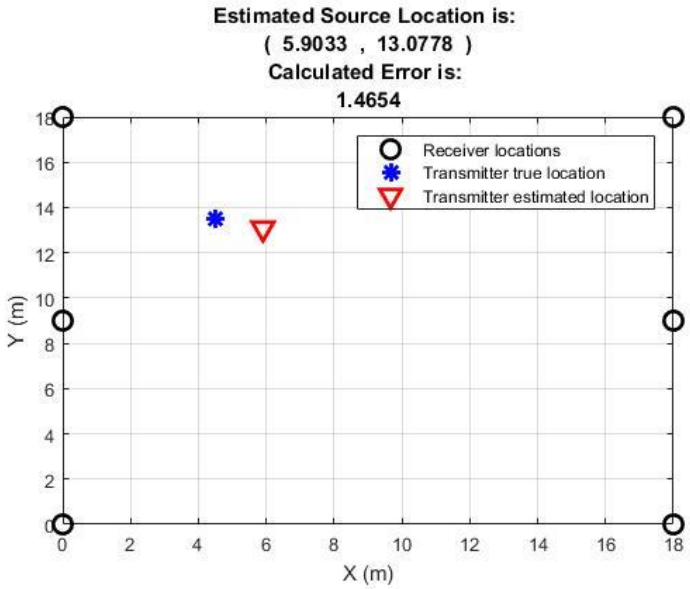

Figure 6.7. Position 3 with six receiving nodes used for localization.

For position 3, the localization error is very much acceptable considering only six measurement nodes were used for localization. The next step is to increase the number of receiving nodes and localize the source for all nine positions to see if the increase in receiving nodes impacts the localization accuracy. Also, path loss optimisation is another important factor that needs to be considered. A node in the receiving system is thus added, and seven receiving nodes are used next.

6.1.1.2 PD localization using seven receiving nodes in an indoor environment.

In this case, PD source localization for nine positions was performed by using seven receiving nodes. The performance parameters were estimated location and the path loss exponent as were in the previous case when six receiving nodes were used. The RMS error was calculated by taking the difference between the estimate and true locations. Results for each position with the error calculations and estimated values of the path loss exponents are shown one by one in Table 6.3 below:

Table 6.3. PD source location estimation with seven sensors used, proposed method.

	True location		Estimated Location			
Source Position	$X\ (m)$	$Y\ (m)$	$X\ (m)$	$Y\ (m)$	Error (m)	Optimum PLE α
Position 1	13.50	4.50	12.37	4.49	1.13	1.75
Position 2	4.50	4.50	5.99	5.02	1.57	2.15
Position 3	4.50	13.50	5.41	13.76	0.94	3.45
Position 4	13.50	13.50	10.94	15.48	3.23	4.25
Position 5	10.00	6.00	12.65	6.95	2.81	1.60
Position 6	6.00	8.00	6.60	8.50	0.78	2.05
Position 7	8.00	12.00	7.89	13.89	1.90	3.30
Position 8	12.00	10.00	13.16	10.86	1.45	2.60
Position 9	4.5.0	-4.50	3.14	-6.43	2.36	2.75

Table 6.3 shows results for the estimated location as well as the optimum path loss exponent which is between 1.60 to 3.45 for the majority of the positions with an exception for position 4 where the error is 4.25 meters. The calculated error is reasonably low for the majority of the positions as well. For two positions it is less than one meter, for four positions it is between 1 to 2 meters, and for three positions it is more than 2 meters. Estimated location for positions 1, 2 and 3 is given in Figures 6.8, 6.9 and 6.10 next:

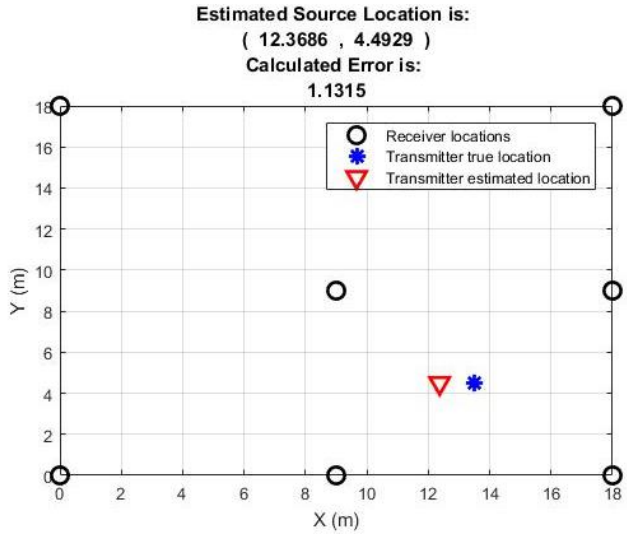

Figure 6.8. Position 1 results with seven receiving nodes used.

For position 1, as shown above, the estimated localization (12.3, 4.49) is quite acceptable considering the actual position of the source is $(13.5, 4.5)$ giving a localization error of 1.13 meters. It can be seen that four nodes are in the vicinity of the source and the estimated location is reasonably good providing the localization error just above 1 meter. In RSS based localization, the geometrical conditions are very important in terms of the localization error.

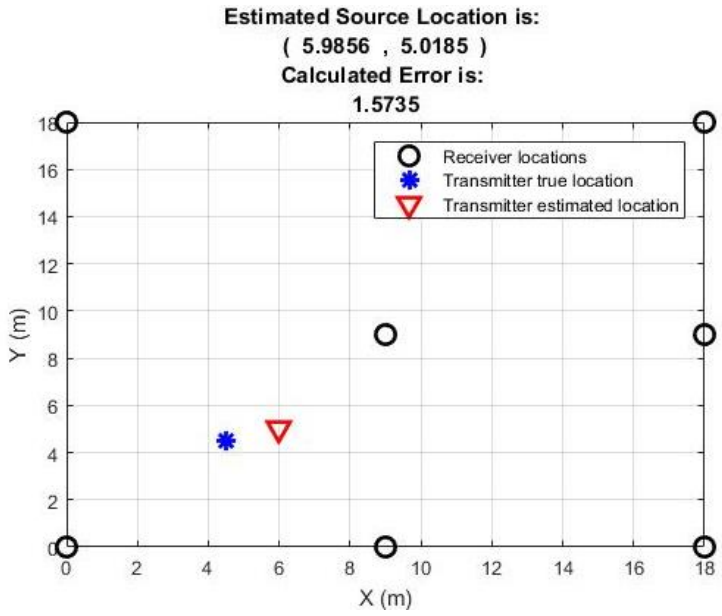

Figure 6.9. Position 2 results with seven receiving nodes used.

For position 2, localization error is 1.57 meters. From the position of the source, it is clear that when estimating the locations, the node in the middle and the first two nodes are in the vicinity.

Considering the positions of the nodes and the localization error is not too bad and remains nearly 1.57 meters which is quite acceptable.

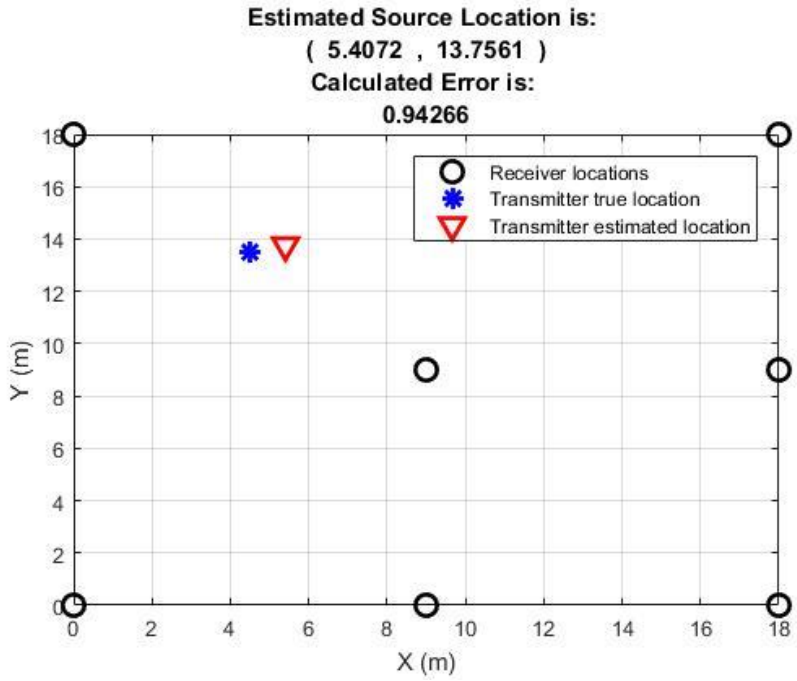

Figure 6.10. Position 3 results with seven receiving nodes used.

Position 3 localization error remains below 1 meter which is a very good result. For this position middle and top left-hand corner nodes are quite near to the location of the source.

For all position for indoor measurements, it is evident that localization errors remain reasonable and the path loss exponent optimised shows the values that are closed to the average value of the propagation environment when using seven receiving nodes. The mean error calculated for all position for indoor measurements remains 1.80 meters, which is quite acceptable as it remains below 2 meters.

6.1.1.3 PD localization using eight receiving nodes in an indoor environment

Source localization was also performed by using eight receiving to evaluate the impact of having more receiving nodes on the localization accuracy and path loss exponent optimisation. When eight receiving nodes used for PD localization, the comparison between the estimated versus true locations, error calculation and the path loss exponent values are shown in Table 6.4 next:

Table 6.4. PD source location estimation with eight sensors used, proposed method.

	True location		Estimated Location			
Source Position	$X\ (m)$	$Y\ (m)$	$X\ (m)$	$Y\ (m)$	Error (m)	Optimum PLE α
Position 1	13.50	4.50	12.44	4.45	1.06	1.75
Position 2	4.50	4.50	5.73	5.22	1.43	2.20
Position 3	4.50	13.50	4.12	14.72	1.28	2.80
Position 4	13.50	13.50	11.35	15.24	2.77	3.55
Position 5	10.00	6.00	12.58	7.20	2.85	1.55
Position 6	6.00	8.00	5.63	9.68	1.72	2.50
Position 7	8.00	12.00	8.95	13.86	2.08	2.95
Position 8	12.00	10.00	13.18	10.83	1.44	2.70
Position 9	4.5.0	-4.50	3.97	-5.63	1.24	2.85

Table 6.4 shows that results have improved significantly in terms of localization accuracy and PLE optimisations. For all nine positions, the PLE values are between 1.55 to 3.35, with the majority between 2 to 3. The localization error for six positions is less than two meters. For three positions it is between 2 to 3 meters. This is an indication of how scalability can enhance the localization accuracy. The localization accuracy also means that PLE values are much closer to the average value of the free space propagation environment, i.e. 2 in this case. Estimated location for positions 1, 2 and 3 is given in figures 6.11, 6.12 and 6.13 next.

The error for position 1 when using eight measurement sensors is reduced from 1.13 meters to 1.06 meters. The error for position 2 is reduced from 1.57 meters to 1.42 meters, in the case of position 3, the error has slightly increased from 0.94 meters to 1.27 meters. This is mainly due to the addition of a single node in the receiving system that is too far from the source position and hence has the greater distance which will mean that the node has contributed towards the error in location estimation rather than improving the overall localization error. This is one of the drawbacks of the RSS based localization.

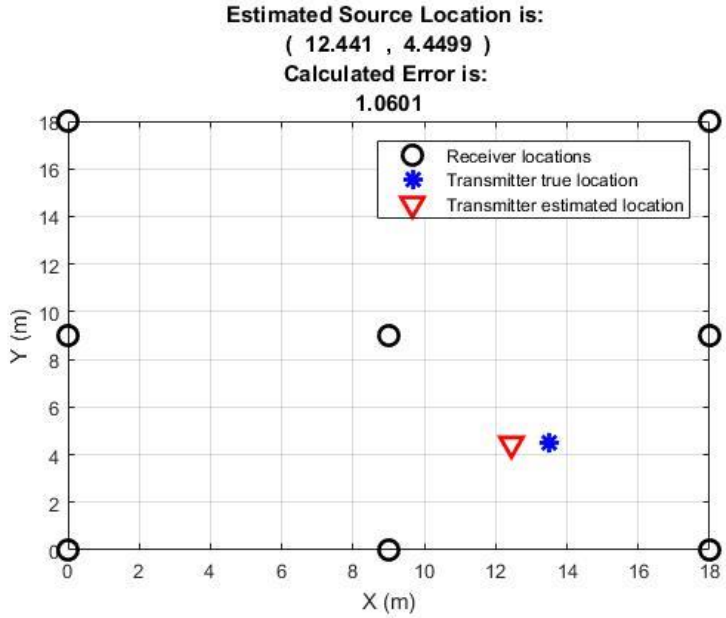

Figure 6.11. Estimated location for position 1 with eight sensors

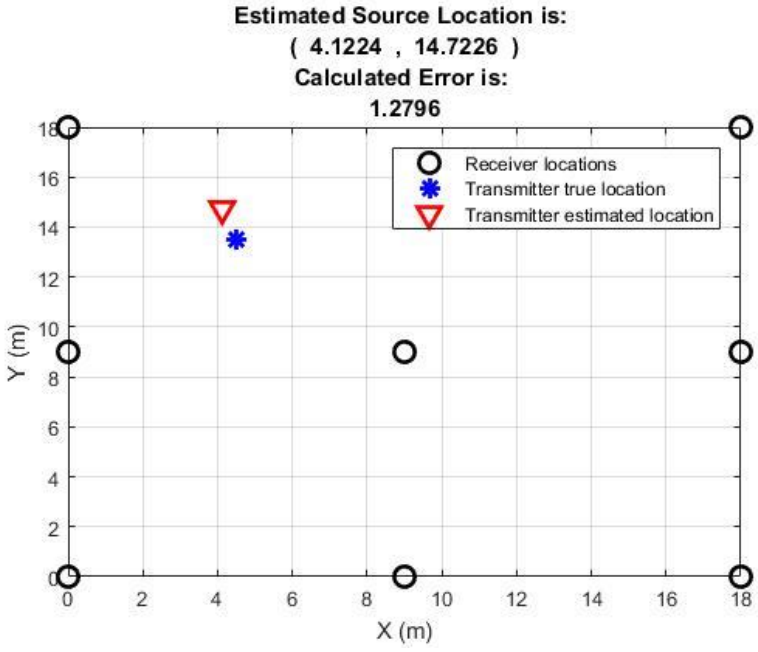

Figure 6.12. Estimated location for position 2 with eight sensors.

When comparing the path loss exponents with the table when seven measurement nodes were used, PLE seems much closer to the average value of the propagation environment. This ensures that increasing the number of receiving nodes, not only contributes to better location estimation; it also improves the path loss exponent values.

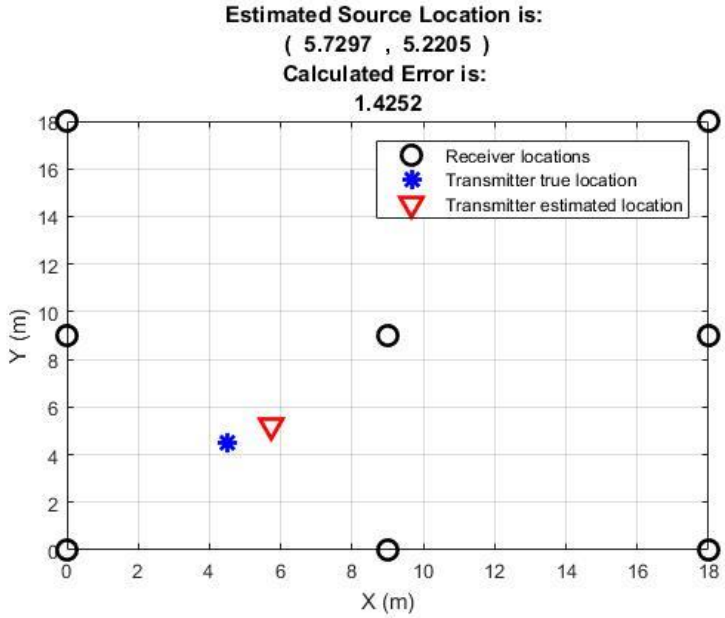

Figure 6.13. Estimated location for position 3 with eight sensors

For all three field scenarios, the mean estimated error for the proposed algorithm can be summarized in Table 6.5 below:

Table 6.5 Mean error comparison for different arrangements of sensors.

	With 6 sensors used	With 7 sensors used	With 8 sensors used
Mean Error (m)	2.80	1.80	1.76

Table 6.5 shows the mean error calculations for three cases. Mean error when using six receiving nodes is 2.80 meters which is reduced to 1.80 meters when seven receiving nodes were used, a mean localization improvement of 1 meter, which reduced further to 1.76 meters, i.e. 0.04m better localization accuracy with the addition of a single node. This implies that RSS based localization is a technique with better properties in PD localization due to its capability to offer scalability at any given time without any modifications in the overall system configuration except the addition of a receiving node. The testing of the algorithm in an outdoor environment is examined next.

6.1.2 Outdoor localization

The above scenario 6.1.1 was based on a homogeneous indoor environment; however, in a real substation, the environment may vary.

To evaluate the performance of the algorithm in a realistic scenario, it is important to find out whether the algorithm will perform well in more complex environments such as substations. To explore this, measurements were performed in two environments. Nine different

measurements were performed at the power distribution network center (PNDC) at Strathclyde University and three distinct measurements were performed at TATA steel in Port Talbot, Wales. PD source localizations were performed by using five, six, seven and eight receiving nodes. To consider the geometrical effects and the scalability, a range of sensor configurations were used. To generator a PD signal the same HVPD pC calibrator was used and a charge of 10nC with repetition rate of 100Hz was generated. The localization results for each of the sensor configurations are explained one by one. An example sensor arrangement at the PNDC site is illustrated in Figure 6.14 below:

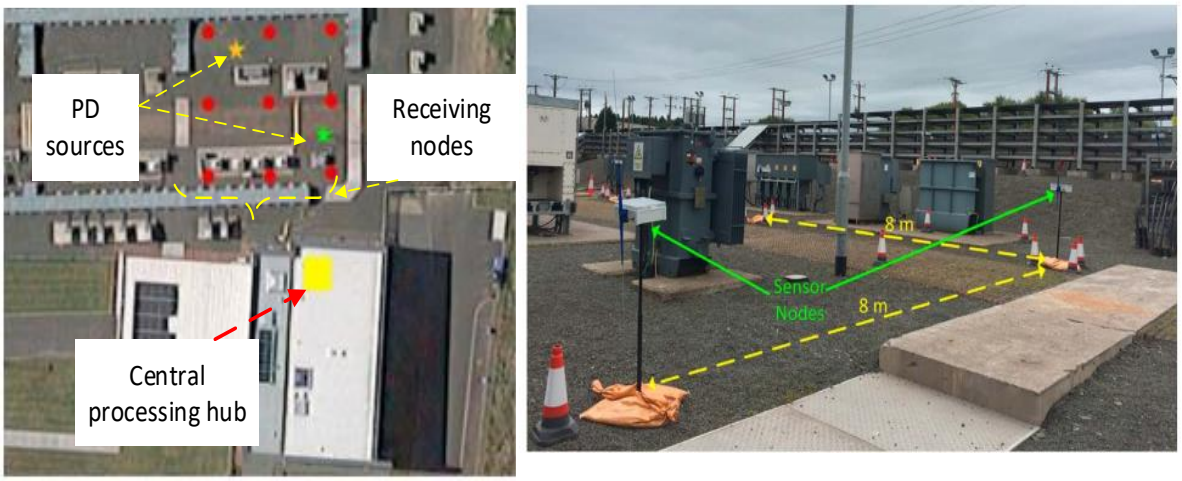

Figure 6.14. An example of a measurement setup at PNDC Strathclyde.

Figure 6.14 (i) illustrates the hypothetical view whereas 6.14 (ii) illustrates the actual nodes deployment at the PNDC site. Localizations performed for various arrangements are described one by one in the next section.

6.1.2.1 Outdoor localization using five receiving nodes

To evaluate the performance of the algorithm, initially, the source localization was performed by using 5 sensors for two different sensors arrangements for two different positions. In the first arrangement, sensors were arranged over a 16 by 16 grids at locations (0,0), (8,0), (0,8), (8,8) and (16,8) respectively. Node deployment example around PNDC site using five sensors can be seen in Figure 6.15 below:

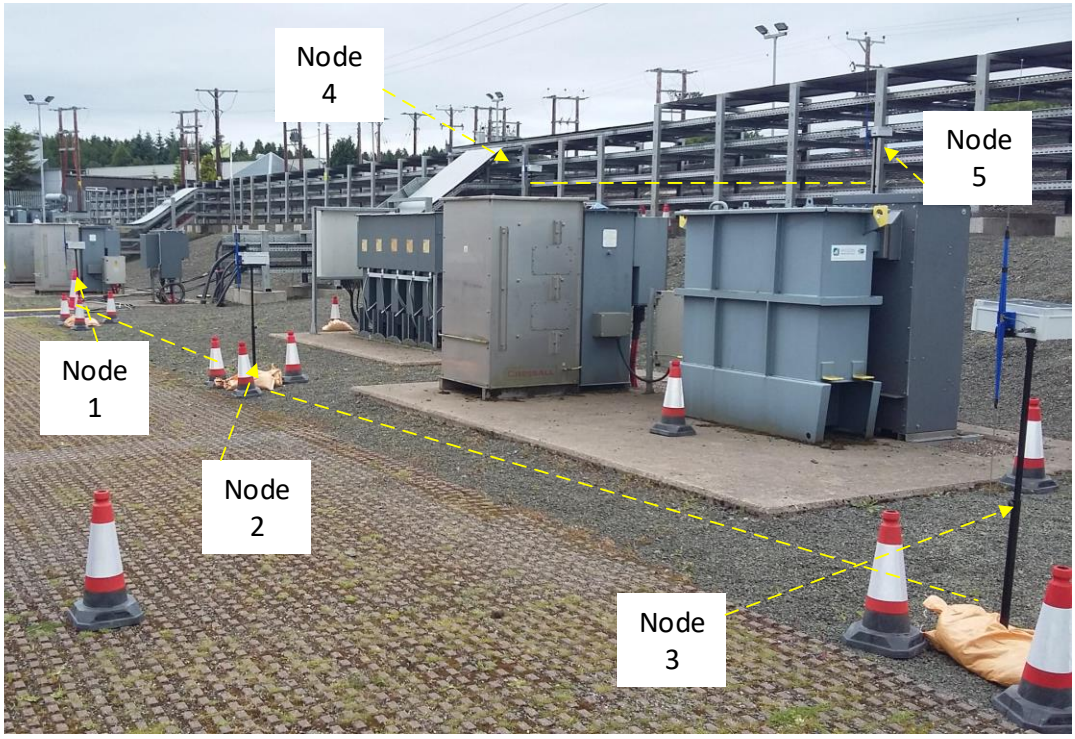

Figure 6.15. PNDC measurement of the PD signal using five receiving nodes.

The source estimation was performed for the locations(2.9,3.0). The received signals converted into dBm as input to the location algorithm are shown in Table 6.6 next:

Table 6.6. Received signal using 5 nodes at (2.90, 3.0) source position (PNDC) in dBm

Source Position	Node 1	Node 2	Node 3	Node 4	Node 5
(2.9,3.0)	-3.4	12.5	-3.2	-3.5	-11.6

The comparison between the estimated versus true location and the path loss exponents is shown in Table 6.7 below:

Table 6.7. Source location estimation and PLE at (2.90, 3.0) source position (PNDC) in dBm

True location		Estimated Location			
$X\ (m)$	$Y\ (m)$	$X\ (m)$	$Y\ (m)$	Error (m)	Optimum PLE α
2.9	3.0	3.51	5.21	2.30	5

The location estimation and the calculated error for the position (2.90, 3.0) is shown in Figure 6.16 below:

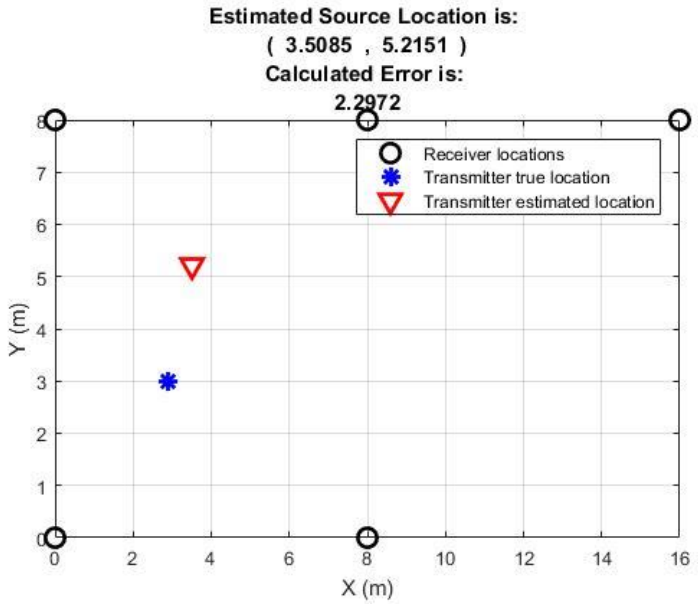

Figure 6.16. Source estimation using five sensors at $(2.90, 3.0)$ source (PNDC).

As evident from Figure 6.16 above, the error is above 2 meters and the path loss exponent is high as well, considering the average path loss value of the environment in free space. Considering only five receiving nodes are used, the results are considered as acceptable.

For the second sensor arrangement, the source location estimation was performed for the source position (14.5,2.3). Sensor arrangement was changed by placing sensors 1 to the location (8,0) and sensor 2 to the location (16,0). Locations of sensors 3, 4 and 5 were kept the same as in case of source position (2.9, 3.0). The received signals converted into dBm as input to the location algorithm is shown in the Table 6.8 below:

Table 6.8. Received signal using 5 nodes at (14.5, 2.30) source (PNDC)

Source Position	Node 1	Node 2	Node 3	Node 4	Node 5
(14.5, 2.3)	-12.0	4.0	-18.1	-7.8	-1.1

The comparison between the estimated versus the true location and the path loss exponents is shown in Table 6.9 below:

Table 6.9. Estimated vs. true location, error and PLE estimation for position 3 using 6 nodes.

True location		Estimated Location			
$X\ (m)$	$Y\ (m)$	$X\ (m)$	$Y\ (m)$	Error (m)	Optimum PLE α
14.5	2.3	11.22	4.56	3.98	4.5

The location estimation and the calculated error for the positions are shown in Figure 6.17 next when five receiving nodes were used for the source location (14.5, 2.3).

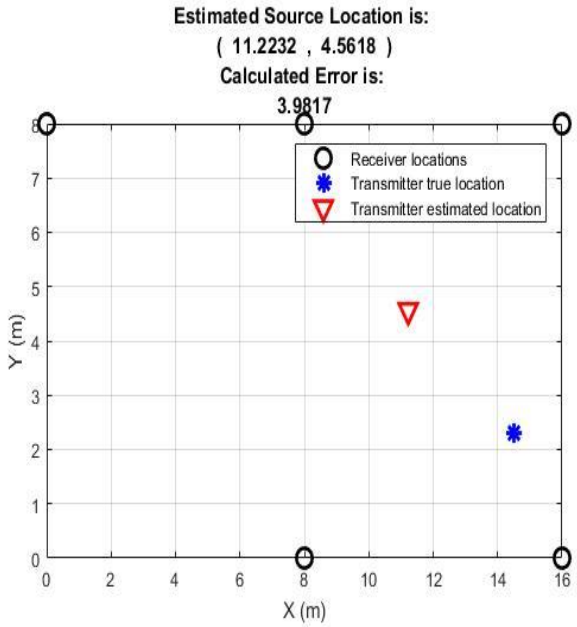

Figure 6.17. Source location estimation at source position (14.5, 2.30) with five receiving nodes.

Figure 6.17 shows a different arrangement of receiving nodes when compared with figure 6.16, however, still five receiving nodes are used for signal measurement. There is no receiving node at position $(0, 0)$ and the source is now placed at the right end of the grid. The results for the position $(14.5, 2.3)$ are acceptable considering that the difference between the received powers is big and the location of the receiving nodes from the source are also far except the nodes 1, 2 and 5. However, the increase in the number of nodes should improve the localization accuracy. The results for positions $(2.9, 3.0)$ and $(14.5, 2.3)$ showed that the algorithm works for the outdoor environment when using five receiving nodes, although the localization accuracy is not very high. To explore the performance of the algorithm further, measurements were taken by using six receiving nodes.

6.1.2.2 Outdoor localization using six receiving nodes

To further explore the algorithm for the outdoor environment, the number of receiving nodes increased to six and the source was placed at four different positions with receiving node positions kept the same as illustrated in Figure 6.18 below:

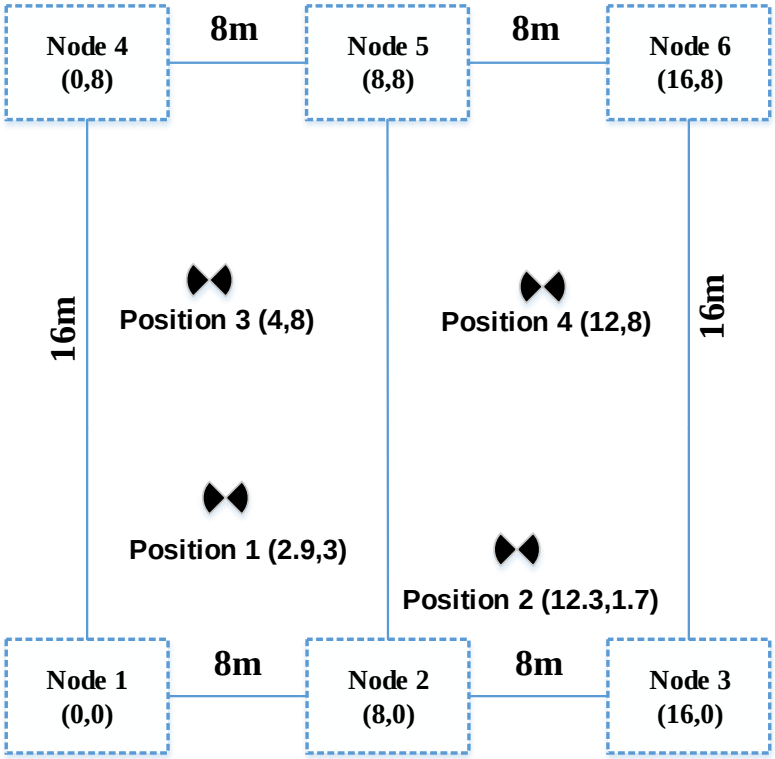

Figure 6.18. Sensor arrangements when six receiving nodes were used to locate PD.

An example setup of the receiving nodes using six measurement sensors is shown in Figure 6.19 next.

The receivers' arrangements show an example of how sensors nodes were arranged to measure a PD signal. A maximum of eight nodes were deployed to form a grid of 16 x 16 meters. Nodes 4, 5, 6 and 9 were elevated at the height of 1.5 meters, while Nodes 7 and 8 were elevated at the height of 3 meters all above the ground.

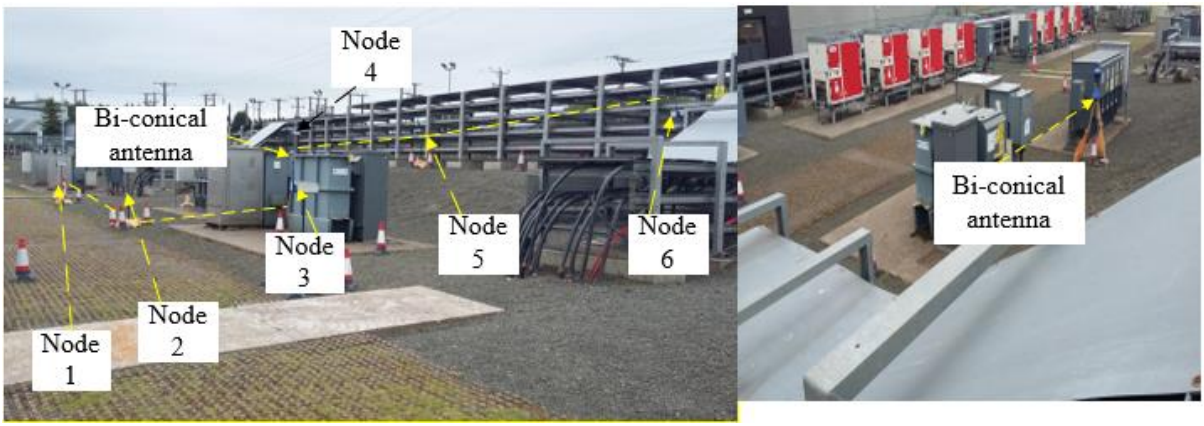

Figure 6.19. An example setup when six measurement nodes were used at the PNDC site.

The received signals converted into dBm as input to the location algorithm for four different positions are shown in Table 6.10 below:

Table 6.10. Received signal in dBm for four different positions using six receiving nodes

Source Position	Node 1	Node 2	Node 3	Node 4	Node 5	Node 6
Position1	-3.30	12.30	-13.30	3.0	-4.0	-11.5
Position2	-19.0	-10.60	-0.80	-14.70	-13.20	-10.60
Position3	-7.90	-11.10	-13.70	-0.30	3.40	-10.50
Position4	-15.60	-11.60	-8.40	-12.70	1.90	0.50

The comparison of the estimated versus true location and the path loss exponents for four positions is shown in Table 6.11 next:

Table 6.11. Comparison between true versus estimated locations when six receiving nodes were used for signal measurement at the PNDC site.

	True location		Estimated Location			
Source Position	$X\ (m)$	$Y\ (m)$	$X\ (m)$	$Y\ (m)$	Error (m)	Optimum PLE α
Position 1	2.90	3.00	3.23	5.30	2.32	2.75
Position 2	12.30	1.70	10.50	2.77	2.09	3.50
Position 3	4.00	8.00	4.55	7.19	0.98	2.70
Position 4	12.00	8.00	11.83	7.85	0.23	3.10

Table 6.11 shows the values for four positions when six measurement sensors were used. The optimised value of the path loss exponent seems reasonable for almost all four positions. Estimated locations are much improved when compared with five measurements nodes with PLE values remain between 2.70 to 3.50. Localizations results for first two positions when six measurement nodes are used are shown in the Figures 6.20 and 6.21 respectively.

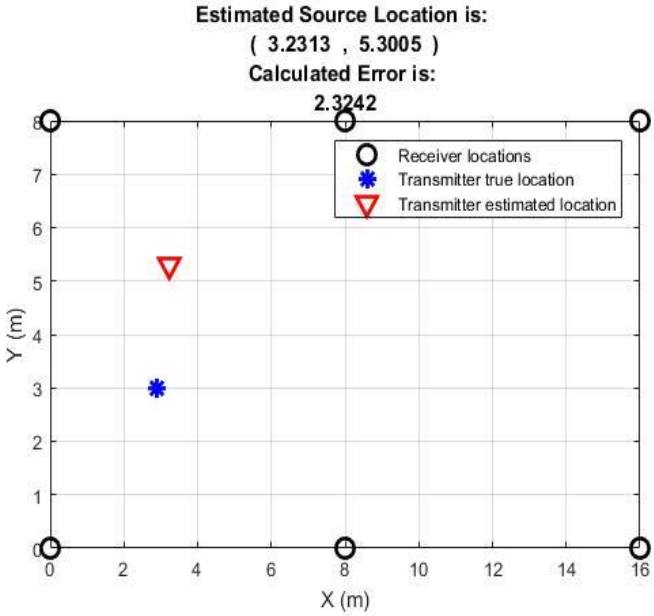

Figure 6.20. Source estimation using six receiving nodes for source position (2.90, 3.0).

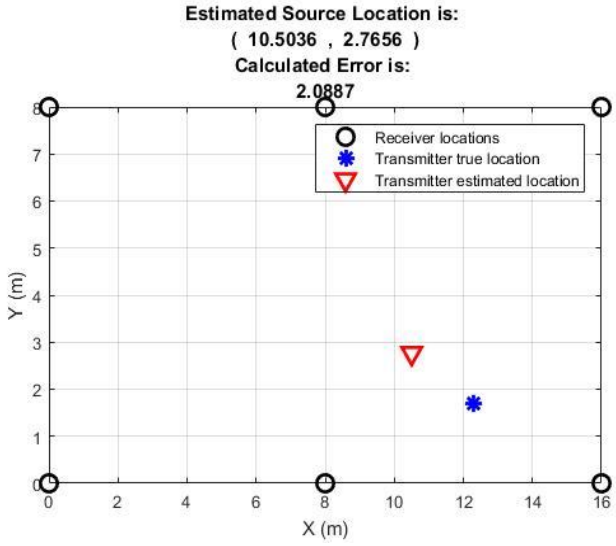

Figure 6.21. Source estimation using six receiving nodes for source position (12.90, 1.70).

The above two results are shown as examples. For all four positions above, the results shown are improved when compared with the five sensors case. Results for positions (4, 8) and (12, 8) are highly encouraging where the localization error is less than a meter. To further evaluate the performance of the proposed algorithm, the number of sensors was increased to seven and eight respectively.

6.1.2.3 Outdoor localization using seven receiving nodes

By using seven receiving nodes, the source localization was performed by using different configurations. Initially, the source was kept at position (14.2, 5.20) and receiving nodes were placed at positions shown in Figure 6.22 below:

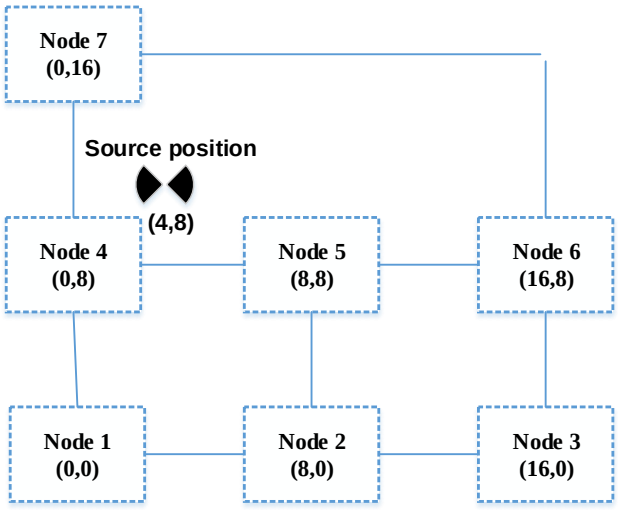

Figure 6.22. Sensor arrangements for the source location (14.5, 2.3) when seven receiving nodes were used for signal measurement.

Source localization was performed by using seven sensors as placed in the above locations. The received signal in the form of dBm is shown in Table 6.12 below:

Table 6.12. Received signals in dBm when seven receiving nodes were used for source location (14.5, 2.3).

Source Position	Node 1	Node 2	Node 3	Node 4	Node 5	Node 6	Node 7
(4.0, 8.0)	-7.90	-11.10	-13.70	-0.30	3.40	-10.50	-10.40

Estimated versus true location comparison is shown in Table 6.13 below:

Table 6.13. True versus estimated location comparison when seven receiving nodes were used for the source position (4.0, 8.0).

True location		Estimated Location			
$X\ (m)$	$Y\ (m)$	$X\ (m)$	$Y\ (m)$	Error (m)	Optimum PLE α
4	8	4.59	7.07	1.09	2.75

The estimated location seems very plausible. The optimised value of PLE is 2.75 which is quite an acceptable value considering the propagation environment. The location estimation performed can be seen in Figure 6.23 below:

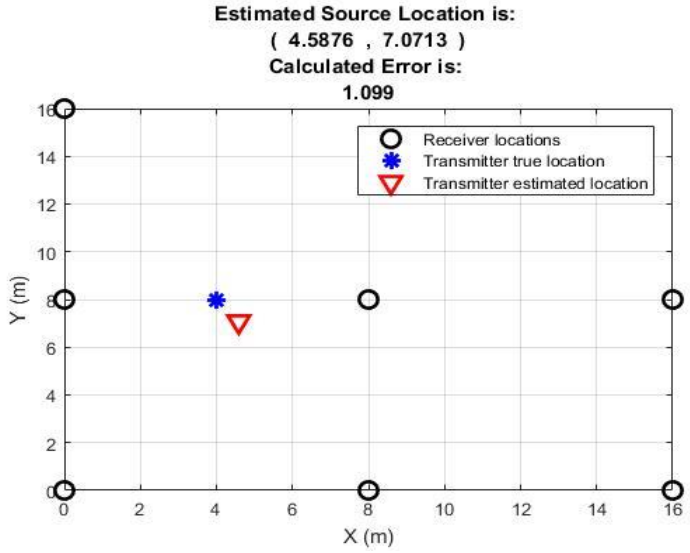

Figure 6.23. Source location estimation for the position (4, 8) when seven receiving nodes were used.

When seven measurement nodes were used, the performance was further explored for two more source positions by using different sensors configurations to above. Firstly, the sensors arrangements were changed to (0,0), (8,0), (16,0), (0,8), (8,8), (16,8) and (8,16) respectively and the source was placed at the position (12, 8) as shown in Figure 6.24 below:

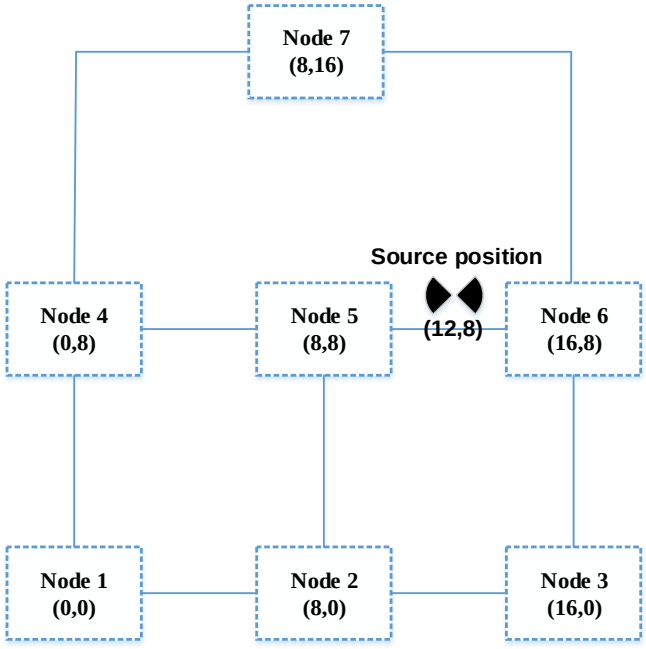

Figure 6.24. Seven measurement sensors arrangement.

The received signal in the form of dBm is shown in Table 6.14 below:

Table 6.14. Source localization for different sensor arrangement when using seven receiving nodes for the source position (12, 8).

Source Position	Node 1	Node 2	Node 3	Node 4	Node 5	Node 6	Node 7
(12, 8)	-15.60	-11.60	-8.40	-12.70	1.90	0.50	-14.60

The estimated vs. true location of the source is shown in Table 6.15 below:

Table 6.15. Estimated versus true location, error calculation and PLE estimation for the source position (12,8).

True location		Estimated Location			
$X\ (m)$	$Y\ (m)$	$X\ (m)$	$Y\ (m)$	Error (m)	Optimum PLE α
12	8	11.60	6.44	1.61	3.50

Table 6.15 above shows the localization error for the given arrangement is nearly 1.6 meters and an optimised value of path loss exponent of 3.5. With RSS based localization, the main issue is that although scalability enhances the localization accuracy, however, it can only enhance localization accuracy, if the location errors were too high due to an insufficient number of nodes. If due to the geometrical position of the source, the localization errors are already low, an addition of a single node may even cause a small increase in error. This will depend upon the location of the additional node. If the additional node is too far from the actual position of the source, this may not be useful. However, such errors will not be too high. In source localizations, the position of the receiver nodes and the position of the source are also important in addition to having more number of receiving nodes. Finally, source localization was performed by using seven nodes and a completely different sensors arrangement, as shown in Figure 6.25 below:

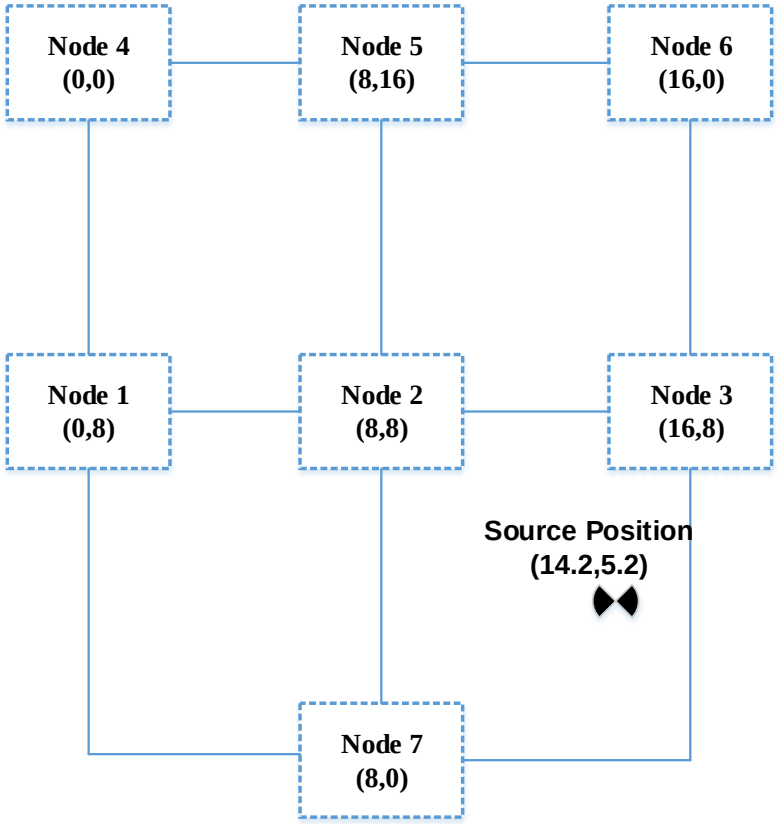

Figure 6.25. Receiving nodes arrangements when seven receiving nodes were used with a different configuration.

As shown in Figure 6.25, sensor 1 corresponds to position (0, 8), and sensor 7 corresponds to position (8, 0). The source positioned at (14.2, 5.2) shows a "difficult" geometry when looking at the sensors arrangement. The localization error is expected in this case to be large. The received signal by each receiving node in dBm is shown in Table 6.16 below:

Table 6.16. Received signal in dBm for the source position (14.2, 5.2) using seven nodes.

Source Position	Node 1	Node 2	Node 3	Node 4	Node 5	Node 6	Node 7
(14.2, 5.2)	-13.50	-3.90	2.20	-15.80	-10.80	-9.90	-13.70

Nodes 2, 3 are much closer to the source; the strength of the signals is high especially for node 3. The rest of the nodes are far away, and in almost all cases, the received signal is quite low compared to nodes 2 and 3. The true versus the estimated location of the source is shown in Table 6.17 below:

Table 6.17. True vs. estimated location when seven sensors used at (14.2,5.20).

True location		Estimated Location			
$X\ (m)$	$Y\ (m)$	$X\ (m)$	$Y\ (m)$	Error (m)	Optimum PLE α
14.2	5.20	12.80	7.92	3.05	3.50

The localization error as expected is higher than in the majority of the other positions, clearly due to the geometrical position of the source and the receiving sensors arrangements.
In general, from the results obtained for seven measurement sensors, it is clear that the location estimation was much better when compared with five and six receiving nodes. The algorithm was further evaluated by using eight measurement nodes which is explained next.

6.1.2.4 Outdoor localization using eight receiving nodes

When eight receiving nodes were used, the algorithm testing was performed under three different arrangements. In arrangement 1, the source was placed at the location $(4, 8)$ and receiving nodes were placed at the locations shown in Figure 6.26 below:

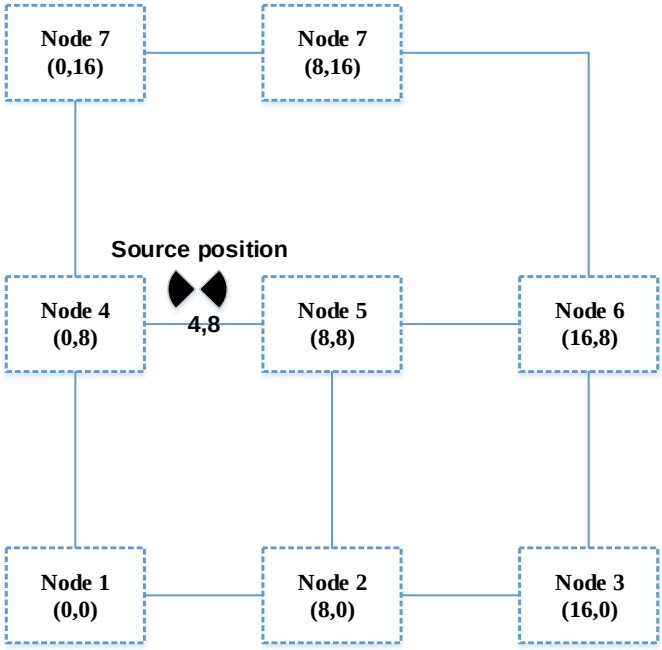

Figure 6.26. Receiving nodes arrangements when eight nodes are used.

The received signal in the form of dBm for eight receiving nodes is shown in Table 6.18 below:

Table 6.18. Measured signal when eight receiving nodes are used.

Source Position	Node 1	Node 2	Node 3	Node 4	Node 5	Node 6	Node 7	Node 8
(4,8)	-7.90	-11.10	-13.70	-0.30	3.40	-10.50	-10.40	-13.30

Table 6.18 shows the measured results in dBm. Results shown above are the average of ten different measurements. Receiving nodes 4 and 5 are closer to the source and show higher signal strength. Source location estimation was performed and path loss exponent was optimised for the configuration of sensors used. The estimated location of the source versus the true location, calculated error and the optimised value of the path loss exponent are shown in Table 6.19 next:

Table 6.19. True versus estimated location when eight receiving nodes were used for the source position (4, 8).

True location		Estimated Location			
$X\ (m)$	$Y\ (m)$	$X\ (m)$	$Y\ (m)$	Error (m)	Optimum PLE α
4	8	4.62	6.72	1.42	2.90

The source location estimation shows the plausible results. The localization error is within the desired limit of two meters, and the optimised value of the PLE is below 3. The estimated location with the error calculation is shown in Figure 6.27 below:

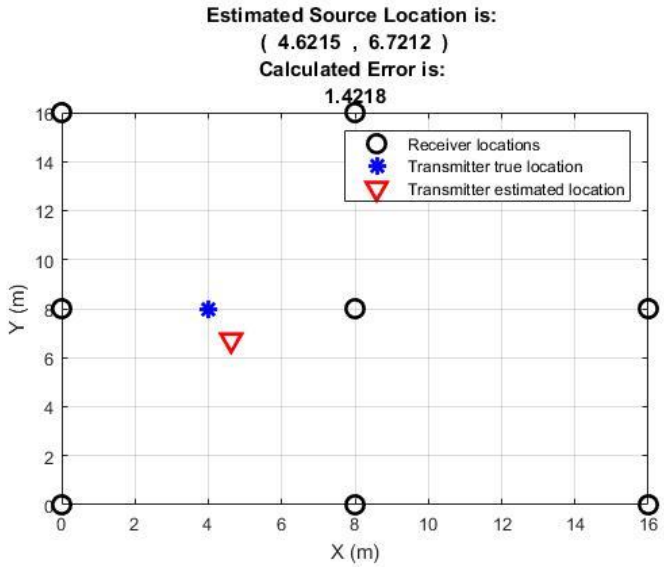

Figure 6.27. Source location estimation is shown when eight receiving nodes are used.

In the second configuration, the source position was chosen to be (8, 12). The location of the receiving nodes changed this time in such a way that node 7 was placed at location (8, 16) and node 8 was placed at location (16, 16). The source location estimation was performed as well as the path loss exponent was optimised. Table 6.20 next shows the true versus estimated location of the source, calculated error and the optimised value of PLE.

Table 6.20. Estimated components when eight receiving nodes were used.

True location		Estimated Location			
$X\ (m)$	$Y\ (m)$	$X\ (m)$	$Y\ (m)$	Error (m)	Optimum PLE α
8	12	6.46	13.11	1.89	3.10

The source location estimation and the calculated error are shown in Figure 6.28 below:

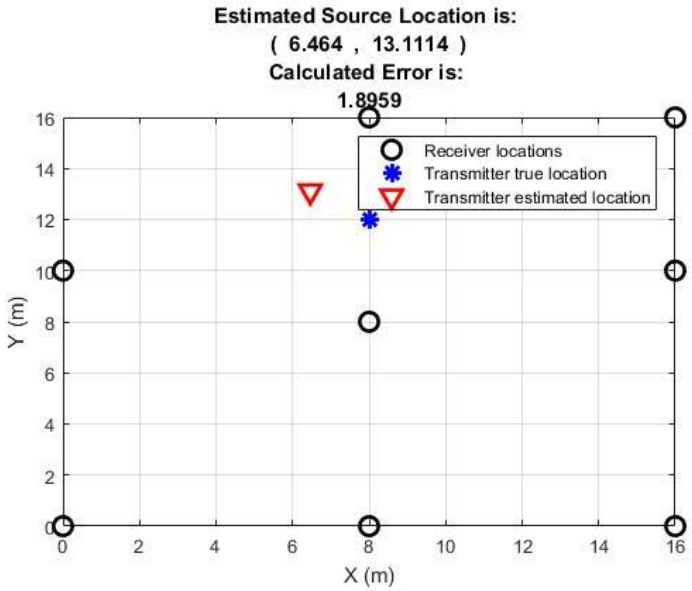

Figure 6.28. Illustration of source estimation using eight receiving nodes.

Figure 6.28 above shows satisfactory results. The error is nearly 1.90 meters which is below 2 meters, and the PLE value is nearly 3.

For the final configuration, by using eight receiving nodes, the source location was chosen as (14.2, 5.2). The receiving node configuration was changed, as shown in such a way that node 1 was placed at (0, 8) and node 8 was placed at (16, 0). The received signal strength in dBm for each of the nodes involved in the system is shown in Table 6.21 below:

Table 6.21. Received signal in dBm when eight receiving nodes were used.

Source Position	Node 1	Node 2	Node 3	Node 4	Node 5	Node 6	Node 7	Node 8
(14,5.2)	-13.50	-3.90	2.20	-15.90	-10.80	-9.90	-13.70	-5.30

Node 2, 3 and 8 are closer to the source. All three nodes have the highest signal strengths due to shorter distances. Node 4 is the farthest nod and has the least value of the received signal strength. Signals measurements were performed for several times, and in all cases, they remained very similar except for very small differences. The overall values shown in the above Table are the average of all received signal values. Table 6.22 below shows the estimated versus the true values as well as the error calculation and the PLE.

Table 6.22. True vs. estimated location, error calculation and PLE for the source position (14.2, 5.2) when eight receiving nodes were used.

True location		Estimated Location			
$X\ (m)$	$Y\ (m)$	$X\ (m)$	$Y\ (m)$	Error (m)	Optimum PLE α
14.2	5.2	13.25	6.40	1.54	2.55

Table 6.22 above shows the reasonable values of the estimated location and the path loss exponent. Having eight receiving nodes has a significant beneficial impact on localization accuracy and PLE optimisation.

6.1.3 Outdoor localization at TATA steel

Source localization performed at PNDC as explained in section 6.1.2 showed encouraging results. To further explore the algorithm, another outdoor environment was selected in the measurements were performed at TATA steel site in Port Talbot, Wales. To measure the performance of the algorithm, sensor nodes were deployed around the substation under various configurations. The performance evaluation was performed by using six, seven and eight receiving nodes at three different positions of the PD source.

6.1.3.1 Outdoor localization using six receiving nodes

Two different configurations were used when measurements were performed by using six receiving nodes. In the first configuration, the receiving nodes were placed at the location shown in Figure 6.29 below for the source locations (11.9, 2.7) and (8, 12) respectively.

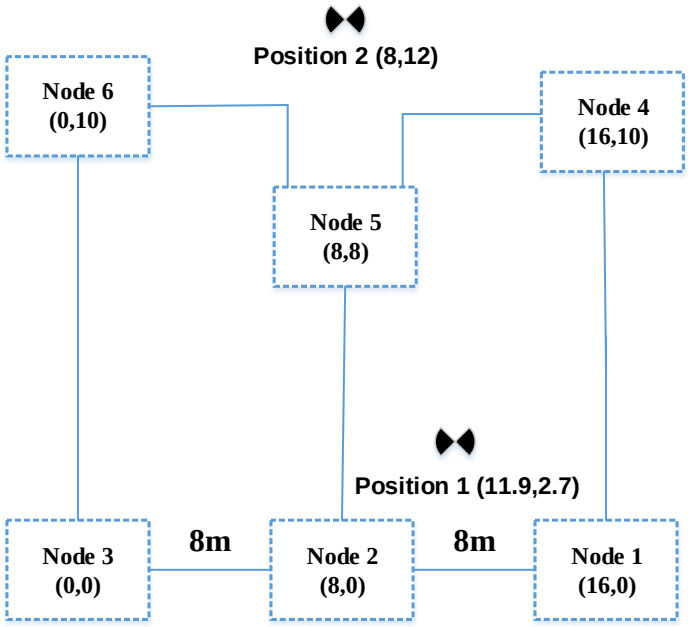

Figure 6.29. Sensors arrangements when six receiving nodes were used to locate PD.

A view of sensor deployment to measure the received signal is shown in Figure 6.30 below:

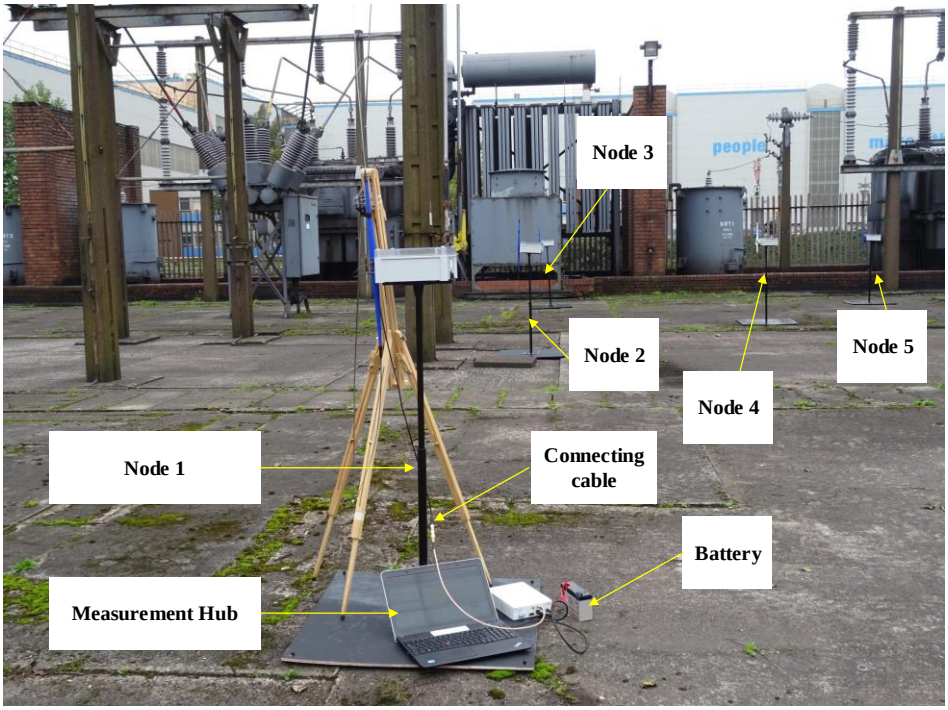

Figure 6.30. An example view of nodes deployment at TATA steel site.

Table 6.23 shows the received signal in dBm for both positions.

Table 6.23. Received signal in dBm for both positions using six receiving nodes

Source Position	Node 1	Node 2	Node 3	Node 4	Node 5	Node 6
Position 1	2.80	2.60	-9.20	-12.60	0.30	-14.10
Position 2	-9.0	-8.10	-9.10	-5.30	-3.00	-3.50

Table 6.24 shows a comparison between the true and estimated location.

Table 6.24. Comparison between true versus estimated locations when six receiving nodes at TATA steel.

	True location		Estimated Location			
Source Position	$X\ (m)$	$Y\ (m)$	$X\ (m)$	$Y\ (m)$	Error (m)	Optimum PLE α
Position 1	11.90	2.70	8.65	3.34	3.31	4.55
Position 2	8.0	12.0	6.64	16.49	4.69	4.75

Table 6.24 above shows a higher error than the desired value. This is mainly due to the limited number of receiving nodes used and also the geometry of the environment. Localization results for both positions are shown in Figures 6.31 and 6.32 respectively.

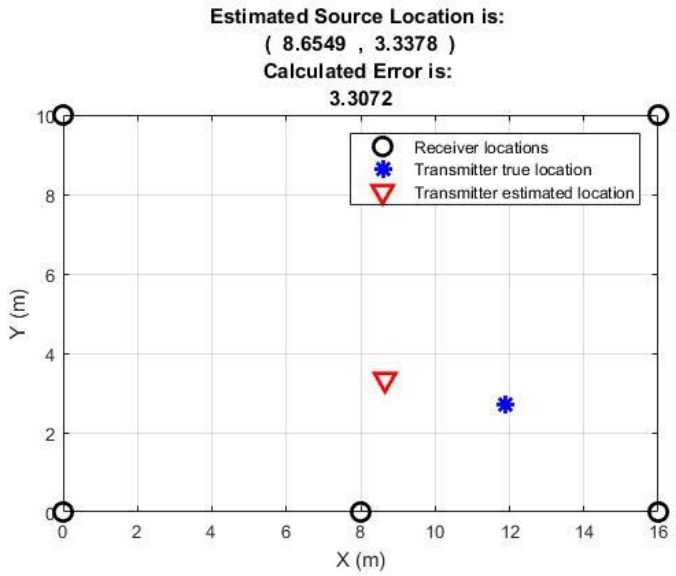

Figure 6.31. Source estimation using six receiving nodes at TATA steel for the position $(11.9, 2.7)$

Results for position 2 using six receiving nodes are shown in Figure 6.32 below:

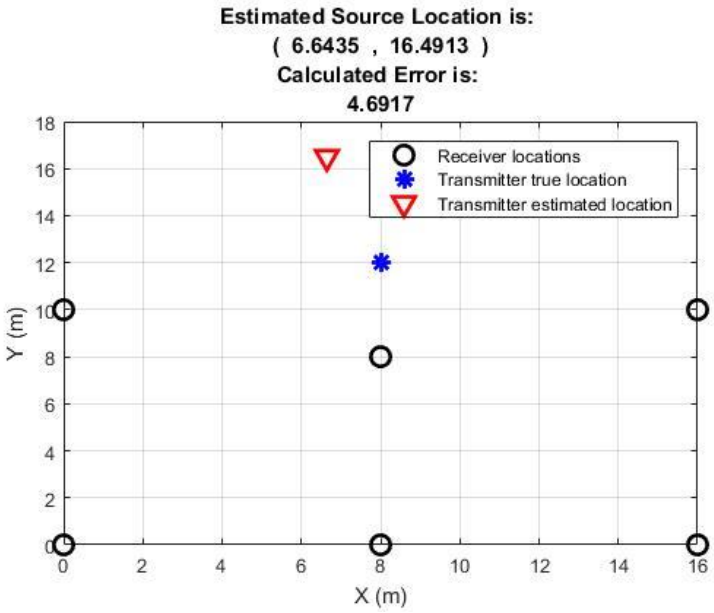

Figure 6.32. Source estimation using six receiving nodes at TATA steel for the position (8,12)

Although the above results show a relatively higher error value than the desired value, however, the performance of the algorithm was analysed by adding another receiving node to the system and by keeping the same source positions to see the effect of scalability on the localization error.

6.1.3.2 Outdoor localization using seven receiving nodes

To check if the increase in a number of receiving nodes will enhance the localization accuracy, another receiving node was added to the measurement system, and now seven nodes were used to receive the signal. The location of the source remained the same for both positions. Figure 6.33 shows the arrangement of receiving nodes.

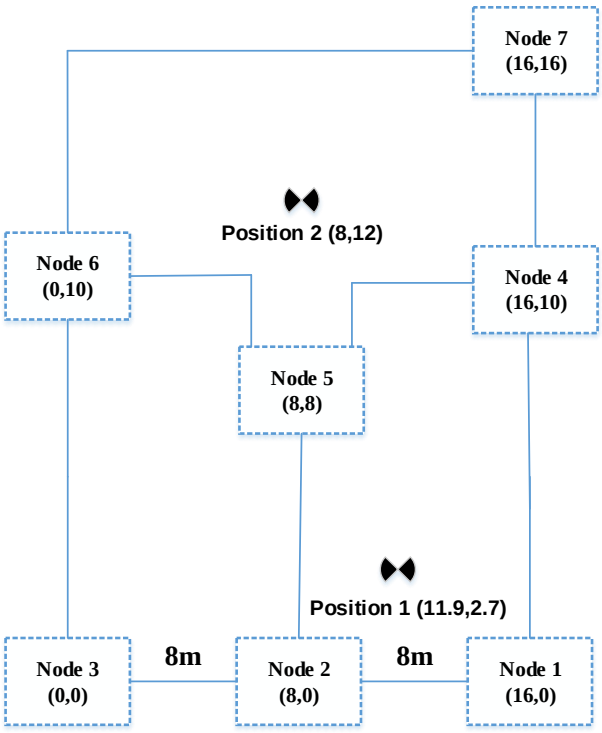

Figure 6.33. Seven receiving nodes arrangement at TATA steel.

An illustration of the sensors placed around the site is also shown in Figure 6.34 next.

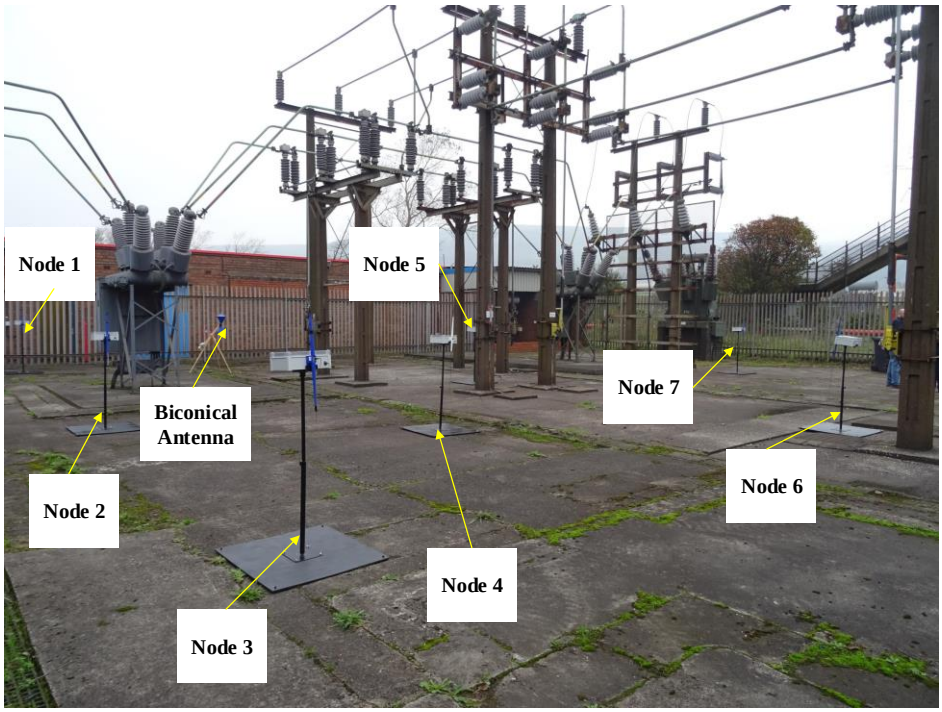

Figure 6.34. TATA steel measurement setup example.

The received signal in dBm for both positions is shown in Table 6.25 below:

Table 6.25. Received signal in dBm for both positions using six receiving nodes

Source Position	Node 1	Node 2	Node 3	Node 4	Node 5	Node 6	Node 7
Position 1	2.70	2.60	-9.25	-12.58	0.30	-14.10	-9.50
Position 2	-9.0	-8.10	-9.20	-5.30	-3.00	-3.46	-7.50

The true versus estimated location, error and PLE values for both positions are shown in Table 6.26 below:

Table 6.26. Comparison between true versus estimated locations when seven receiving nodes at TATA steel.

	True location		Estimated Location			
Source Position	$X\ (m)$	$Y\ (m)$	$X\ (m)$	$Y\ (m)$	Error (m)	Optimum PLE α
Position 1	11.90	2.70	10.97	3.87	1.50	2.55
Position 2	8.0	12.0	6.42	13.47	2.15	1.75

When the results of Table 6.26 are compared with the table 6.24 results, a significant improvement can be seen by just adding a single receiving node to the measurement system. For both positions, when seven receiving nodes were used, Figures 6.35 and 6.36 show the results respectively.

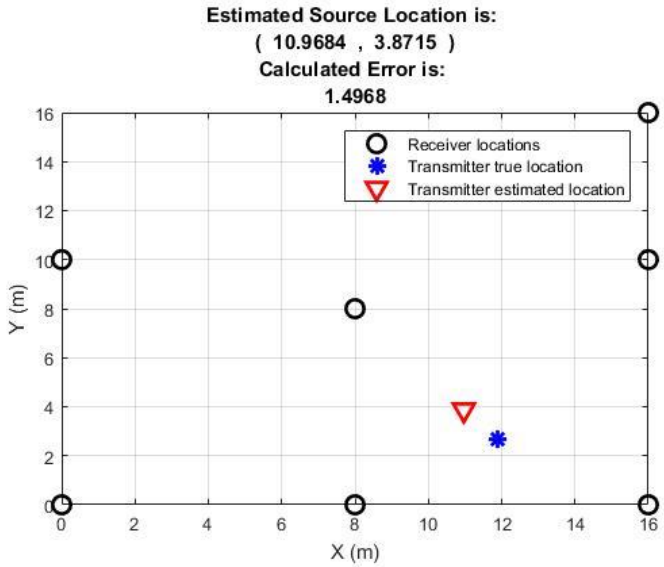

Figure 6.35. Results for the position $(11.90, 2.70)$ by using seven receiving nodes.

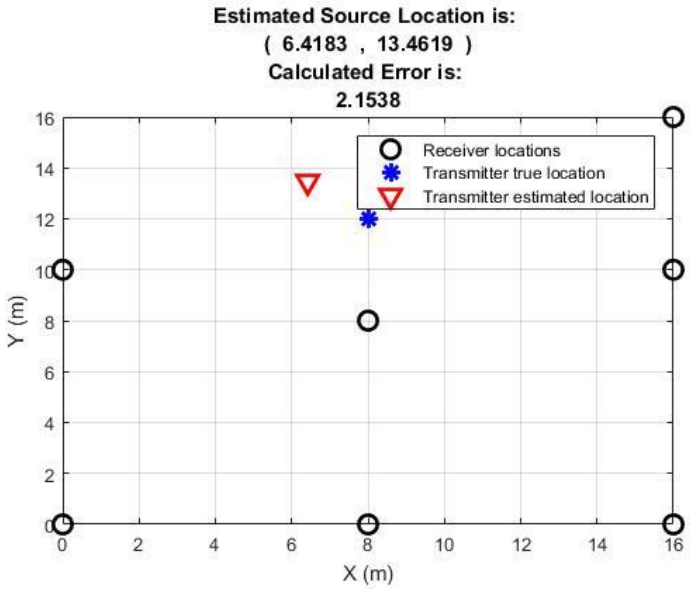

Figure 6.36. Results for the position (8,12) by using seven receiving nodes.

Both results are highly satisfactory when compared with the results obtained by using six measurement nodes. This ensures that in RSS based localization, scalability has a significant impact on localization accuracy and the PLE estimation. Localization was also performed for position 3, i.e. (3.7, 12.8). However, node 7 was placed at the position (8,16) instead of position (16,16). The received signal is shown in Table 6.27 below:

Table 6.27. Received signal using seven receiving nodes when seven nods were used at TATA steel

Source Position	Node 1	Node 2	Node 3	Node 4	Node 5	Node 6	Node 7
Position 3	-14.73	-5.91	-4.70	-9.40	0.80	2.60	-0.50

Comparison between estimated and the true locations is shown in Table 6.28 below:

Table 6.28. Comparison of true vs. estimated location for the source position (3.7, 12.8) when using seven receiving nodes.

	True location		Estimated Location			
Source Position	$X\ (m)$	$Y\ (m)$	$X\ (m)$	$Y\ (m)$	Error (m)	Optimum PLE α
Position 3	3.70	12.80	4.22	11.006	1.87	1.40

The result is also illustrated in Figure 6.37 below:

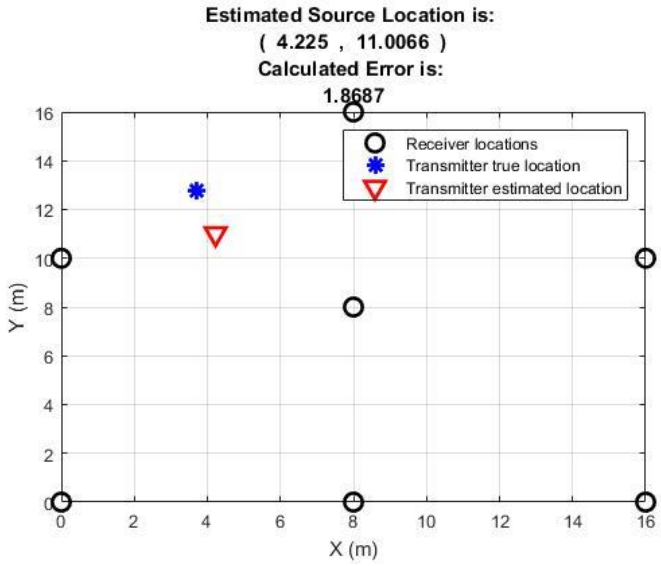

Figure 6.37. Results for position 3 when seven receiving nodes were used.

Finally, the performance of the algorithm was evaluated by using eight receiving nodes at the TATA steel for three positions. How the algorithm performed when compared with the performance when six and seven receiving nodes were used, is explained in the next section.

6.1.3.3 Outdoor localization using eight receiving nodes

The source location estimation at TATA steel site was performed by using eight measurement sensors for the same three positions. Figure 6.38 below shows the locations of the receiving nodes for the first two positions which include $(11.90, 2.70)$ and $(8, 12)$ respectively.

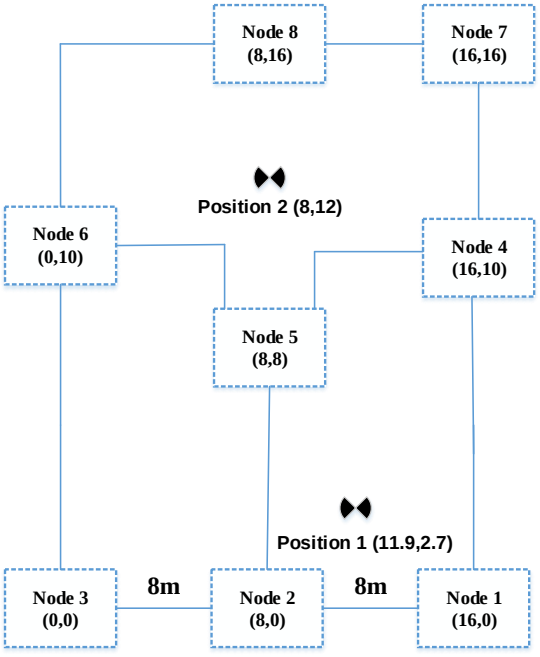

Figure 6.38. Receivers locations for the first two positions when eight nodes were used.

Receive signal in dBm for both positions is shown in Table 6.29 below:

Table 6.29. Received signal in dBm for both positions using six receiving nodes

Source Position	Node 1	Node 2	Node 3	Node 4	Node 5	Node 6	Node 7	Node 8
Position 1	2.80	2.60	-10.20	-12.60	0.30	-14.10	-9.50	-8.1
Position 2	-9.0	-8.10	-9.10	-5.30	-3.00	-3.50	-7.50	1.9

True versus estimated locations comparison is shown in Table 6.30 below:

Table 6.30. Comparison between true versus estimated locations when six receiving nodes at TATA steel.

	True location		Estimated Location			
Source Position	$X\ (m)$	$Y\ (m)$	$X\ (m)$	$Y\ (m)$	Error (m)	Optimum PLE α
Position 1	11.90	2.70	11.60	4.11	1.44	1.65
Position 2	8.0	12.0	6.46	13.11	1.89	1.55

For both positions, Figures 6.39 and 6.40 respectively, show the results

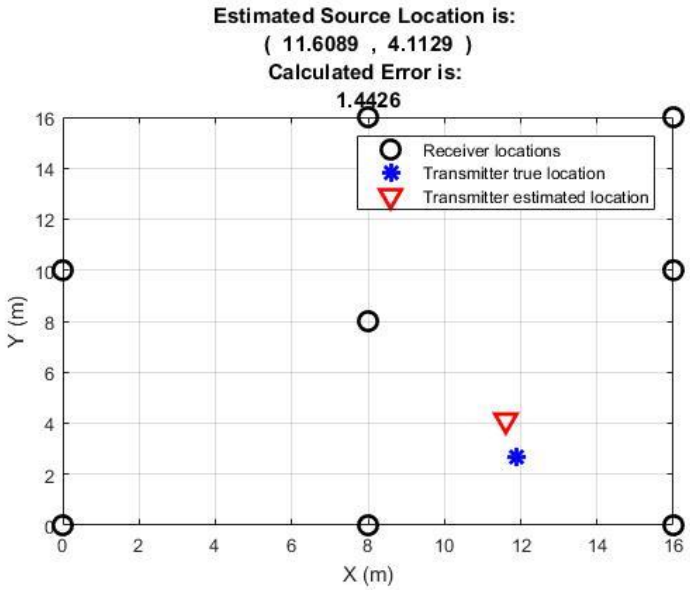

Figure 6.39. Position 1 results using eight receiving nodes.

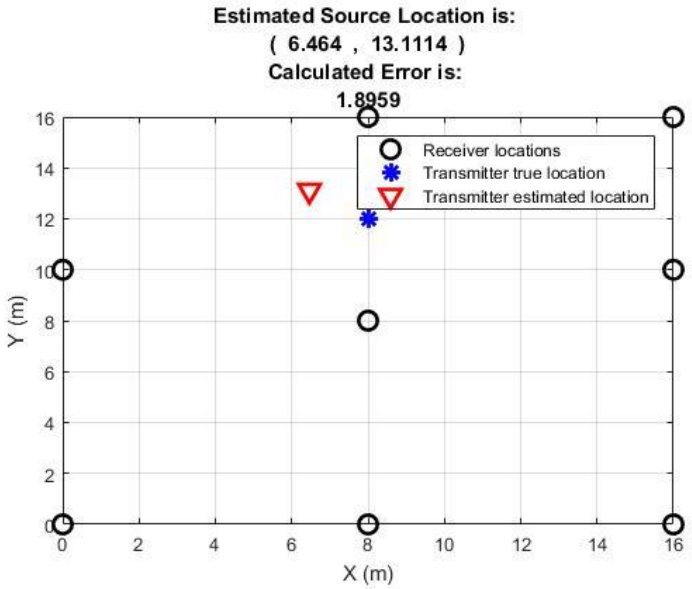

Figure 6.40. Position 2 results using eight receiving nodes.

In both cases, localization accuracy has improved. For position 1, localization error has reduced from 1.50 meters to 1.44 meters, and for position 2, the error has reduced from 2.15 meters to 1.89 meters. For position 3, locations of the first six nodes remained the same and nodes 7 and 8 were placed at $(8,16)$ and $(0,16)$ respectively. The received signal in dBm for position 3 is shown in Table 6.31below:

Table 6.31. Received signal using seven receiving nodes when eighth nodes were used at TATA steel

Source Position	Node 1	Node 2	Node 3	Node 4	Node 5	Node 6	Node 7	Node 8
Position 3	-9.70	-5.90	-4.70	-9.40	0.80	2.60	-0.50	0.20

Comparison between estimated and the true locations is shown in Table 6.32 below:

Table 6.32. Position 3 results using eight receiving nodes.

	True location		Estimated Location			
Source Position	$X\ (m)$	$Y\ (m)$	$X\ (m)$	$Y\ (m)$	Error (m)	Optimum PLE α
Position 3	3.70	12.80	3.66	11.1	1.71	2.0

There is an improvement in localization accuracy. The error was reduced from 1.87 meters to 1.71 meters. Figure 6.41 below shows the estimated location and the calculated error.

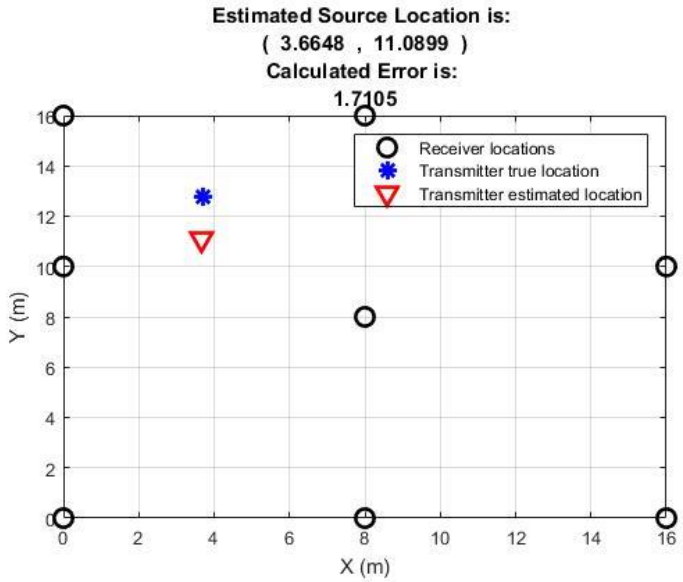

Figure 6.41. Estimated location and error calculation for position 3.

When six, seven and eight receiving nodes were used, it is clear from the results that every time a node is added in the measurements system, the localization accuracy is improved and the PLE was optimised to converge to the average value of the propagation environment.

6.2 Chapter 6 summary

To evaluate the performance of the algorithm, measurements were taken in a substation environment for indoor and outdoor localization of the source by using the radiometric sensors described in Chapter 5. Indoor measurements were performed in the University of Huddersfield sports hall, and outdoor measurements were performed at the University of Strathclyde and Scottish Power PNDC and TATA steel sites at Port Talbot, Wales site. Indoor and outdoor localization results give highly encouraging results by using the proposed algorithm. There were a range of configurations used as well as a number of sensors for each configuration. Estimated source locations, calculated errors and optimised values of estimated PLE for each of the source position are given in the corresponding Tables. It can be concluded that field trials were highly successful and localization results achieved are very satisfactory.

Chapter 7: PERFORMANCE EVALUATION OF THE PROPOSED ALGORITHM WITH OTHER ALGORITHMS

The performance of the proposed algorithm was evaluated against the ratio and search and least squares (LS) algorithms. All three algorithms use RSS for localization in an anonymous environment i.e. having no prior information of source transmitted power and path loss exponent. The performance of the algorithms was evaluated in terms of localization error and optimised estimated values of the path loss exponent in three field-trial scenarios. The least squares algorithm is quite simple and does not optimise the path loss exponent. The proposed algorithm and ratio and search algorithms both optimise the value of path loss exponent within a given range as described in chapter 4.

7.1.1 Performance evaluation by using six receiving nodes based on indoor results obtained at University of Huddersfield sports hall.

When six measurement nodes were used, the comparison of true versus estimated locations between the three algorithms is shown in Table 7.1.

Table 7.1 Comparison of estimated versus true location with six measurement sensors for three algorithms.

	Actual Locations		LS Estimated Locations		R&S Estimated Locations		Proposed algorithm Estimated Locations	
Source position	$X\ (m)$	$Y\ (m)$	$X\ (m)$	$Y\ (m)$	$X\ (m)$	$Y\ (m)$	$X\ (m)$	$Y\ (m)$
1	13.50	4.50	10.32	6.05	10.19	5.50	10.30	7.62
2	4.50	4.50	6.93	7.63	6.95	7.08	7.04	6.56
3	4.50	13.50	4.30	16.12	5.27	15.32	5.90	13.08
4	13.50	13.50	9.18	12.57	9.18	12.57	8.68	11.95
5	10.00	6.00	8.82	8.49	8.82	8.49	8.75	8.66
6	6.00	8.00	6.85	9.32	6.85	9.32	6.29	9.17
7	8.00	12.00	7.80	11.97	7.80	11.97	7.38	11.57
8	12.00	10.00	9.04	10.51	9.04	10.51	8.91	9.84
9	4.50	-4.50	8.42	6.24	6.41	0.79	7.64	-3.23

Table 7.1 shows true versus estimated locations of three algorithms rounded to two decimal places. It is worth mentioning that all three algorithms do not have any prior information about the path loss exponent parameters. For each of the three algorithms, errors are calculated for three scenarios and are compared for each position in Tables 7.2, 7.3 and 7.4 that show the error comparison.

Table 7.2 Error comparison for 6 measurement sensors.

Source position	LS Error (m)	R&S Error (m)	Proposed algorithm Error (m)
1	3.54	3.46	4.47
2	3.96	3.56	3.27
3	3.63	1.98	1.46
4	4.42	4.42	5.06
5	2.98	2.76	2.60
6	1.57	1.57	1.21
7	0.20	0.50	0.75
8	3.00	3.00	3.09
9	4.43	5.62	3.39
Mean Error	3.08	2.98	2.81

From the computed errors shown in Table 7.2 above, it is clear that the LS algorithm has the maximum error and the mean error computed is 3.08 meters. Ratio and search and the proposed algorithms deliver mean errors of 2.95 and 2.81 meters respectively. These error values are appropriate considering the number of receiving nodes used are only six in this case. The error comparison is illustrated in Figure 7.1 below:

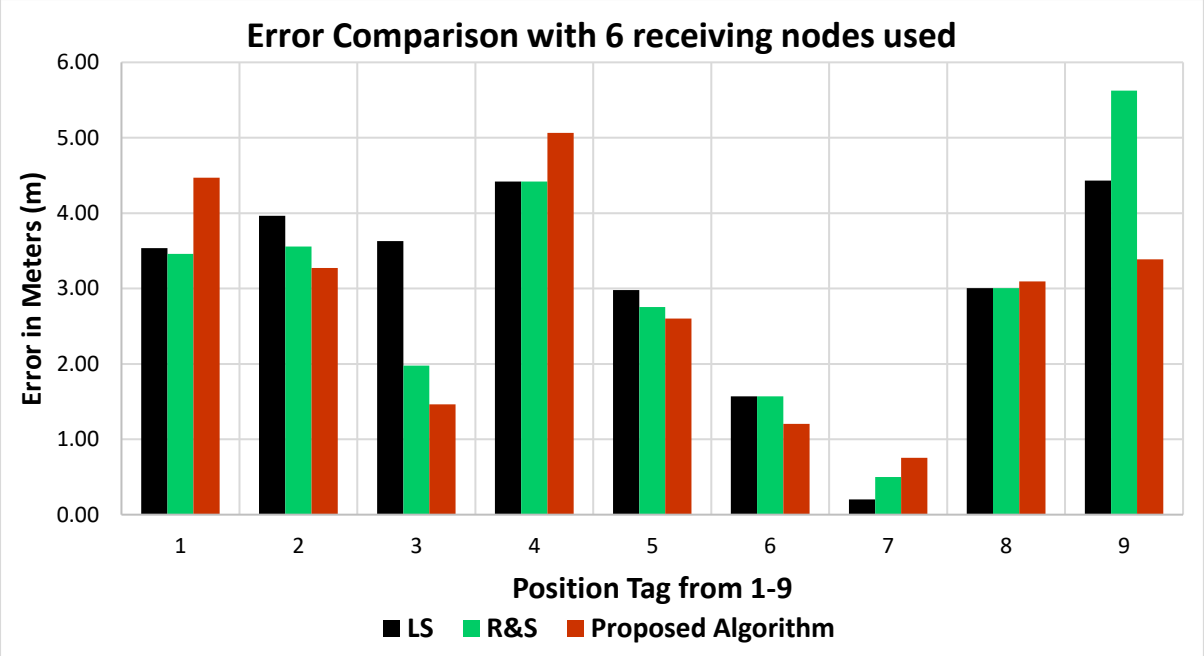

Figure 7.1. Error comparison between the three algorithms when six receiving nodes were used.

The performance in terms of the path loss exponent was also evaluated. For the LS algorithm, it does not matter to a great extent because the algorithm does not optimise the PLE. The chosen value for the algorithm was 2 because it is the closest average value of the propagation environment. Table 7.3 shows the comparison between the optimised values of the PLE for each algorithm when six receiving nodes were used.

Table 7.3 PLE comparison for six measurement sensors.

Source Position	LS α_{OPT}	R&S α_{OPT}	Proposed Algorithm α_{OPT}
1	2	2.7	2.7
2	2	2.95	3.1
3	2	3.35	4.5
4	2	5	5
5	2	5	5
6	2	5	5
7	2	5	4.7
8	2	5	5
9	2	2.8	4.65

Table 7.3 summarises the optimised values of the PLE. For the ratio and search and the proposed algorithm, the PLE remains high for the majority of the positions. The optimised value should improve by increasing the number of receiving nodes, however, by using only six receiving nodes, it remains a bit high than the desired value of around 2 to 3. Performance evaluation of the algorithm by using seven receiving nodes is discussed next.

7.1.2 Performance evaluation by using seven receiving nodes.

When seven measurement nodes were used, the comparison of true versus estimated locations between the three algorithms is shown in Table 7.4 below:

Table 7.4. Comparison of estimated versus true location with seven measurement sensors.

	Actual Locations		LS Estimated Locations		R&S Estimated Locations		Proposed algorithm Estimated Locations	
Source Position	$X\ (m)$	$Y\ (m)$	$X\ (m)$	$Y\ (m)$	$X\ (m)$	$Y\ (m)$	$X\ (m)$	$Y\ (m)$
1	13.50	4.50	11.88	4.77	12.08	4.82	12.37	4.49
2	4.50	4.50	5.55	5.19	5.26	5.58	5.99	5.02
3	4.50	13.50	7.07	12.66	4.33	14.87	5.41	13.76
4	13.50	13.50	12.60	13.77	11.63	14.56	10.94	15.48
5	10.00	6.00	11.99	8.20	12.64	8.88	12.65	6.95
6	6.00	8.00	5.80	8.75	5.40	9.86	6.60	8.50
7	8.00	12.00	11.64	12.45	7.86	14.59	7.89	13.89
8	12.00	10.00	13.35	11.71	12.57	12.31	13.16	10.86
9	4.50	-4.50	3.78	-6.73	3.46	-5.40	3.14	-6.43

Estimated location values shown in Table 7.4 above are rounded to two decimal places. Comparing the true versus estimated locations, it is evident that all three algorithms estimate the coordinates of the source within reasonable accuracy. For the majority of the locations, the estimated versus the true locations seem reasonably close. A comparison of error calculation for each position when seven measurement sensors are used is shown in Table 7.5 next.

Table 7.5 Error Comparison for seven measurement sensors.

Source Position	LS Error (m)	R&S Error (m)	Proposed algorithm Error (m)
1	1.65	1.45	1.13
2	1.26	1.32	1.57
3	2.70	1.38	0.94
4	0.94	2.15	3.23
5	2.97	3.91	2.81
6	0.78	1.95	0.78
7	3.66	2.60	1.90
8	2.18	2.38	1.45
9	2.34	1.37	2.36
Mean Error	2.05	2.06	1.80

Table 7.5 shows the error comparison for each position. The results show that for the majority of the positions, the proposed algorithm offers better accuracy and lower mean error.

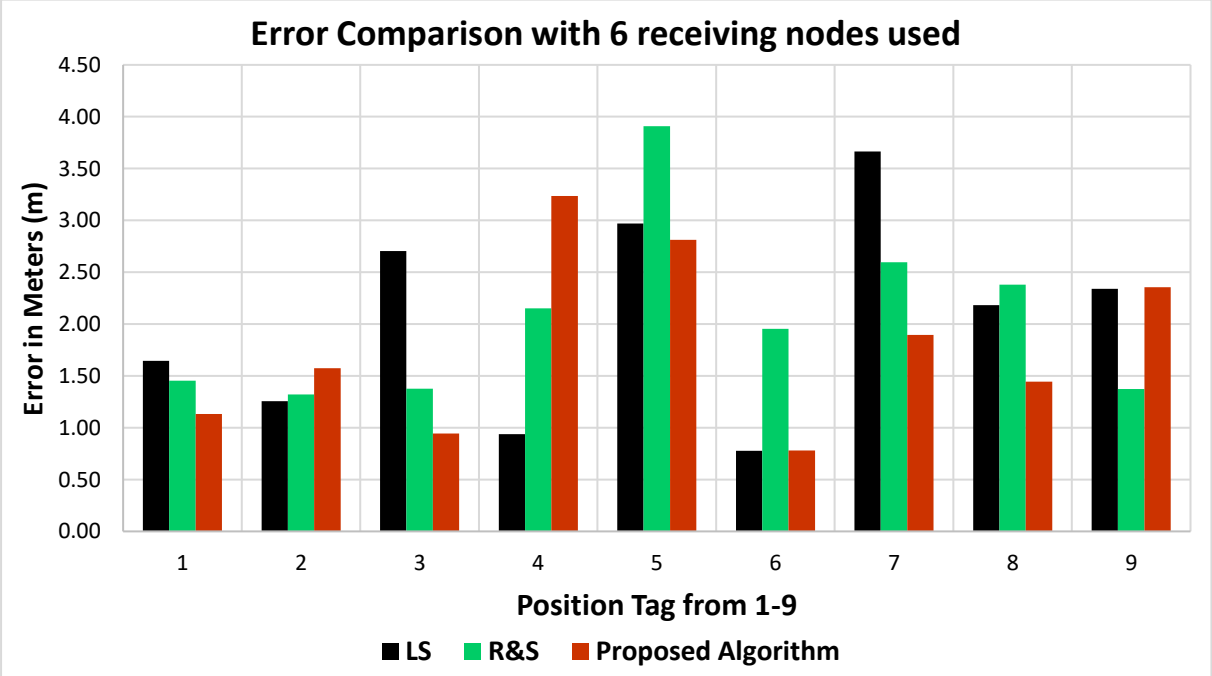

Figure 7.2 Error Comparison with seven measurement sensors used.

An error comparison between the algorithms can be seen in Figure 7.2 above, where seven measurement sensors were used.

From the above comparison, it is evident that the proposed algorithm offers the least error when compared with the other algorithms. Also comparing results with Figure 7.1, the localization accuracy has improved for the majority of the positions and the mean localization error reduced as well. This ensures that an increase in a single node in the receiving system enhances the overall localization accuracy. The path PLE comparison between three algorithms when seven receiving nodes were used is shown in Table 7.6 below:

Table 7.6 PLE Comparison for seven measurement sensors.

Source Position	LS α_{OPT}	R&S α_{OPT}	Proposed Algorithm α_{OPT}
1	2	1.65	1.75
2	2	2.15	2.15
3	2	3.20	3.45
4	2	1.50	4.25
5	2	1.50	1.60
6	2	2.50	2.05
7	2	3.20	3.30
8	2	2.80	2.60
9	2	2.80	2.75

Results for the optimised value of PLE when seven receiving nodes were used are far better and improved when compared with the results of Table 7.3. It validates that an increase in a number of receivers improves the accuracy as well as PLE is optimised as well to converge closer to the average PLE value of the propagation environment.

7.1.3 Performance evaluation by using eight receiving nodes.

To evaluate the performance of the proposed algorithm further, a node is added in the receiving system and this time eight measurement sensors are used. A comparison between the estimated and true locations has been made and error is computed for each position as well as the optimised PLE. When eight measurement sensors are used, the comparison between the true and estimated locations for each algorithm is shown in Table 7.7.

Table 7.7 Comparison of estimated versus true locations with eight measurement sensors

	Actual Locations		LS Estimated Locations		R&S Estimated Locations		Proposed algorithm Estimated Locations	
Source Position	$X\ (m)$	$Y\ (m)$	$X\ (m)$	$Y\ (m)$	$X\ (m)$	$Y\ (m)$	$X\ (m)$	$Y\ (m)$
1	13.50	4.50	12.04	4.69	12.21	4.77	12.44	4.45
2	4.50	4.50	5.41	5.27	5.38	5.52	5.73	5.22
3	4.50	13.50	4.91	14.26	4.33	14.63	4.12	14.72
4	13.50	13.50	11.89	14.11	11.68	14.50	11.35	15.24
5	10.00	6.00	11.81	8.67	12.55	9.25	12.58	7.20
6	6.00	8.00	5.15	9.26	5.45	9.86	5.63	9.68
7	8.00	12.00	8.80	15.21	7.89	14.60	8.95	13.86
8	12.00	10.00	13.32	11.86	12.53	12.37	13.18	10.83
9	4.50	-4.50	3.91	-7.91	3.91	-5.60	3.97	-5.63

Table 7.7 results are based on eight receiving nodes. With the addition of a single node to the receiving system, the source location estimations have improved for the majority of positions for the ratio and search and the proposed algorithms. An error comparison between three algorithms when eight receiving nodes were used is shown in Table 7.8 next.

Table 7.8 Error comparison for eight measurement sensors.

Source Position	LS Error (m)	R&S Error (m)	Proposed algorithm Error (m)
1	1.47	1.32	1.06
2	1.19	1.35	1.43
3	0.86	1.15	1.28
4	1.72	2.08	2.77
5	3.22	4.13	2.85
6	1.52	1.94	1.72
7	3.31	2.60	2.08
8	2.28	2.43	1.44
9	3.46	1.25	1.24
Mean Error	2.11	2.03	1.76

The least squares algorithm performance has improved for positions 1, 2 and 3, however, the mean error has slightly increased although not to a great extent. This is mainly because the least squares algorithm does not optimise the PLE. For the ratio and search and the proposed algorithm, the results have improved in terms of localization accuracy for the majority of the positions with a lower mean error for all nine positions. For the ratio and search algorithm the mean error has slightly improved i.e. from 2.06 to 2.03 an improvement of 0.03 meters. For the proposed algorithm, the mean error has improved from 1.80 meters to 1.76 meters i.e. an improvement of 0.04 meter. This shows that by increasing the number of nodes, the overall location accuracy of the PD source estimation is improved. An error comparison between the algorithms can be seen in Figure 7.3, where eight measurement sensors were used.

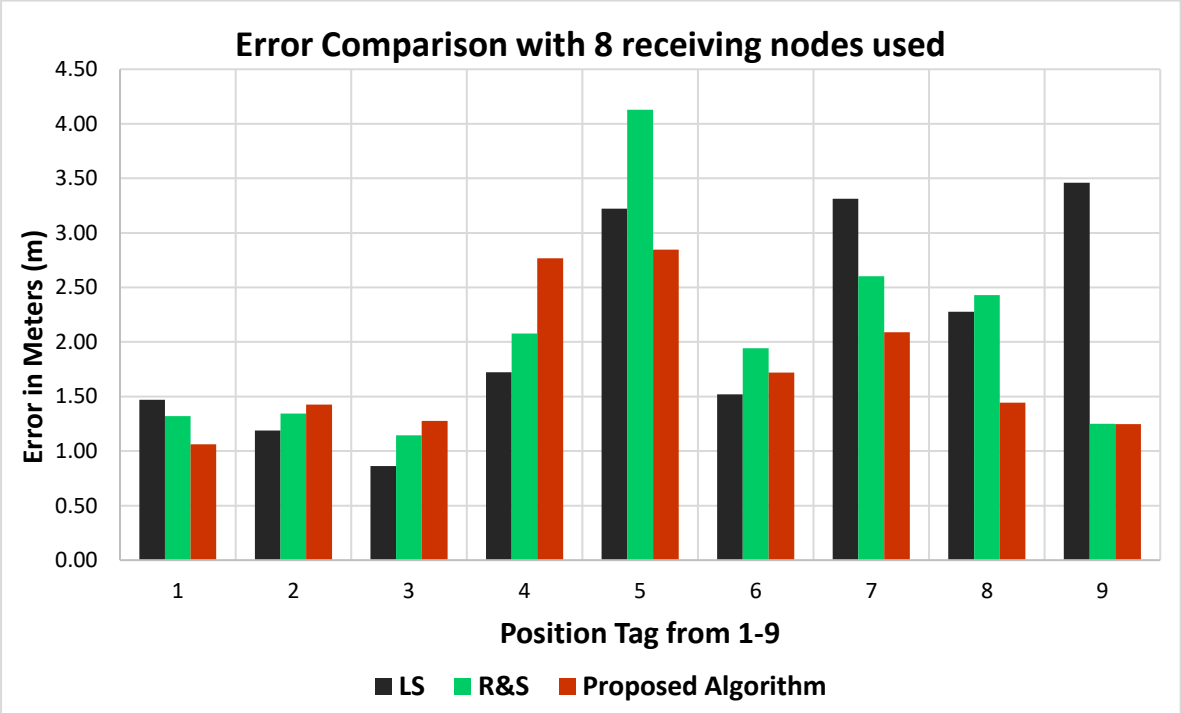

Figure 7.3 Error Comparison with eight measurement sensors used.

Finally, Table 7.9 shows the PLE comparison between the three algorithms when eight receiving nodes were used.

In Table 7.9 next, the optimised value of PLE remains between 2 and 3 for eight out of the nine positions for the proposed and the ratio and search algorithms. Localization errors have improved as well from the proposed algorithm. This means that an increase in the receiving nodes has a positive effect on the overall accuracy as well as the PLE optimisation.

Table 7.9 PLE Comparison for eight measurement sensors.

Source Position	LS α_{OPT}	R&S α_{OPT}	Proposed Algorithm α_{OPT}
1	2	1.65	1.75
2	2	2.15	2.20
3	2	3.20	2.80
4	2	1.50	3.55
5	2	1.50	1.55
6	2	2.50	2.50
7	2	3.20	2.95
8	2	2.80	2.70
9	2	2.80	2.85

A graph of mean error versus the changing number of receivers is given below

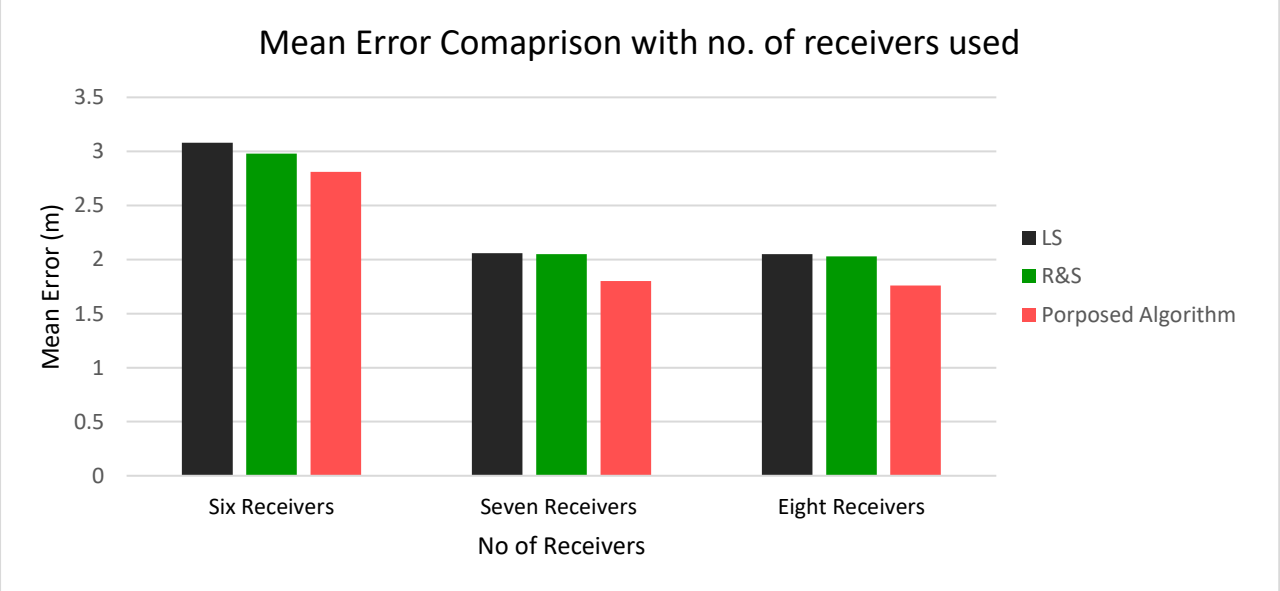

Figure 7.4. Mean error VS changing number of receivers.

The performance evaluation in outdoor environment is described next.

7.1.4 Performance evaluation in outdoor environment using six receiving nodes.

Performance evaluation of the algorithms was also performed for outdoor measurements. The results obtained by using six and eight measurement nodes were compared to evaluate the proposed algorithm with the ration and search and leas squares algorithm.

When six measurement nodes were used, the comparison of true versus estimated locations between the three algorithms is shown in Table 7.10.

Table 7.10. Estimated VS true locations using six sensors in outdoor environment.

	Actual Locations		LS Estimated Locations		R&S Estimated Locations		Proposed algorithm Estimated Locations	
Source position	$X\ (m)$	$Y\ (m)$	$X\ (m)$	$Y\ (m)$	$X\ (m)$	$Y\ (m)$	$X\ (m)$	$Y\ (m)$
1	2.90	3.00	4.40	3.36	3.35	7.67	3.23	5.30
2	12.30	1.70	12.20	7.63	11.89	7.89	10.50	2.77
3	4.00	8.00	4.60	12.20	3.92	11.02	4.55	7.19
4	12.00	8.00	13.89	9.97	13.04	10.60	11.83	7.85
5	11.90	2.70	7.23	2.10	8.40	3.95	8.65	3.34
6	8.00	12.00	4.96	16.88	7.10	15.90	6.64	16.49

Table 7.10 shows true versus estimated locations of three algorithms rounded to two decimal places for outdoor measurements. Calculated errors for four positions when six measurement nodes were uses are shown in Table 7.11 that show the error comparison.

Table 7.11. Error comparison between three algorithms when six sensors used in outdoor environment.

Source position	LS Error (m)	R&S Error (m)	Proposed algorithm Error (m)
1	1.55	4.68	2.32
2	3.34	6.02	2.09
3	4.24	3.02	0.98
4	2.72	2.80	0.23
5	3.80	3.92	3.31
6	5.11	4.32	4.69
Mean Error	3.46	4.13	2.27

From the computed errors shown in Table 7.11 above, it is clear that the proposed algorithm has the minimum mean error which is 2.27 meters. Ratio and search has the highest mean error which is 4.13 meters and the least squares has the mean error of 3.46 meters. The error comparison is illustrated in Figure 7.5 below:

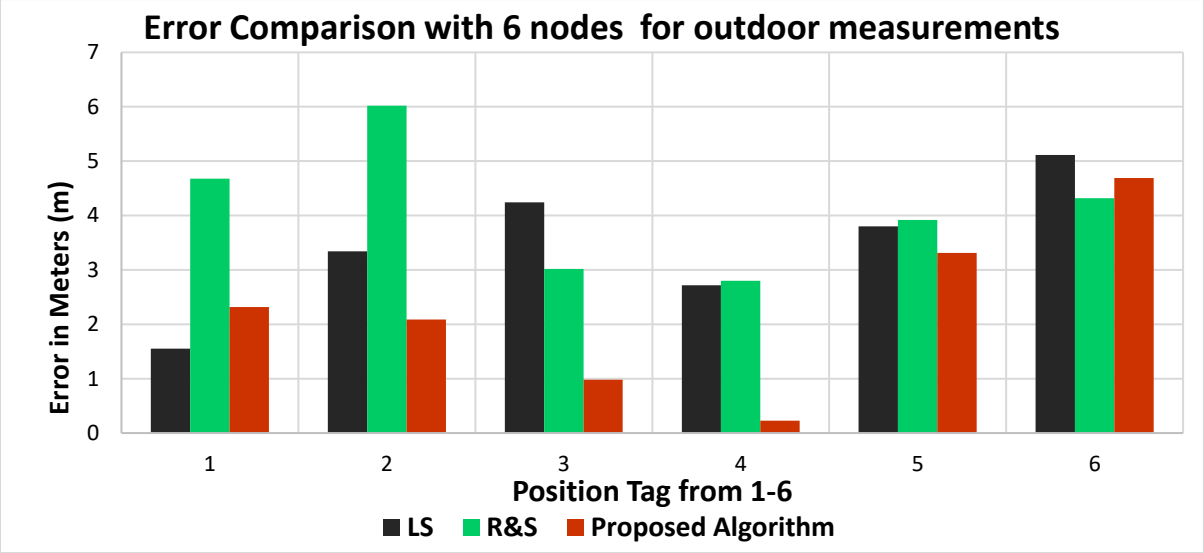

Figure 7.5. Outdoor measurements error comparison using six receivers.

The performance in terms of the path loss exponent was also evaluated. Similar to indoor measurement, the LS algorithm does not have any effect in terms of PLE optimisation. Table 7.12 shows the comparison between the optimised values of the PLE for each algorithm when six receiving nodes were used.

Table 7.12. PLE comparison between three algorithms.

Source Position	LS α_{OPT}	R&S α_{OPT}	Proposed Algorithm α_{OPT}
1	2	1.00	2.75
2	2	1.50	3.50
3	2	3.10	2.70
4	2	3.70	3.10
5	2	4.30	3.70
6	2	3.85	3.10

Table 7.12 summarises the optimised values of the PLE. Performance evaluation of the algorithm by using eight receiving nodes is discussed next.

7.1.5 Performance evaluation by using eight receiving nodes.

To evaluate the performance of the proposed algorithm further, a node is added in the receiving system and this time eight measurement sensors are used. Table 7.13 shows the comparison between three algorithms for three different positions.

Table 7.13. Comparison of estimated versus true location with eight measurement sensors in outdoor environment.

	Actual Locations		LS Estimated Locations		R&S Estimated Locations		Proposed algorithm Estimated Locations	
Source Position	$X\ (m)$	$Y\ (m)$	$X\ (m)$	$Y\ (m)$	$X\ (m)$	$Y\ (m)$	$X\ (m)$	$Y\ (m)$
1	4.00	8.00	5.40	6.70	4.92	7.12	4.62	6.72
2	12.00	8.00	9.90	5.55	10.69	9.93	6.46	13.11
3	14.20	5.20	12.88	3.97	12.21	7.25	13.25	6.40
4	11.90	2.70	13.10	1.98	11.95	4.47	11.60	4.11
5	8.0	12.0	7.00	13.51	6.56	13.35	6.46	13.11
6	3.70	12.80	2.91	10.88	4.12	10.98	3.66	11.10

Table 7.14 below shows the error comparison for three algorithms as calculated on the basis of the above estimated values.

Table 7.14 Error comparison for eight measurement sensors in outdoor environment.

Source Position	LS Error (m)	R&S Error (m)	Proposed algorithm Error (m)
1	1.90	1.28	1.42
2	3.29	2.33	1.89
3	1.80	2.85	1.54
4	1.49	1.57	1.44
5	2.51	2.15	1.89
6	2.13	1.92	1.71
Mean Error	2.35	2.09	1.65

The mean error calculated for three postions when eight measurement nodes were used again shows that the proposed algorithm performs better than both LS and R&S algorithms with the mean localization error of 1.65 meters. Figure 7.6 shows the error comparison where eight measurement sensors were used.

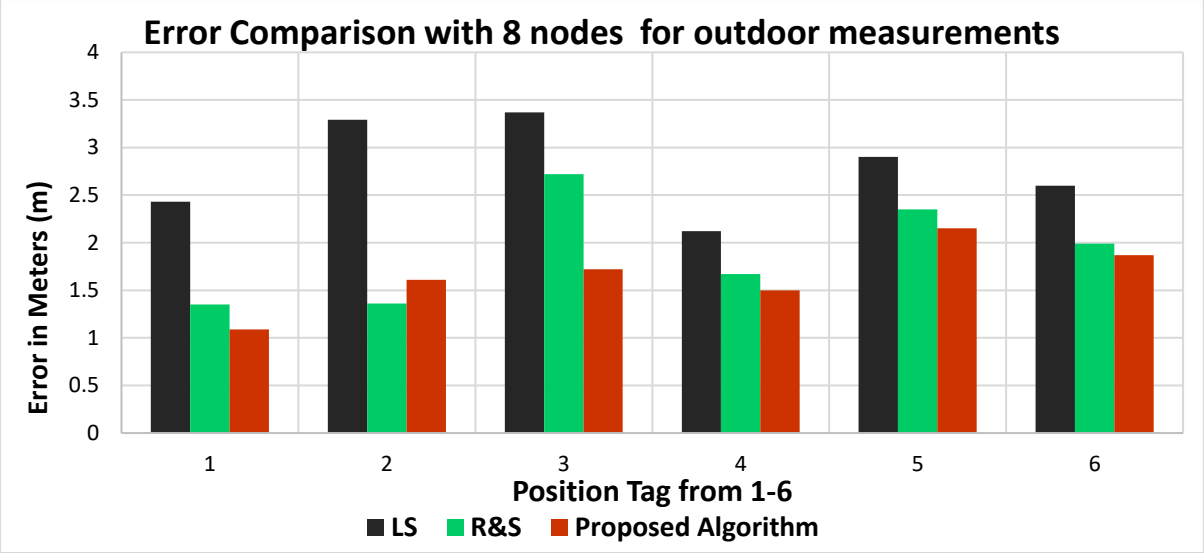

Figure 7.6. Mean error comparison when eight nodes were used in outdoor environment.

Finally, Table 7.15 shows the PLE comparison between the three algorithms when eight receiving nodes were used.

Table 7.15. PLE comparison using eight receiving nodes in outdoor environment.

Source Position	LS α_{OPT}	R&S α_{OPT}	Proposed Algorithm α_{OPT}
1	2	2.45	2.75
2	2	2.95	3.50
3	2	3.75	3.50
4	2	2.45	1.65
5	2	1.95	1.55
6	2	2.30	2.00

The average PLE values seems much closer to the average value of the propagation environment.

7.2 Chapter 7 summary

Evaluation of the proposed algorithm against the LS and the ratio and search algorithms was performed in termed of source location estimation, computed error and the optimised values of the PLE. The LS algorithm does not optimise PLE though. With six, seven and eight receiving nodes used, the results obtained show that the proposed algorithm performs better for the majority of the positions when compared with other algorithms. Overall it can be said that RSS

based localization proves a potential technique for future autonomous and continuous monitoring of PD in substations.

Chapter 8: CONCLUSION AND FUTURE WORK

8.1 Conclusion

There is an exponential growth in demand and supply of electricity. Safe and uninterrupted supply is now paramount to ensure the smooth running of systems. The dependency amongst various systems has even increased the need for safety and reliability more than before. Electrical equipment manufacturers need to ensure that the equipment used is efficient and cost-effective.

Safe and reliable operation of HV is highly dependent on the insulation materials used for equipment manufacturing. Due to loads and stresses as well as ageing, insulation materials deteriorate with time. This may lead to unexpected failures and outages of the equipment which can lead to power disruptions and catastrophic failures resulting in economic, energy or even losses. This brings the need to continuously monitor the health of HV systems to ensure that if there is any unexpected behaviour that it is fixed and thus revenue losses can be avoided. Partial discharge detection and localization is one of the most useful and important ways to prevent such outages and failures. Partial discharge is a process of ionization that can take place in HV systems due to various reasons such as voids, joints, and treeing. If the discharge is kept unresolved, it will lead to a change in the structure of the insulation materials and will eventually cause the failure of the system. Power companies have the mechanisms in place to monitor the health of the systems, but only on a periodic basis and not continuously.

In this research, a range of PD detection and localization mechanisms have been explored including TOA, TDOA, AOA, acoustic emissions etc. Some of these methods are commercially used by the power companies to monitor the health of the HV systems. None of these methods have been employed for continuous monitoring due to their complexity for PD type applications. One of the main challenges in PD detection is the duration of the PD pulse; it occurs for a very short duration which can be very low or less than 1ns. For example, the TOA method proves expensive due to time based synchronizations between the source and the receiving nodes. A small synchronization error can lead to big localization errors. Similarly, the TDOA mechanism although it does not require source synchronization, however, still there is a need for time synchronization between node pairs as it works on the difference of the arrival

time of the EM wave. The AOA technique is also not easy to implement as it requires an array of antennas and line of sight (LOS) to the source.

Considering that the need for continuous PD monitoring is critically important, there was a requirement to explore a method that uses just the energy of the pulse. RSS based localization explored in this study uses energy of the received signal. In this study, a signal propagated by the source is captured, and its received energy is converted into distance by an algorithm that has as input the power signal levels. The RSS based technique is the simplest of the available techniques, easy to implement and cost-effective for the following reasons:

- In RSS based localization there is no requirement of the source and nodes time synchronization because the technique processes the energy on the signals rather than the pulse of the PD pulse.
- In RSS based localization, LOS is again not very important in contrast to the techniques where LOS is a key requirement.
- Due to the lack of synchronization requirement, scalability does not remain an issue in RSS based localization. If the scope of the problem gets bigger due to more area coverage, an additional receiving node can be added in the receiving systems without any modification requirements.
- Due to the simplicity of the technique, it is a cost-effective technique and easy to implement in harsh industrial environments such as localization of PD sources.

8.1.1 Conclusion on the feasibility of RSS technique by developing RSS based location algorithm

The feasibility of the techniques was first evaluated in this research by simulations. An RSS based location algorithm was modelled using the path loss model equation. The main challenge to be resolved to model the location algorithm was that there was no prior information about the source transmitted power and the path loss exponent. To resolve source transmitted power issues, a ratio of distances approach was used and to resolve the PLE issue a measure of the spread approach between spatially separate nodes was used.

To prove the principle, simulations were performed first. Simulations were performed in two main stages. In the first stage, it was assumed that there is a noiseless system due to the fact that under noiseless conditions, the estimated location should be the same as the location of the source. This was proved successful and ensured that the algorithm works correctly.

In the second part of the simulations, artificial noise was injected in the received signal and the performance of the algorithm was evaluated again. The performance of the algorithm was tested with typical values of system noise figure and RF bandwidth. The results obtained were satisfactory and were published at the 2nd URSI Atlantic radio science meeting (AT_RASC).

8.1.2 Conclusion on indoor field trials performed

Upon proving the principle, the next stage was to perform field trials and evaluate the algorithm performance. Three field trial scenarios were performed at the University of Huddersfield's sports hall. An artificial PD signal of 10 nC at 100 Hz repetition frequency was generated. The signal was received by using the radiometric sensors explained in chapter 4 of the thesis. The received signal voltage levels were converted into dBm as input to the location algorithm. The source location was estimated by using six, seven and eight receiving nodes respectively over an 18 by 18 meter grid. The performance parameters were the localization error, path loss exponent optimisation and the scalability. Artificial PD signals were generated from nine different positions and for each of the nine positions, the source location was estimated. The mean error calculated was 2.80 meters. The performance of the algorithm by using seven receiving sensors improved in terms of localization error and path loss exponent optimisation. By adding just, a single node in the receiving system, the mean error was reduced from 2.80 meters to 1.80 meters as well as path loss exponent optimised for each position seemed more realistic when compared with the results of six measurement sensors. Finally, the algorithm's performance was evaluated by using eight measurement sensors and this time the mean localization error was reduced from 1.80 meters to 1.76 meters giving an improved accuracy of 0.04 meter. The path loss exponent seemed even more realistic and closer to the average PLE of the propagation environment. Overall from indoor localization, it was concluded that for the first set of measurements that are based on nearly a real substation environment, the results were highly satisfactory.

8.1.3 Conclusion on outdoor field trials

To see if the algorithm will perform adequately in a real substation environment it was necessary to take outdoor measurements and to estimate the source localization by using the algorithm developed. There were two sets of measurements performed at two different places. Firstly, measurements were performed at the power network demonstration centre (PNDC) of Scottish Power at the University of Strathclyde. There were a range of sensor configurations used and the number of sensors used varied as well. Results for various configurations are

shown in chapter 6 and demonstrate that RSS based localization is highly plausible in a real substation environment and also location algorithm provides satisfactory results for the explored configurations.

The second set of results were obtained by deploying the system at TATA steel Port Talbot site in Wales and results were obtained for two different positions of the source. Again, the location estimation performed showed very encouraging results.

8.2 Future work

The proposed algorithm provided highly satisfactory results for PD source localization and was the key part of the PD detection and localization system. The algorithm provides the basis for source localization in an anonymous environment. In the future, the algorithm can be tested for other applications as well.

The proposed algorithm optimises an average path loss exponent. However, PLE remains the same between node pairs. In a real environment, it may vary between pairs of nodes. The algorithm provides the basis for research based on different path loss exponents between node pairs. This will be a basic future research direction on improved localization algorithm.

Another future research direction is to further explore the performance of the location algorithm in a real power station environment and to make it available commercially for power companies as part of the whole system integration where the algorithm can be used to locate unknown PD sources based on measured signals autonomously and continuously in order to monitor the health of HV systems.

The study conducted may become the basis for providing the diagnostic information about the PD. Upon localizing the source, the next step would be to obtain the diagnostic information. More field trails scenario can be used to obtain more information about the PD signal characteristics that will help to diagnose the PD as well as localizing it. PD detection, localization and diagnosis will become a completely autonomous system that can add significant value in the power industry.

The scope of the algorithm can be extended to locate multiple PD sources. The algorithm is the basis for enhancing it to localize multiple PD sources in a substation environment and also to differentiate between the PD types by categorising the type of the source.

REFERENCES

1. Danikas, M.G., *The definitions used for partial discharge phenomena.* IEEE transactions on electrical insulation, 1993. 28(6): p. 1075-1081.
2. Arief, Y., W. Izzati, and Z. Adzis, *Modeling of partial discharge mechanisms in solid dielectric material.* International Journal of Engineering and Innovative Technology, 2012. 1(4): p. 1-6.
3. Satish, L. and W. Zaengl, *Can fractal features be used for recognizing 3-d partial discharge patterns.* IEEE Transactions on Dielectrics and Electrical Insulation, 1995. 2(3): p. 352-359.
4. Boggs, S. and J. Densley, *Fundamentals of partial discharge in the context of field cable testing.* IEEE Electrical Insulation Magazine, 2000. 16(5): p. 13-18.
5. Li, Z., et al. *Classification of different types of partial discharge based on acoustic emission techniques*. in *Measurement, Information and Control (ICMIC), 2013 International Conference on*. 2013. IEEE.
6. Sahoo, N., M. Salama, and R. Bartnikas, *Trends in partial discharge pattern classification: a survey.* IEEE Transactions on Dielectrics and Electrical Insulation, 2005. 12(2): p. 248-264.
7. Grubic, S., et al., *A survey on testing and monitoring methods for stator insulation systems of low-voltage induction machines focusing on turn insulation problems.* IEEE Transactions on Industrial Electronics, 2008. 55(12): p. 4127-4136.
8. Illias, H., et al. *Partial discharge patterns in high voltage insulation*. in *IEEE International conference on Power and Energy (PECon)*. 2012. Sabah.
9. Ouatah, E., et al., *Characteristics of partial discharge pulses propagation in shielded power cable.* Electric Power Systems Research, 2013. 99: p. 38-44.
10. Jennings, E. and A. Collinson. *A partial discharge monitor for the measurement of partial discharges in a high voltage plant by the transient earth voltage technique*. in *Partial Discharge, 1993., International Conference on*. 1993. IET.
11. Chang, C., et al., *Source classification of partial discharge for gas insulated substation using waveshape pattern recognition.* IEEE Transactions on Dielectrics and Electrical Insulation, 2005. 12(2): p. 374-386.
12. Chang, J.-S., P.A. Lawless, and T. Yamamoto, *Corona discharge processes.* IEEE Transactions on plasma science, 1991. 19(6): p. 1152-1166.
13. Massines, F., et al., *Experimental and theoretical study of a glow discharge at atmospheric pressure controlled by dielectric barrier.* Journal of Applied Physics, 1998. 83(6): p. 2950-2957.
14. Morshuis, P.H., *Degradation of solid dielectrics due to internal partial discharge: some thoughts on progress made and where to go now.* IEEE Transactions on Dielectrics and Electrical Insulation, 2005. 12(5): p. 905-913.
15. Morshuis, P.H. and J.J. Smit, *Partial discharges at DC voltage: their mechanism, detection and analysis.* IEEE Transactions on Dielectrics and Electrical Insulation, 2005. 12(2): p. 328-340.
16. Gataullin, A., *Recording and processing of partial discharge signals.* Instruments and Experimental Techniques, 2014. 57(4): p. 426-430.

17. Jaber, A.A., et al., *Calibration of free-space radiometric partial discharge measurements.* IEEE Transactions on Dielectrics and Electrical Insulation, 2017. 24(5): p. 3004-3014.
18. Li, W., J. Zhao, and S. Meng. *Partial Discharge Time-Frequency Spectrum Analysis and Extraction for Power Cable*. in *Power and Energy Engineering Conference (APPEEC), 2012 Asia-Pacific*. 2012. IEEE.
19. Zekavat, R. and R.M. Buehrer, *Handbook of position location: Theory, practice and advances*. Vol. 27. 2011: John Wiley & Sons.
20. Champion, J. and S.J. Dodd, *Simulation of partial discharges in conducting and non-conducting electrical tree structures.* Journal of Physics D: Applied Physics, 2001. 34(8): p. 1235.
21. Glover, I.A., *Scalable Non-invasive Radiometric Wireless Network for Partial Discharge Monitoring in Future Smart Grid*. 2014.
22. Hui, X., et al., *TDOA localization algorithm with compensation of clock offset for wireless sensor networks.* China Communications, 2015. 12(10): p. 193-201.
23. Judd , M.D. *Radiometric partial discharge detection*. in *Condition Monitoring and Diagnosis*. 2008. Beijing: IEEE.
24. Aziz, N., M. Judd, and V. Catterson. *Identifying prognostic indicators for electrical treeing in solid insulation through PD analysis*. in *Solid Dielectrics (ICSD), 2013 IEEE International Conference on*. 2013. IEEE.
25. Judd, M.D., L. Yang, and I.B. Hunter, *Partial discharge monitoring of power transformers using UHF sensors. Part I: sensors and signal interpretation.* IEEE Electrical Insulation Magazine, 2005. 21(2): p. 5-14.
26. Patwari, N., et al., *Locating the nodes: cooperative localization in wireless sensor networks.* IEEE Signal processing magazine, 2005. 22(4): p. 54-69.
27. Majidi, M., et al., *Partial discharge pattern recognition via sparse representation and ANN.* Dielectrics and Electrical Insulation, 2015. 22(2): p. 1061-1070.
28. Khan, U.I., K. Pahlavan, and S. Makarov. *Comparison of TOA and RSS based techniques for RF localization inside human tissue*. in *2011 Annual International Conference of the IEEE Engineering in Medicine and Biology Society*. 2011. IEEE.
29. Bargshady, N., N.A. Alsindi, and K. Pahlavan. *Performance of TOA-and RSS-based indoor geolocation for cooperative robotic applications*. in *International Workshop on Mobile Entity Localization and Tracking in GPS-less Environments*. 2009. Springer.
30. Park, J.-W., et al., *Comparisons of error characteristics between TOA and TDOA positioning in dense multipath environment.* 2009. 58(2): p. 415-421.
31. Seyed, A. and M. Buehrer, *Handbook of position location: Theory, practice and advances*. 2012: John Wiley and sons
32. Shin, D.-H., T.-K.J.I.T.o.A. Sung, and E. Systems, *Comparisons of error characteristics between TOA and TDOA positioning.* 2002. 38(1): p. 307-311.
33. Portugues, I., et al., *RF-Based Partial Discharge Early Warning System for Air-Insulated Substations.* Power Delivery, 2008. 24(1): p. 20-29.
34. Khan, U., et al. *Localization of Partial Discharge by Using Received Signal Strength*. in *2018 2nd URSI Atlantic Radio Science Meeting (AT-RASC)*. 2018. IEEE.
35. Jaber, A., et al. *Validation of partial discharge emulator simulations using free-space radiometric measurements*. in *Students on Applied Engineering (ICSAE), International Conference for*. 2016. IEEE.
36. Van Brunt, R.J., *Physics and chemistry of partial discharge and corona. Recent advances and future challenges.* IEEE Transactions on dielectrics and Electrical Insulation, 1994. 1(5): p. 761-784.

37. Wu, M., et al., *An overview of state-of-the-art partial discharge analysis techniques for condition monitoring.* IEEE electrical insulation magazine, 2015. 31(6): p. 22-35.
38. Strachan, S., et al., *Intelligent diagnosis of defects responsible for partial discharge activity detected in power transformers.* 12th Intelligent Systems Application to Power Systems (ISAP 2003), 2003.
39. Gockenbach, E. and H. Borsi. *Condition monitoring and diagnosis of power transformers*. in *Condition Monitoring and Diagnosis, 2008. CMD 2008. International Conference on*. 2008. IEEE.
40. Bartnikas, R., *Partial discharges. Their mechanism, detection and measurement.* IEEE Transactions on Dielectrics and Electrical Insulation, 2002. 9(5): p. 763-808.
41. Kreuger, F., E. Gulski, and A. Krivda, *Classification of partial discharges.* IEEE transactions on Electrical Insulation, 1993. 28(6): p. 917-931.
42. Takala, M., et al., *Dielectric properties and partial discharge endurance of polypropylene-silica nanocomposite.* IEEE Transactions on Dielectrics and Electrical Insulation, 2010. 17(4).
43. Harbaji, M., K. Shaban, and A. El-Hag, *Classification of common partial discharge types in oil-paper insulation system using acoustic signals.* IEEE Transactions on Dielectrics and Electrical Insulation, 2015. 22(3): p. 1674-1683.
44. Howells, E. and E. Norton, *Detection of partial discharges in transformers using acoustic emission techniques.* IEEE Transactions on Power Apparatus and Systems, 1978(5): p. 1538-1549.
45. Krivda, A., *Automated recognition of partial discharges.* Dielectrics and Electrical Insulation, 1995. 2(5): p. 796 - 821.
46. Niemeyer, L., *A generalized approach to partial discharge modeling.* IEEE transactions on Dielectrics and Electrical insulation, 1995. 2(4): p. 510-528.
47. Pham, H., *Reliability analysis of a high voltage system with dependent failures and imperfect coverage.* Reliability Engineering & System Safety, 1992. 37(1): p. 25-28.
48. Stone, G., *Partial Discharges in Electrical Insulation*, in *Iris power*. 2014.
49. Deshpande, A.S., A.N. Cheeran, and H.A. Mangalvedekar, *Spectrum Analysis of Pratial Discharge Signals* International Journal of Engineering Science and Emerging Technologies 2013. 4(2): p. 37-43.
50. Srinivas, N.N. and H.C. Doepken. *Electrochemical treeing in PE and XLPE insulated cables - frequency effects and impulse degradation*. in *1978 IEEE International Conference on Electrical Insulation*. 1978. New York
51. Suzuoki, Y., F. Komori, and T. Mizutani, *Partial discharges due to electrical treeing in polymers: phase-resolved and time-sequence observation and analysis.* Journal of Physics D: Applied Physics, 1996. 29(11): p. 2922.
52. Paoletti, G. and A. Golubev. *Partial discharge tehrory and applications to electrical systems*. in *Pulp and Paper, 1999. Industry Technical Conference* 1999. Seattle.
53. Horii, K. and M. Kosaki. *Partial discharge and treeing phenomena of polyethylene in liquid nitrogen*. in *Electrical Insulation & Dielectric Phenomena-Annual Report 1973, Conference on*. 1973. IEEE.
54. Zhang, Y., et al., *Radiometric wireless sensor network monitoring of partial discharge sources in electrical substations.* International Journal of Distributed Sensor Networks, 2015. 11(9): p. 438302.
55. Boggs, S.A., *Partial discharge: overview and signal generation.* IEEE Electrical Insulation Magazine, 1990. 6(4): p. 33-39.
56. Ma, X., C. Zhou, and I. Kemp, *Interpretation of wavelet analysis and its application in partial discharge detection.* IEEE Transactions on Dielectrics and Electrical Insulation, 2002. 9(3): p. 446-457.

57. Cavallini, A., G. Montanari, and F. Ciani. *Analysis of partial discharge phenomena in paper-oil insulation systems as a basis for risk assessment evaluation*. in *Dielectric Liquids, 2005. ICDL 2005. 2005 IEEE International Conference on*. 2005. IEEE.
58. Stone, G. and S. Boggs. *Propagation of partial discharge pulses in shielded power cable*. in *Electrical Insulation & Dielectric Phenomena, 1982. Annual Report 1982. Conference on*. 1982. IEEE.
59. Densley, J., *The Effect of Aggressive Chemicals on Extruded Insulation Shields.* Appendix A1D (5-30). 3: p. 44-49.
60. Ahmed, N. and N. Srinivas. *Partial discharge measurements in distribution class extruded cables*. in *Transmission and Distribution Conference, 1999 IEEE*. 1999. IEEE.
61. Bamji, S., A. Bulinski, and R. Densley. *Final breakdown mechanism of water treeing*. in *Electrical Insulation and Dielectric Phenomena, 1991. CEIDP. 1991 Annual Report. Conference on*. 1991. IEEE.
62. Boggs, S., J. Densley, and J. Kuang, *Mechanism for Conversion of Water Trees to Electrical Trees in XLPE.* IEEE Power Engineering Review, 1997. 17(9): p. 30-30.
63. Tenbohlen, S., et al., *Experienced-based evaluation of economic benefits of on-line monitoring systems for power transformers.* Cigré Session 2002, 2002: p. 12-110.
64. Stone, G., et al., *Practical implementation of ultrawideband partial discharge detectors.* IEEE Transactions on Electrical Insulation, 1992. 27(1): p. 70-81.
65. Wang, Z.D., et al. *An algorithm for partial discharge location in distributed power transformers*. in *IEEE Power Engineering Society*. 2000.
66. Deshpande, A., H. Mangalvedekar, and A. Cheeran, *Partial discharge analysis using energy patterns.* International Journal of Electrical Power & Energy Systems, 2013. 53: p. 184-195.
67. Bell, R., et al., *High-voltage onsite commissioning tests for gas-insulated substations using UHF partial discharge detection.* IEEE Transactions on Power Delivery, 2003. 18(4): p. 1187-1191.
68. Headquarters, A., *Wi-Fi Location-Based Services 4.1 Design Guide*. 2008, Cisco.
69. Mohamed, H., et al. *Partial discharge detection using low cost RTL-SDR model for wideband spectrum sensing*. in *Telecommunications (ICT), 2016 23rd International Conference on*. 2016. IEEE.
70. Miao, P., et al. *Location algorithm for partial discharge based on radio frequency (RF) antenna array*. in *Power and Energy Engineering Conference (APPEEC), 2012 Asia-Pacific*. 2012. IEEE.
71. Illias, H., et al. *Partial discharge patterns in high voltage insulation*. in *Power and Energy (PECon), 2012 IEEE International Conference on*. 2012. IEEE.
72. Pinpart, T. and M. Judd, *Differentiating between partial discharge sources using envelope comparison of ultra-high-frequency signals.* IET science, measurement & technology, 2010. 4(5): p. 256-267.
73. Portugues, I.E., et al., *RF-based partial discharge early warning system for air-insulated substations.* IEEE Transactions on Power Delivery, 2009. 24(1): p. 20-29.
74. Mohamed, H., et al. *Partial discharge localization based on received signal strength*. in *Automation and Computing (ICAC), 2017 23rd International Conference on*. 2017. IEEE.
75. Mohamed, H., et al. *Partial discharge detection using software defined radio*. in *Students on Applied Engineering (ICSAE), International Conference for*. 2016. IEEE.
76. Boggs, S. and G. Stone, *Fundamental limitations in the measurement of corona and partial discharge.* IEEE Transactions on Electrical Insulation, 1982. 17(2): p. 143-150.

77. *Sensor Response Characteristics for UHF Location of PD Sources*. in *Condition Monitoring and Diagnosis*. 2008. Beijing
78. Niroomand, M., M. Rezaeian, and Z. Amini. *Partial discharge localization and classification using acoustic emission analysis in power transformer*. in *Telecommunications Energy Conference, 2009. INTELEC 2009. 31st International*. 2009. IEEE.
79. Moore, P.J., I.E. Portugues, and I.A. Glover *Radiometric location of partial discharge sources on energized high-Voltage plant.* IEEE Transactions on Power Delivery, 2005. 20(3): p. 2264-2272.
80. Miao , P., et al. *Location Algorithm for Partial Discharge Based on Radio Frequency (RF) Antenna Array*. in *Power and Energy Engineering Conference (APPEEC)*. 2012. Shanghai.
81. Huang , J., et al., *RSS-Based Method for Sensor Localization with Unknown Transmit Power and Uncertainty in Path Loss Exponent.* MDPI, 2016. 16: p. 1-20.
82. Koo, J. and H. Cha, *Localizing WiFi access points using signal strength.* IEEE communication letters, 2011. 15(2): p. 187-189.
83. Rencheng, J., et al. *Research on RSSI-Based Localization in Wireless Sensor Networks*. in *Wireless Communications, Networking and Mobile Computing*. 2008. Dalian.
84. Sheng, X. and Y.-H. Hu, *Maximum likelihood multiple-source localization using acoustic energy measurements with wireless sensor networks.* IEEE Transactions on Signal Processing, 2005. 53(1): p. 44-53.
85. Zhu, M., et al., *Optimization of Antenna Array Deployment for Partial Discharge Localization in Substations by Hybrid Particle Swarm Optimization and Genetic Algorithm Method.* Energies, 2018. 11(7): p. 1-18.
86. Moore, P.J., I.E. Portugues, and I.A. Glover, *Partial discharge investigation of a power transformer using wireless wideband radio-frequency measurements.* IEEE Transactions on Power Delivery, 2006. 21(1): p. 528-530.
87. Sinaga, H.H., B.T. Phung, and T.R. Blackburn, *Partial discharge localization in transformers using UHF detection method.* Dielectrics and Electrical Insulation, 2012. 19(6): p. 1891-1900.
88. Sikorski, W., et al., *Location of partial discharge sources in power transformers based on advanced auscultatory technique.* IEEE Transactions on Dielectrics and Electrical Insulation, 2012. 19(6).
89. So, H.C. and L. Lin, *Linear Least Squares Approach for Accurate Received Signal Strength Based Source Localization.* IEEE transactions on signal processing 2011. 59(8): p. 4035-4040.
90. CISCO, *Wi-Fi Location-Based Services 4.1 Design Guide*. 2008, San Jose: CISCO.
91. Xiong, H., et al., *Robust TDOA Localization Algorithm for Asynchronous Wireless Sensor Networks.* International Journal of Distributed Sensor Networks, 2014: p. 1-10.
92. Hettiwatte, S.N., Z. Wang , and P.A. Crossley. *Estimating transformer parameters for partial discharge location*. in *Power Engineering Conference (AUPEC)*. 2014. Perth, WA.
93. Cheng, Y.-C., et al. *Accuracy characterization for metropolitan-scale Wi-Fi localization*. in *Proceedings of the 3rd international conference on Mobile systems, applications, and services*. 2005. ACM.
94. Gonzalez, M.A., et al., *GUIDE-gradient: A guiding algorithm for mobile nodes in WLAN and Ad-hoc networks.* Wireless Personal Communications, 2011. 57(4): p. 629-653.

95. Zhang, Z., et al. *I am the antenna: accurate outdoor AP location using smartphones*. in *Proceedings of the 17th annual international conference on Mobile computing and networking*. 2011. ACM.
96. Xu, Y., J. Zhou, and P. Zhang, *RSS-based source localization when path-loss parameters are unknown* IEEE communication letters 2014. 18(6): p. 1055-1058.
97. Kunze, K. and P. Lukowicz. *Symbolic object localization through active sampling of acceleration and sound signatures*. in *International Conference on Ubiquitous Computing*. 2007. Springer.
98. Rajalakshmi, A.M., P, et al. *Centroid Based 3D Localization Technique Using RSSI With a Mobile Robot*. in *International Symposium on Wireless Personal Multimedia Communications* 2014.
99. Hany, U. and L. Akter. *Performance of Distance based and Path Loss based Weighted Centroid Localization Algorithms for Video Capsule Endoscope*. in *International Conference on Signal and Image Processing Applications (IEEE ICSIPA 2017)*. 2017. Malysia.
100. Shi, H. *A New Weighted Centroid Localization Algorithm based on RSSI*. in *Proceeding of the IEEE International Conference on Information and Automation*. 2012. Shenyang.
101. Kim, K.-Y. and Y. Shin, *A Distance Boundary with Virtual Nodes for the Weighted Centroid Localization Algorithm.* Sensors, 2018. 18(4): p. 1054.
102. Madhan, M.G., et al., *RSSI based location estimation: An experimental study.* ICTACT Journal on communication technology, 2014. 5(4): p. 1015-1018.
103. Bandiera, F., A. Coluccia, and G. Ricci, *A Cognitive Algorithm for Received Signal Strength Based Localization.* IEEE TRANSACTIONS ON SIGNAL PROCESSING, 2015: p. 1726-1736.
104. Xu, Y., J. Zhou, and P. Zhang, *RSS-based source localization when path-loss model parameters are unknown.* IEEE communications letters, 2014. 18(6): p. 1055-1058.
105. Vaghefi, R.M., et al., *Cooperative received signal strength-based sensor localization with unknown transmit powers.* IEEE Transactions on Signal Processing, 2013. 61(6): p. 1389-1403.
106. Upton, D.W., et al., *Low power radiometric partial discharge sensor using composite transistor-reset integrator.* IEEE Transactions on Dielectrics and Electrical Insulation, 2018. 25(3): p. 984-992.
107. Saeed, B., et al. *A supervisory system for partial discharge monitoring*. in *2018 2nd URSI Atlantic Radio Science Meeting (AT-RASC)*. 2018. IEEE.
108. Upton, D.W., et al., *Wireless Sensor Network for Radiometric Detection and Assessment of Partial Discharge in High-Voltage Equipment.* Radio Science 2018. 53(5): p. 357-364.
109. Upton, D., et al., *Wireless Sensor Network for Radiometric Detection and Assessment of Partial Discharge in High-Voltage Equipment.* Radio Science, 2018. 53(3): p. 357-364.
110. Albarracín, R., J.A. Ardila-Rey, and A.A.J.S. Mas'ud, *On the use of monopole antennas for determining the effect of the enclosure of a power transformer tank in partial discharges electromagnetic propagation.* 2016. 16(2): p. 148.
111. Khan, U.F., et al., *An Efficient Algorithm for Partial Discharge Localization in High-Voltage Systems Using Received Signal Strength.* 2018. 18(11): p. 4000.
112. Upton, D.W., et al., *Low power radiometric partial discharge sensor using composite transistor-reset integrator.* 2018.

113. Jaber, A., et al. *Diagnostic potential of free-space radiometric partial discharge measurements*. in *General Assembly and Scientific Symposium of the International Union of Radio Science (URSI GASS), 2017 XXXIInd*. 2017. IEEE.

APPENDICES

A range of figures are given in appendix A of the report.

Appendix A General PD spectrum and the localization results in mV

The PD spectral view in a generalised form is shown in figure A.1 below:

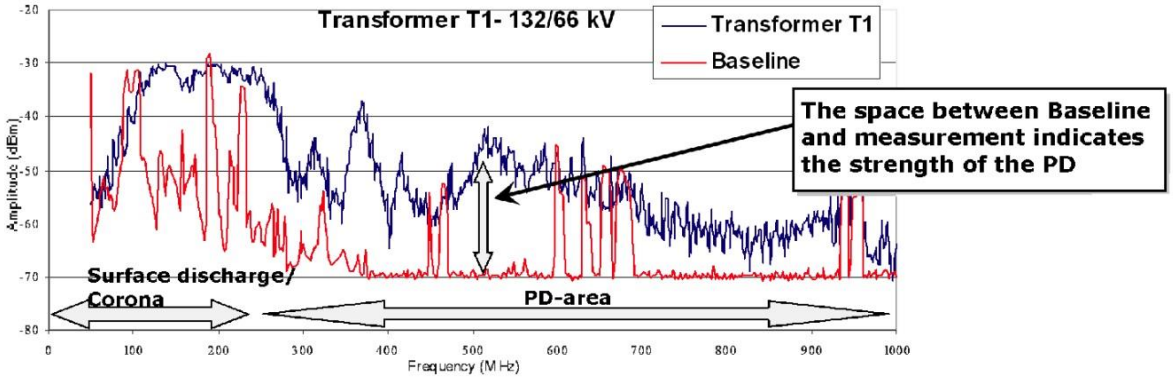

Figure A.1. Radiation pattern of a PD pulse.

Within the indoor localization, the average step size of the received signal in mv is given in table A.1 below for all nine locations.

Table A.1. Average step size of the received signal in (mV)

PD source location	Node 1	Node 2	Node 3	Node 4	Node 5	Node 6	Node 7	Node 8
P1	86.73	69.30	63.39	371.10	312.08	160.25	381.65	259.60
P2	76.78	47.84	275.71	387.57	107.25	236.79	324.57	43.43
P3	457.80	81.10	332.24	239.09	72.83	49.55	72.33	17.56
P4	169.52	444.16	77.02	327.06	282.05	50.71	48.86	12.25
P5	99.38	105.01	103.89	717.40	356.14	134.31	168.46	112.04
P6	163.32	62.82	392.25	650.35	123.13	132.32	165.14	39.08
P7	276.61	179.32	170.29	558.27	192.92	58.59	65.26	16.22
P8	115.03	272.49	66.40	651.03	512.37	71.82	128.78	52.61
P9	27.65	11.46	29.62	56.03	28.41	437.39	321.16	61.63

The nodes layout is shown A.2 below:

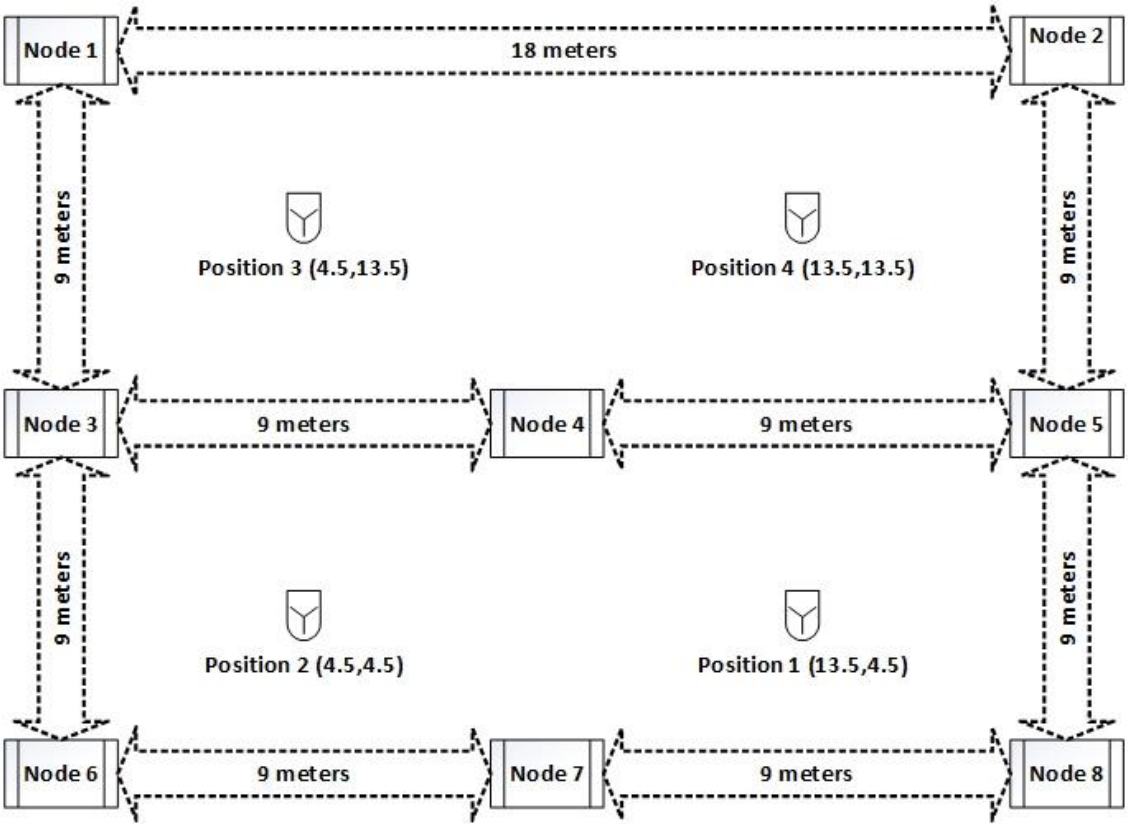

Figure A.2. Nodes layout of the receivers inside the sports hall.

PD calibrator used for PD generation is shown in figure A.3 below:

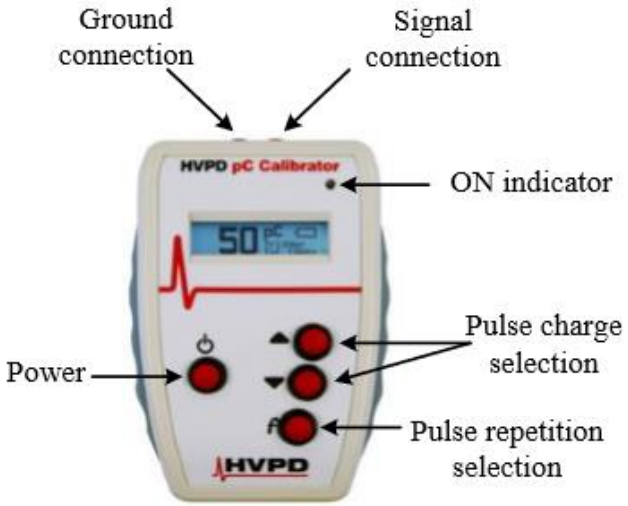

Figure A.3. PD calibrator.

A view of measurement setup inside the lab is shown in the figure below:

Figure A.4. An illustration of equipment used in RF lab.

The calibration of the emulators was performed as an example shown in figure A.5 below:

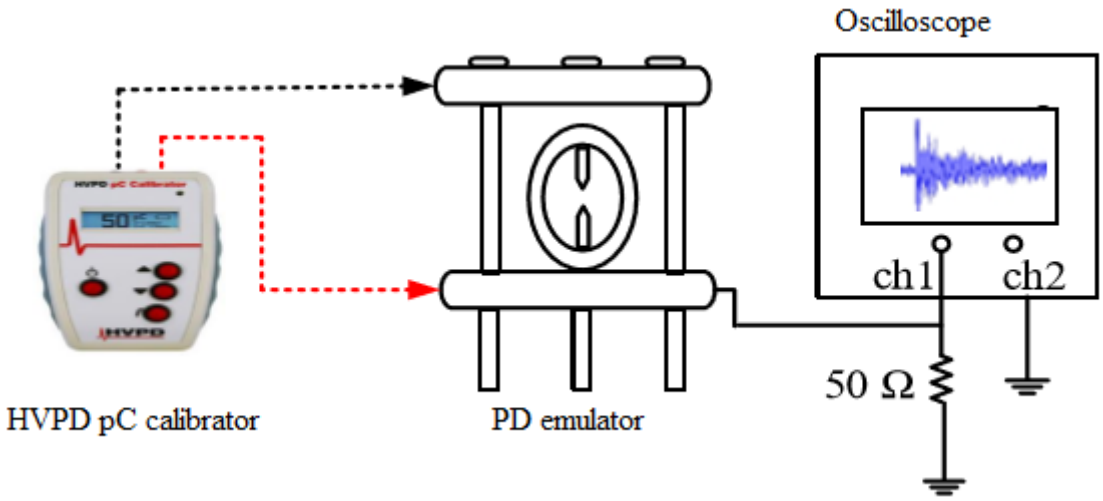

Figure A.5. Example of PD calibration.

Figures A.6 to A.10 show the estimated locations of the source of six nodes were used.

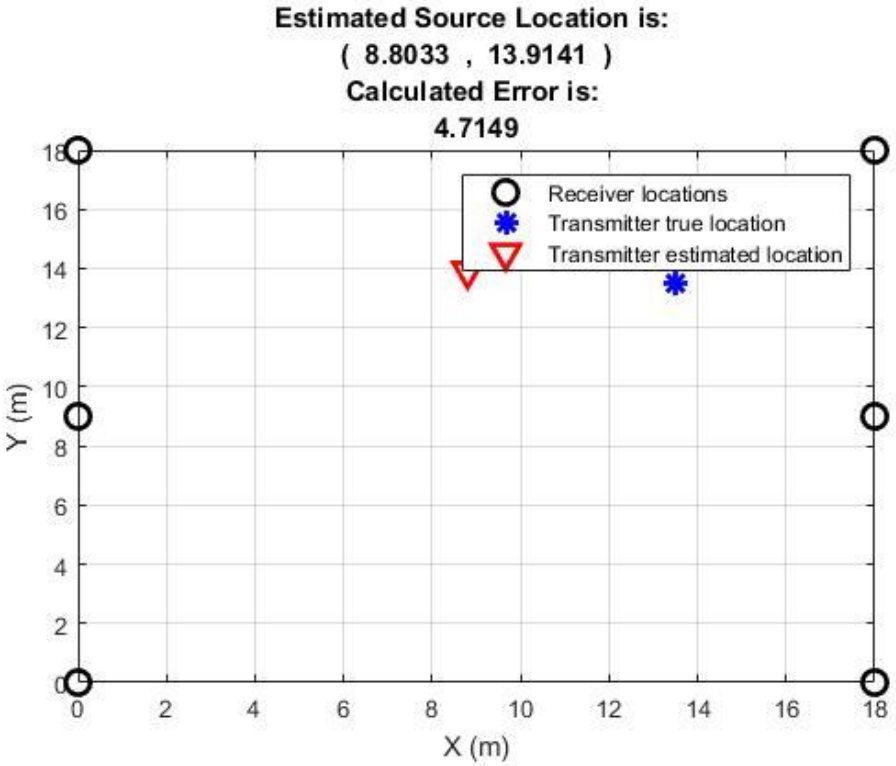

Figure A.6. Position 4, six nodes.

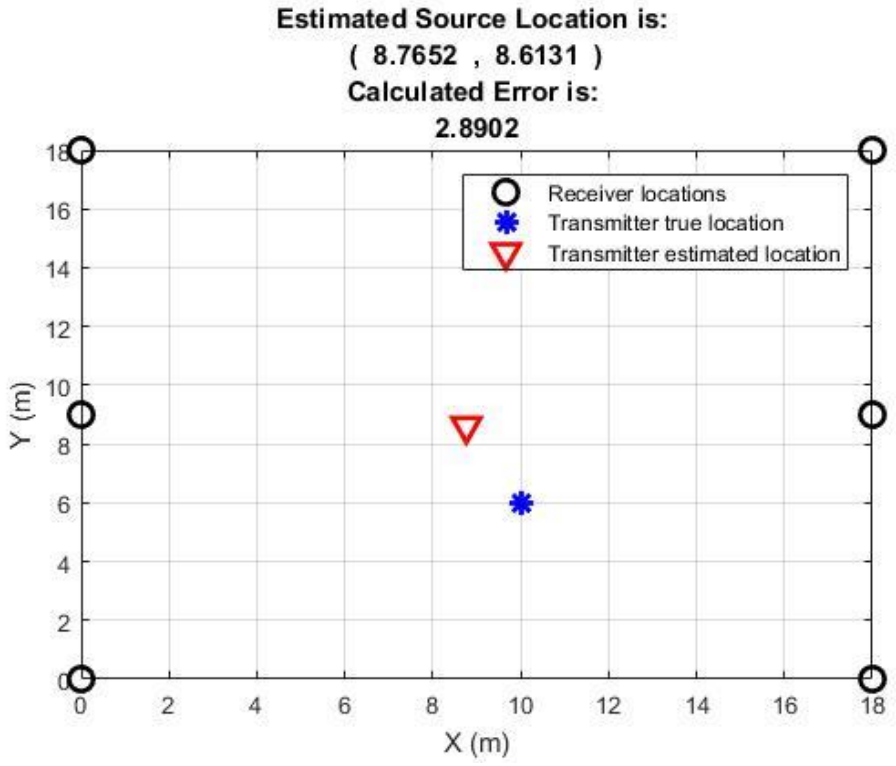

Figure A.7. Position 5, six nodes.

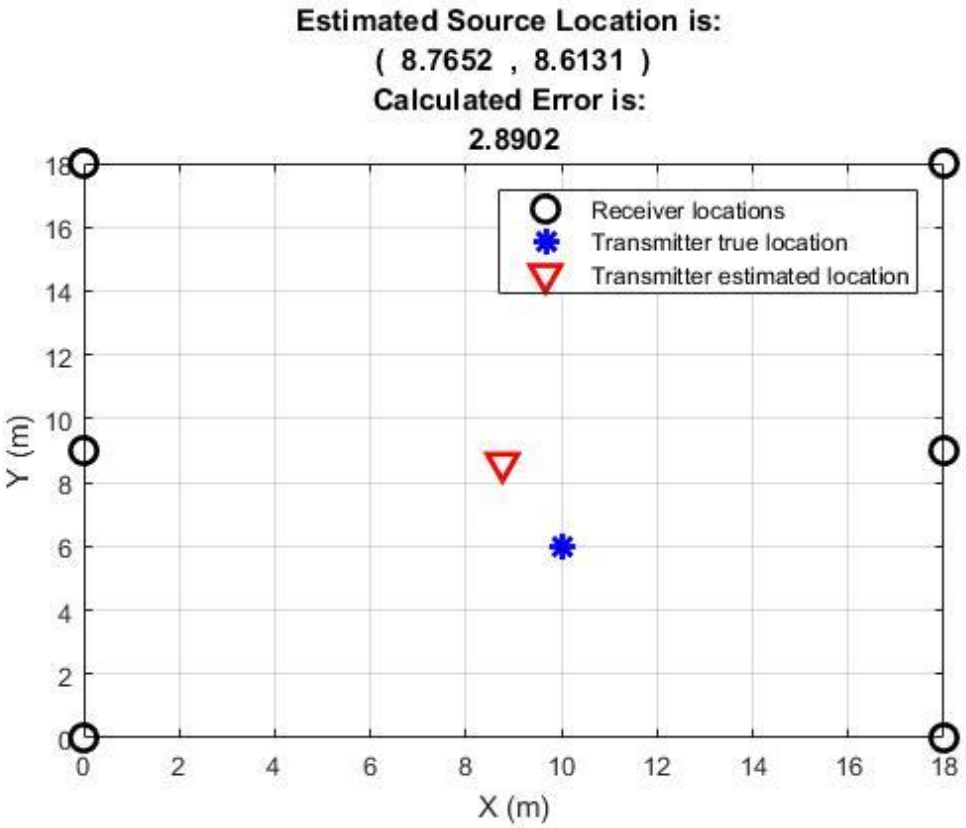

Figure A.8 Position 6, six nodes

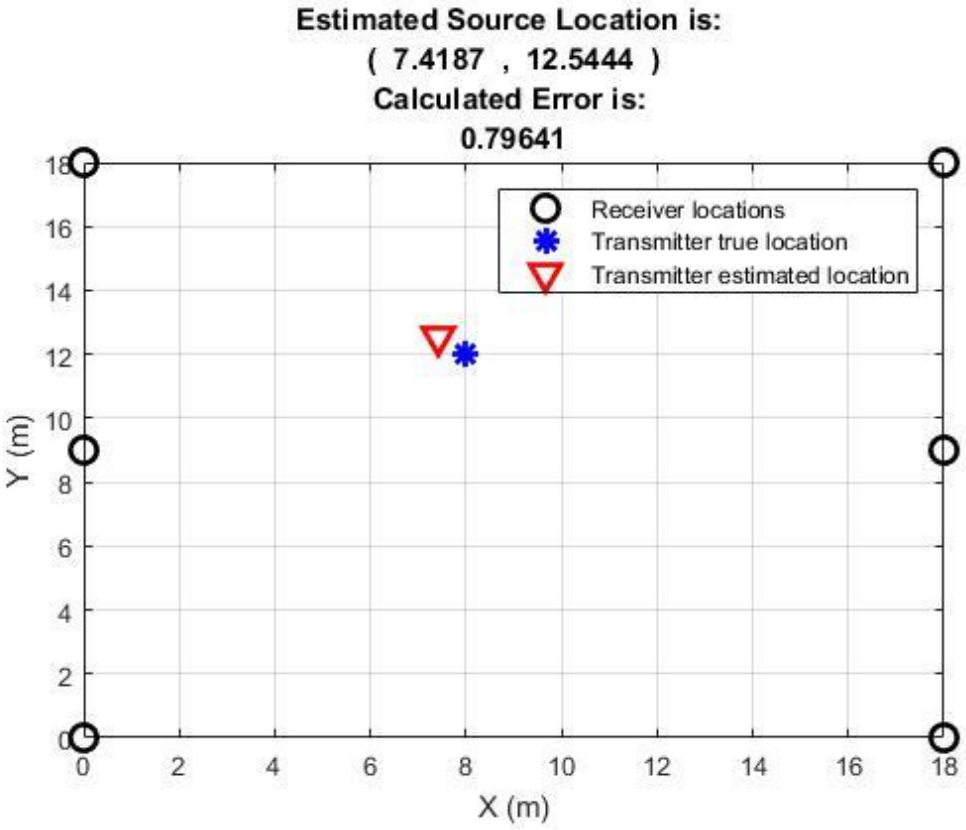

Figure A.9 Position 7, six nodes.

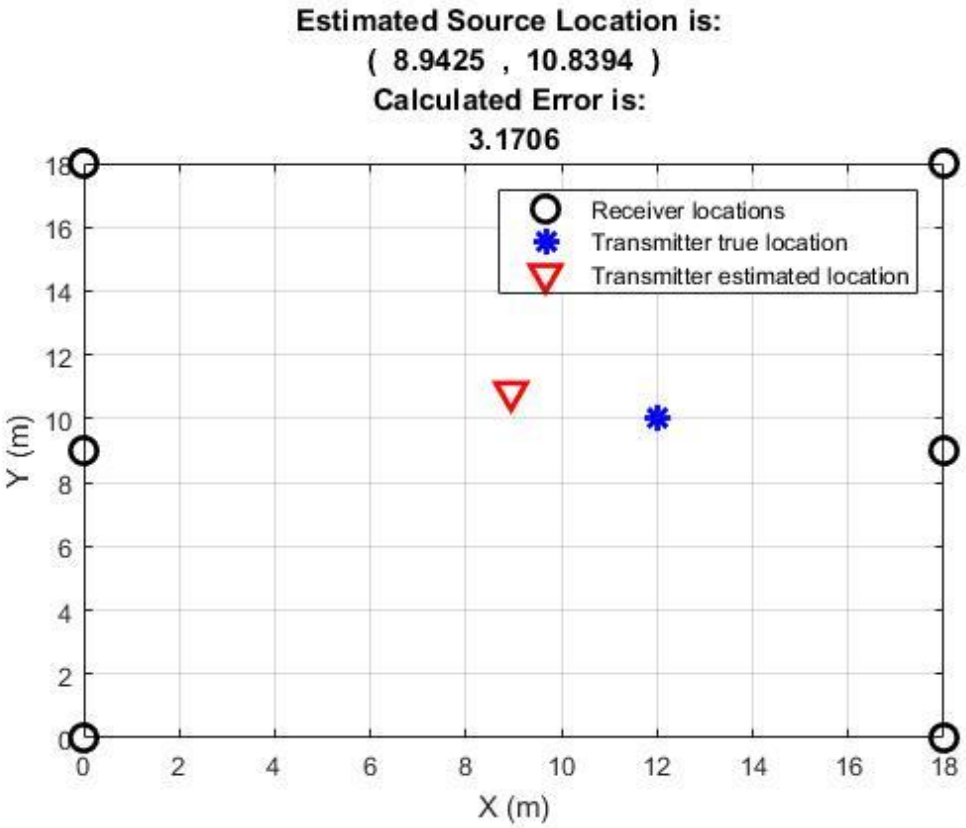

Figure A.10. Position 8, six nodes

Figures A.11 to A.16 show the results from positions 4 to 9 when seven nodes were used.

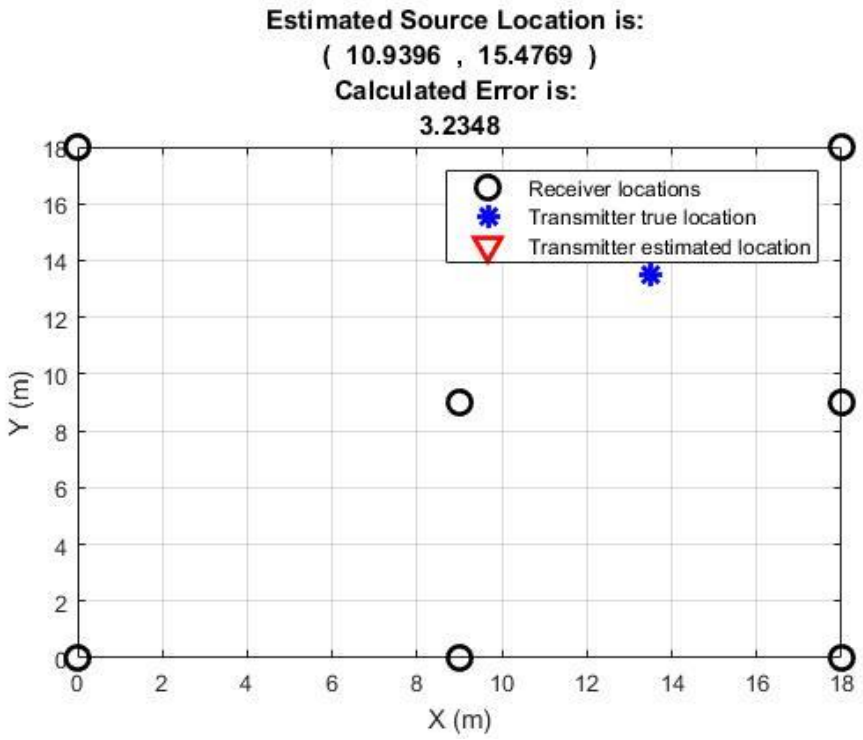

Figure A.11. Position 4, seven nodes used.

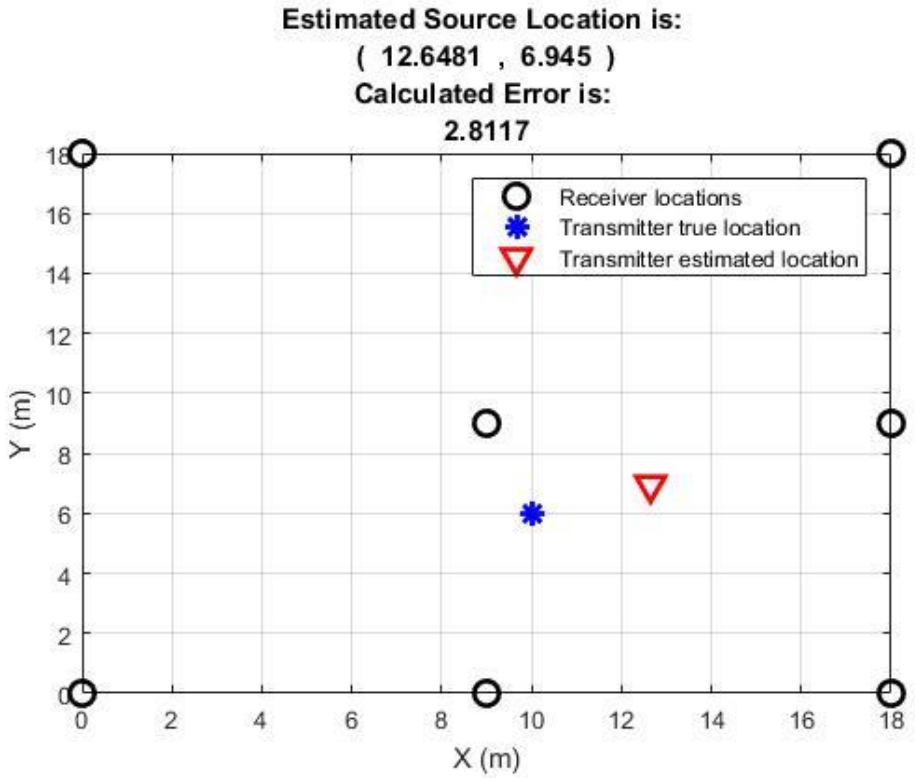

Figure A.12. Position 5, seven nodes used.

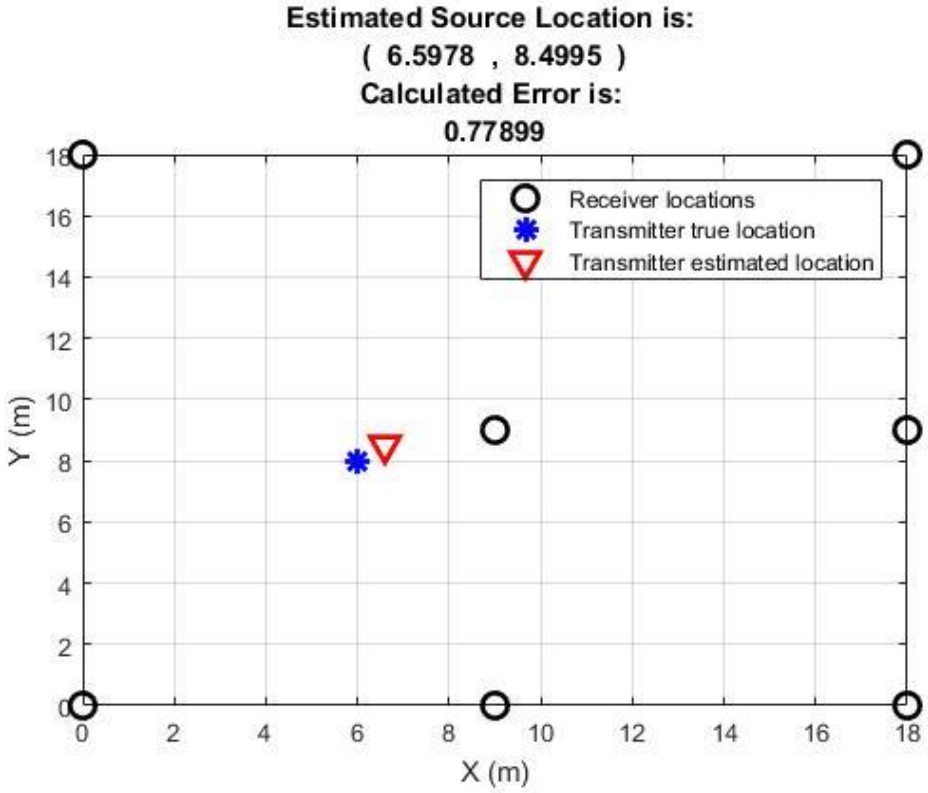

Figure A.13. Position 6, seven nodes used.

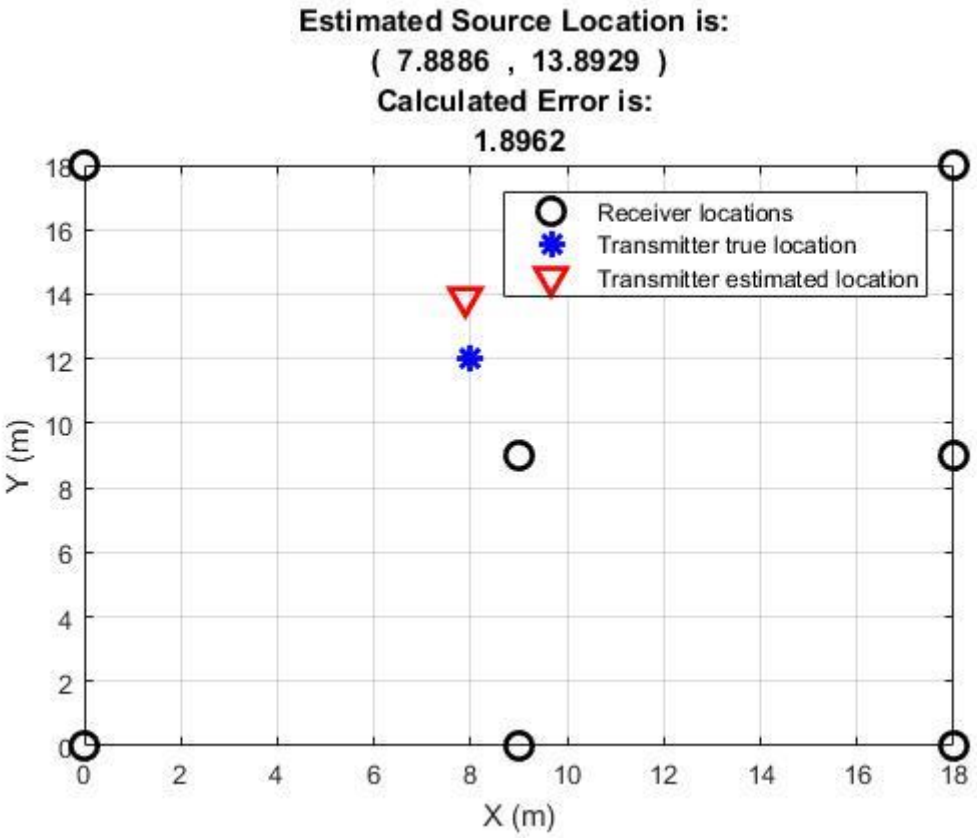

Figure A.14. Position 7, seven nodes used.

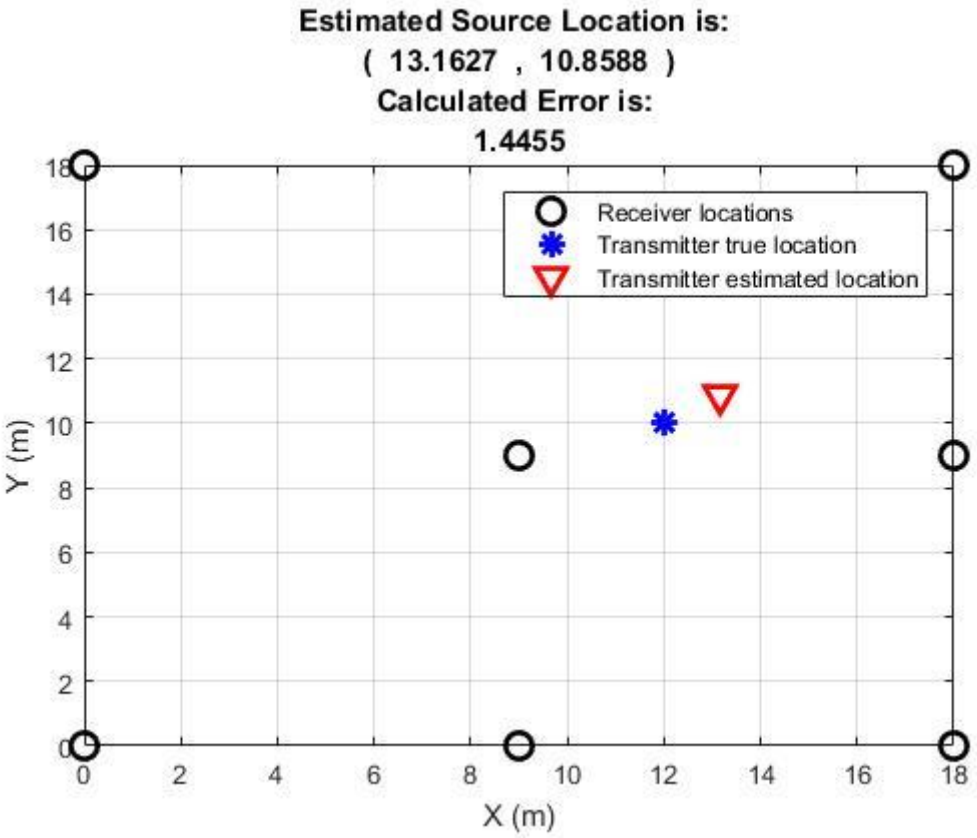

Figure A.15. Position 8, seven nodes used.

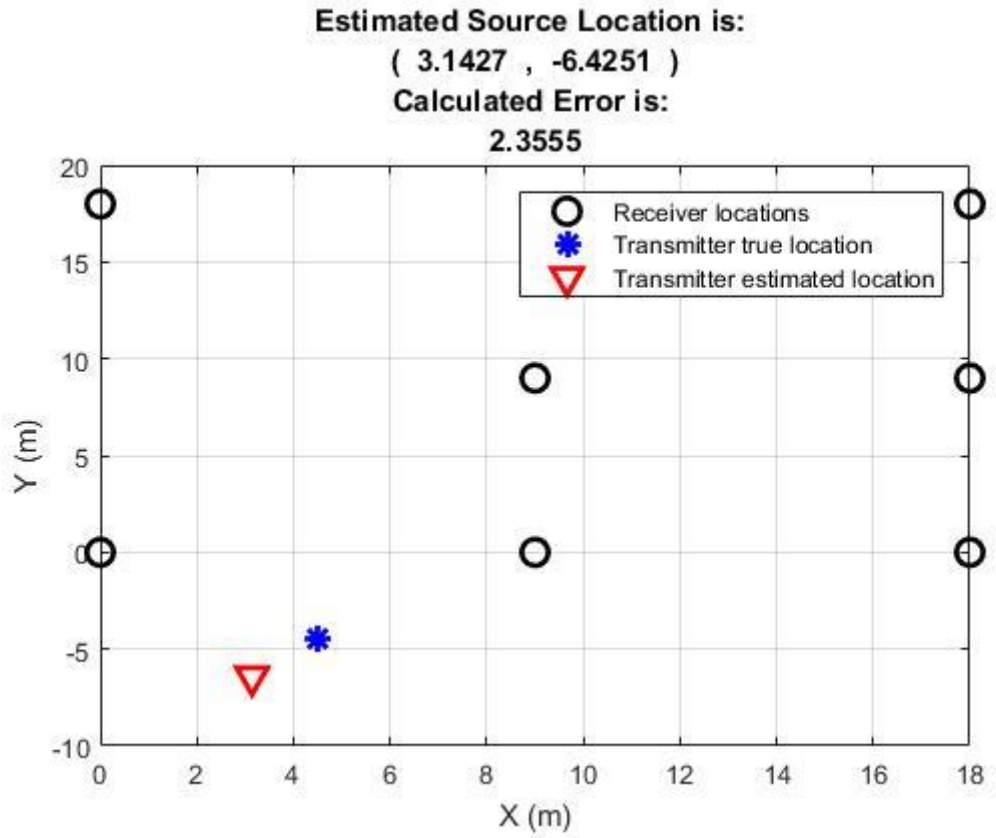

Figure A.16. Position 9, seven nodes used.

Figures A.17 to A.22 show the results from positions 4 to 9 when eight nodes were used.

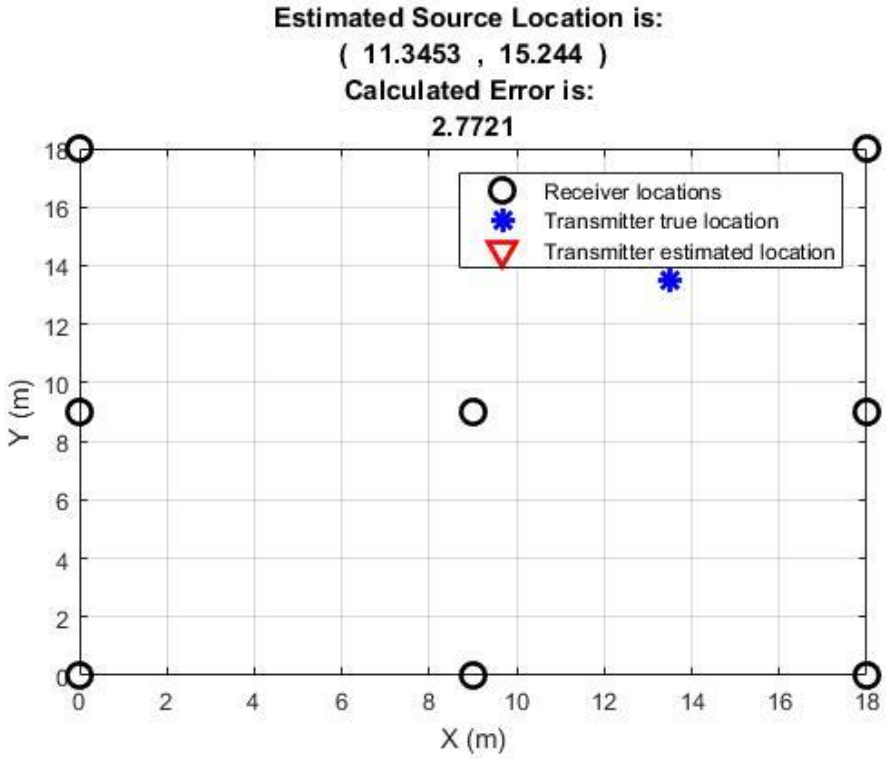

Figure A.17. Position 4, when eight receiving nodes were used.

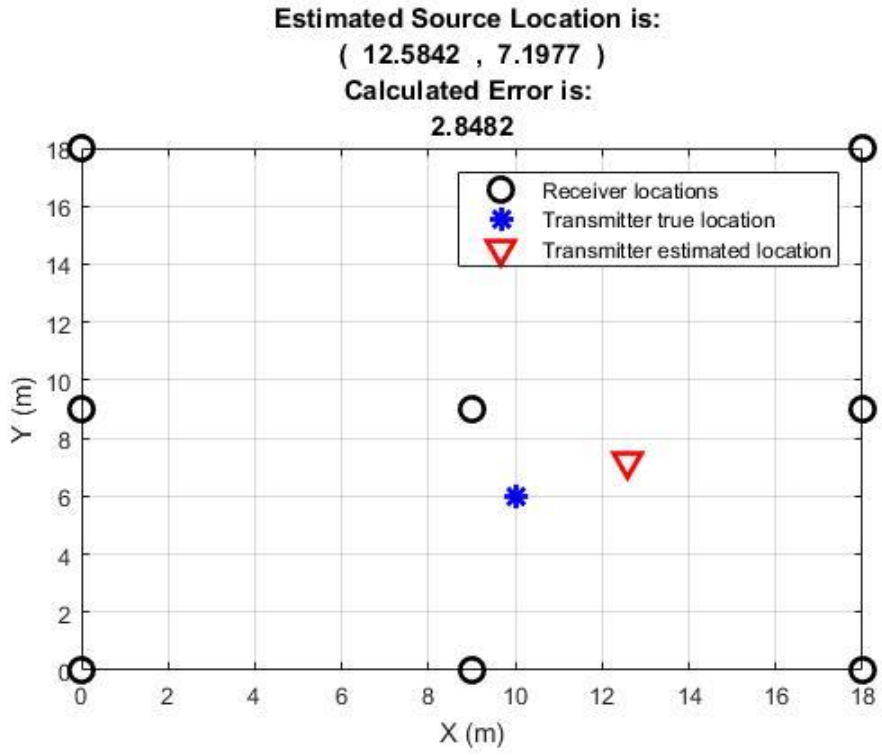

FigureA.18. Position 5, when eight receiving nodes were used.

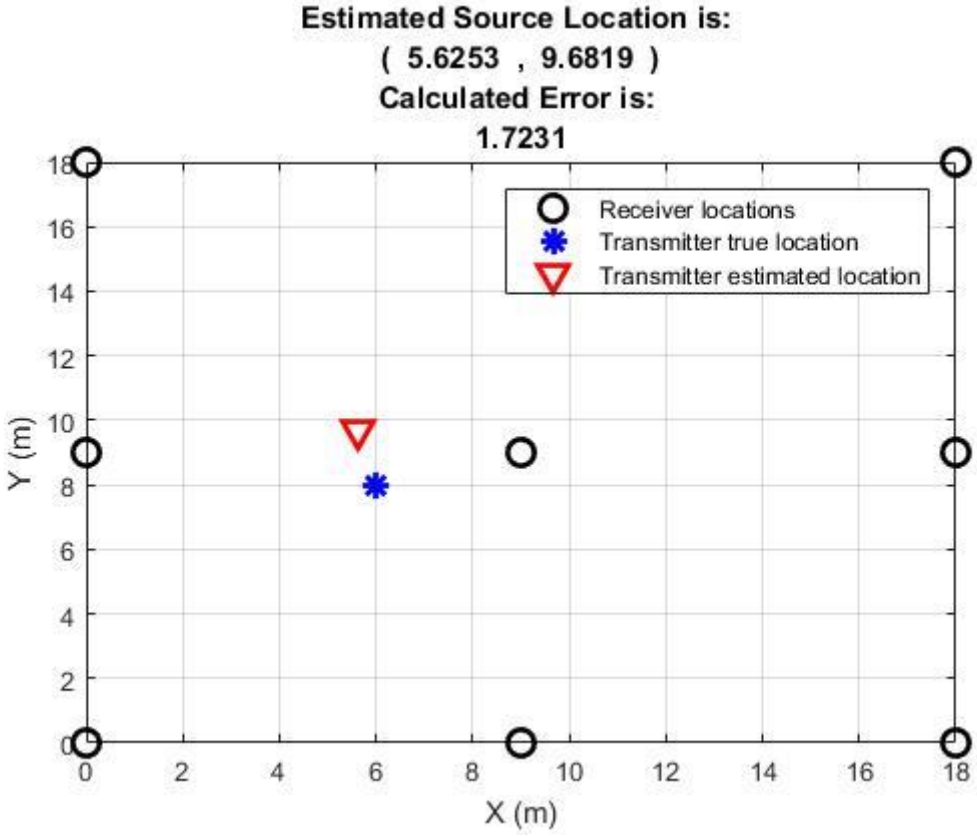

Figure A.19. Position 6, when eight receiving nodes were used.

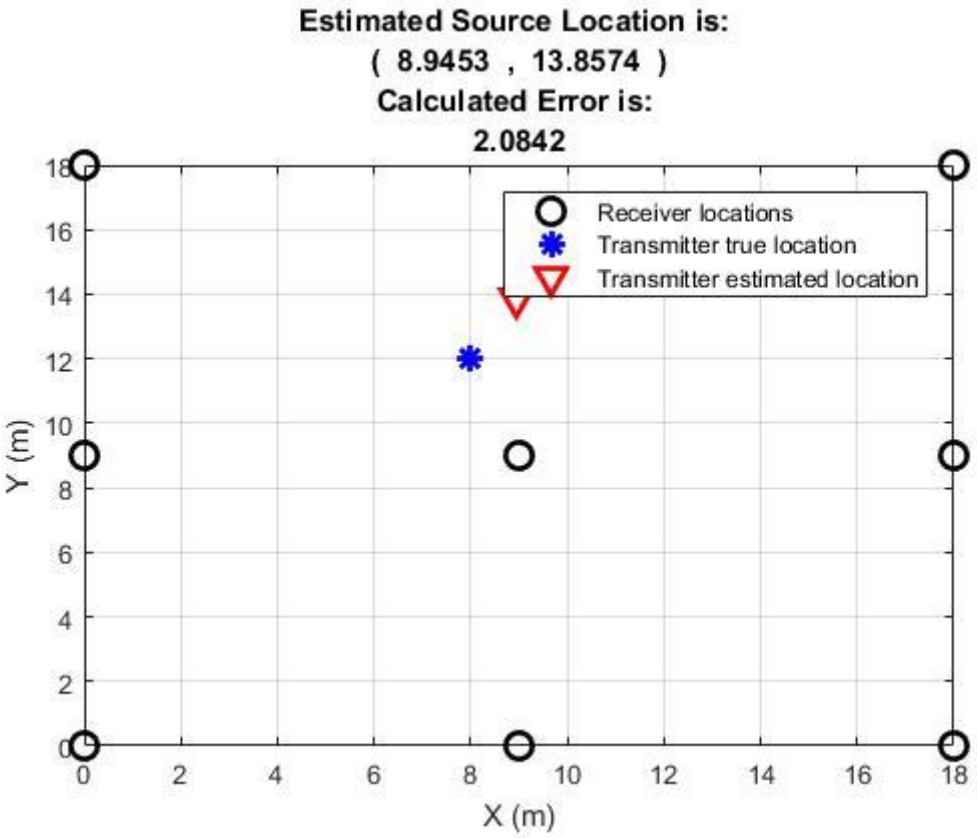

Figure A.20. Position 7, when eight receiving nodes were used.

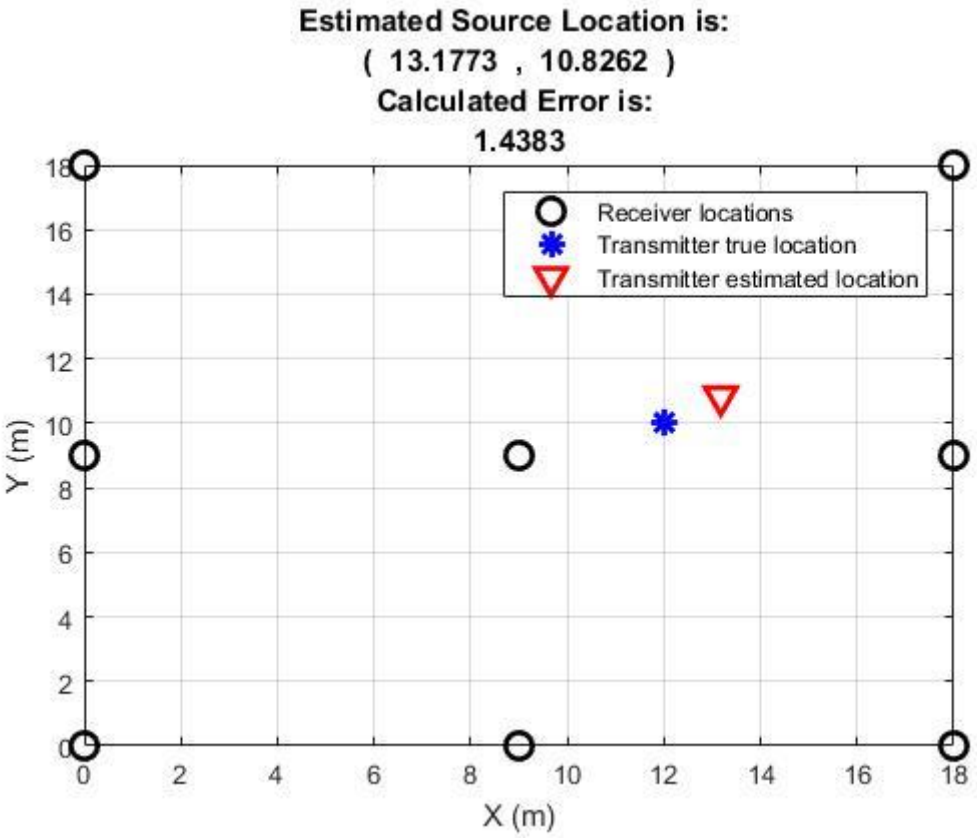

Figure A.21. Position 8, when eight receiving nodes were used.

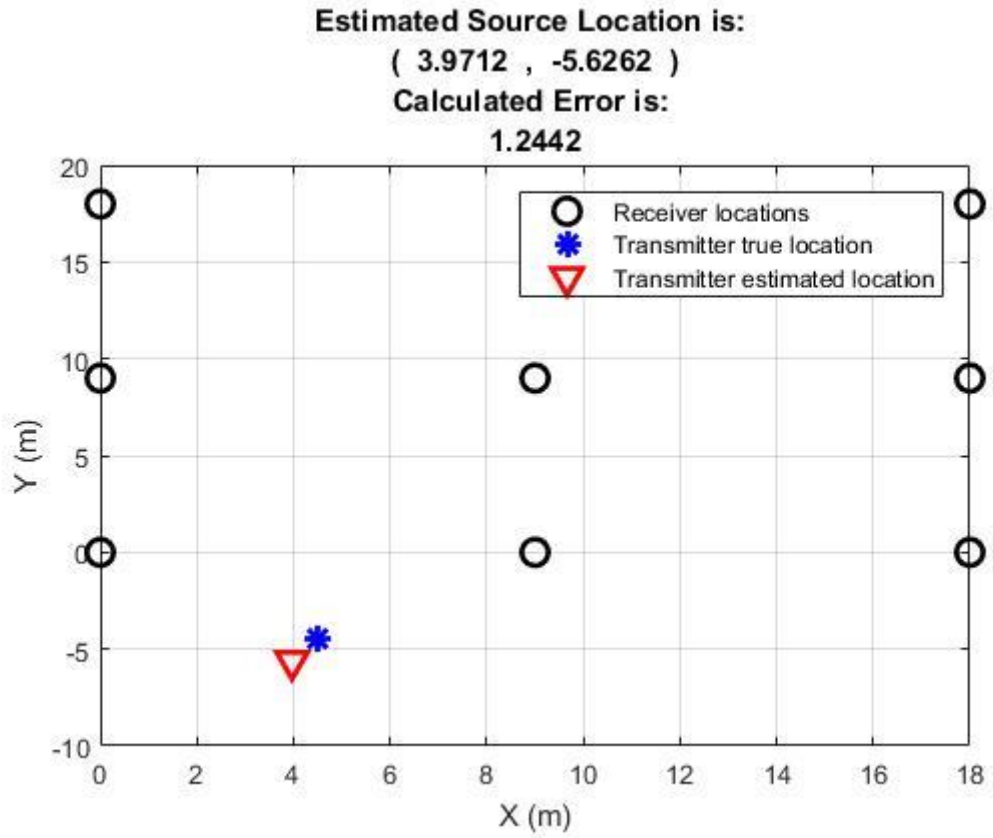

Figure A.22. Position 9, when eight receiving nodes were used.